AEDC-TR-76-62

ANALYTICAL, NUMERICAL, AND EXPERIMENTAL

RESULTS ON TURBULENT BOUNDARY LAYERS

PROPULSION WIND TUNNEL FACILITY
ARNOLD ENGINEERING DEVELOPMENT CENTER
AIR FORCE SYSTEMS COMMAND
ARNOLD AIR FORCE STATION, TENNESSEE 37389

July 1976

Final Report for Period September 1974 — January 1975

Prepared for

DIRECTORATE OF TECHNOLOGY (DY)
ARNOLD ENGINEERING DEVELOPMENT CENTER
ARNOLD AIR FORCE STATION, TENNESSEE 37389

This report has been reviewed by the Information Office (OI) and is releasable to the National Technical Information Service (NTIS). At NTIS, it will be available to the general public, including foreign nations.
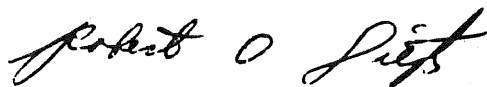
APPROVAL STATEMENT

This technical report has been reviewed and is approved for publication.

FOR THE COMMANDER

ELTON R. THOMPSON
Research & Development
  Division
Directorate of Technology

ROBERT O. DIETZ
Director of Technology

REPORT DOCUMENTATION PAGE		READ INSTRUCTIONS BEFORE COMPLETING FORM
1. REPORT NUMBER AEDC-TR-76-62	2. GOVT ACCESSION NO.	3. RECIPIENT'S CATALOG NUMBER
4. TITLE (and Subtitle) ANALYTICAL, NUMERICAL, AND EXPERIMENTAL RESULTS ON TURBULENT BOUNDARY LAYERS		5. TYPE OF REPORT & PERIOD COVERED Final Report – September 1974 – January 1975
		6. PERFORMING ORG. REPORT NUMBER
7. AUTHOR(s) David L. Whitfield, ARO, Inc.		8. CONTRACT OR GRANT NUMBER(s)
9. PERFORMING ORGANIZATION NAME AND ADDRESS Arnold Engineering Development Center (DY) Air Force Systems Command Arnold Air Force Station, Tennessee 37389		10. PROGRAM ELEMENT, PROJECT, TASK AREA & WORK UNIT NUMBERS Program Element 65807F
11. CONTROLLING OFFICE NAME AND ADDRESS Arnold Engineering Development Center (DYFS) Arnold Air Force Station, Tennessee 37389		12. REPORT DATE July 1976
		13. NUMBER OF PAGES 102
14. MONITORING AGENCY NAME & ADDRESS(if different from Controlling Office)		15. SECURITY CLASS. (of this report) UNCLASSIFIED
		15a. DECLASSIFICATION/DOWNGRADING SCHEDULE N/A

16. DISTRIBUTION STATEMENT (of this Report)

Approved for public release; distribution unlimited.

17. DISTRIBUTION STATEMENT (of the abstract entered in Block 20, if different from Report)

18. SUPPLEMENTARY NOTES

Available in DDC

19. KEY WORDS (Continue on reverse side if necessary and identify by block number)

laminar boundary layer	experimental data
turbulent boundary layer	Reynolds number
numerical analysis	Prandtl number
mathematical analysis	

20. ABSTRACT (Continue on reverse side if necessary and identify by block number)

This report describes the results of analytical, numerical, and experimental investigations of incompressible and compressible boundary layers. The subjects considered are (1) laminar and/or turbulent numerical boundary-layer calculations in which the Reynolds stress is related to the turbulent kinetic energy; (2) an analytical investigation of turbulence near a wall which is not founded on classical mixing-length theory; (3) analytical

DD FORM 1473 (1 JAN 73) EDITION OF 1 NOV 65 IS OBSOLETE

20. ABSTRACT (Continued)

solutions for relating velocity and temperature throughout
turbulent boundary layers for nonunity Prandtl numbers; (4) a
description of the data reduction of pitot pressure measurements
utilizing these analytical results in order to obtain velocity,
temperature, skin friction, and various boundary-layer parameters;
and (5) the application of these numerical and analytical
results to the analysis of turbulent boundary-layer measurements
made in the Propulsion Wind Tunnel Facility (PWT). Listings of
the computer programs used for the boundary-layer computations
and data reduction are included.

AFSC
Arnold AFS Tenn

PREFACE

The work reported herein was conducted by the Arnold Engineering Development Center (AEDC), Air Force Systems Command (AFSC), under Program Element 65807F. The results presented were obtained by ARO, Inc. (a subsidiary of Sverdrup & Parcel and Associates, Inc.), contract operator of AEDC, AFSC, Arnold Air Force Station, Tennessee. The work was done under ARO Project Nos. P33A-36A and P32A-31D. The author of this report was David L. Whitfield, ARO, Inc. The manuscript (ARO Control No. ARO-PWT-TR-75-132) was submitted for publication on August 15, 1975.

CONTENTS

ILLUSTRATIONS

APPENDIXES

1.0 INTRODUCTION

The material presented herein is a result of work done in support of various research, test, and test facility development projects conducted in the Propulsion Wind Tunnel Facility (PWT). The topics considered are somewhat independent, and an effort is made to develop each in an essentially self-contained section. This permits the results to be reviewed and extracted for particular applications as desired without sorting through the entire report. However, an important use of these results is their application as a unit to the analysis of experimental data. Such an application is made, not only as an example to illustrate this point, but to analyze experimental turbulent boundary-layer measurements made in PWT.

The first topic considered (Section 2.0) is a laminar and/or turbulent numerical boundary-layer calculation technique in which the Reynolds stress is related to the local turbulent kinetic energy of the flow, e, and a modified form of the turbulent kinetic energy equation is used to solve for e throughout the boundary layer. This approach has certain advantages over the classical mixing-length approach. For example, computations can be performed of transition flow, initial and free-stream turbulence levels can be taken into account, and the integration is carried completely to the wall where natural boundary conditions can be imposed. This numerical calculation technique is developed for the purpose of performing reasonable engineering predictions of incompressible and compressible turbulent boundary layers. The major effort of this portion of the report is in the modeling of the various terms of the turbulent kinetic energy equation.

Section 3.0 contains the development of an analytical investigation of turbulence near a wall. The approach is unique in that it is based on the turbulent kinetic energy equation developed in Section 2.0, and it does not depend on mixing-length or damping-factor concepts. The results include closed-form expressions for the velocity, Reynolds stress, production of turbulence, and dissipation of turbulence. Moreover, the results show good agreement with experimental data and are valid from the wall through the so-called sublayer and buffer layer and into the fully turbulent portion of the boundary layer. An important application of these results is that of providing information of the region near the wall where experimental measurements are not routinely made (usually never made during wind-tunnel tests because of the experimental difficulties and/or data acquisition time). These analytical results are used to more accurately determine boundary-layer parameters from experimental data such as displacement thickness and momentum thickness as discussed in Section 5.0.

Section 4.0 is concerned with the development of analytical relationships between velocity and temperature throughout turbulent boundary layers on constant temperature or adiabatic walls for nonunity Prandtl numbers. Analytical solutions are of interest as opposed to numerical ones for purposes of data reduction of, e.g. pitot pressure measurements and holographic interferometric measurements. In addition, Reynolds analogy is calculated from these solutions which is shown to be in good agreement with previous results for near adiabatic wall conditions, and predicts the quantity $2\,c_h/c_f$ to decrease with decreasing wall temperature. This prediction is also shown to be supported by comparisons with experimental data, and apparently such a variation has not previously been predicted.

In Section 5.0 the result for the velocity distribution and the velocity-temperature relations (Sections 3.0 and 4.0) are included in the development of a data reduction computer program for the purpose of reducing pitot pressure measurements made in turbulent boundary layers. The code is written to obtain spatial distributions of velocity and temperature, local skin friction, and various boundary-layer parameters.

The results of Sections 2.0 through 5.0 are applied in Section 6.0 to the analysis of turbulent boundary-layer measurements made in Propulsion Wind Tunnels 16S, 16T, and the Acoustic Research Tunnel (ART) in PWT. The experimental data considered include previously reported measurements made in Tunnel 16S and recently acquired unpublished data in Tunnels 16S, 16T, and ART. Results of this analysis which are of particular interest include (1) new skin-friction coefficients determined from measurements made in Tunnel 16S and their impact on transition correlations of data taken in 16S and (2) the nature of the flow in the nozzle boundary layer of Tunnel 16T.

This report contains a fair amount of new results. For example, (1) the particular modeling of the turbulent kinetic energy equation developed in Section 2.0 has not been used previously, (2) the analytical results obtained in Section 3.0 concerning turbulence near a wall are new, but more importantly this particular development (i.e. without mixing-length theory) has not been followed previously, and (3) the analytical velocity-temperature relations and Reynolds analogy for nonunity Prandtl numbers obtained in Section 4.0 are also new. Therefore, because these results are not common nor time tested, effort was expended in assessing the accuracy of each by numerous comparisons with experimental data. In Sections 2.0 through 4.0, these experimental comparisons follow the theoretical development of the results. The computer programs for the boundary-layer calculations and the data reduction procedure (Sections 2.0 and 5.0) are included in Appendixes A and B, respectively.

2.0 NUMERICAL BOUNDARY-LAYER CALCULATIONS

This numerical technique draws heavily from that of previous investigators. Portions of several sources have been extracted and modified where deemed necessary for the purpose of improving the results. The objective was to obtain as accurate results as possible (the standard for which was comparisons with experimental data) for various flow conditions, while attaining a physically reasonable model with minimum empiricism (the constants of which were not allowed to change for the various flow conditions). The result is a fairly easy to use numerical method which yields results in relatively good agreement with experimental data for the flows considered. However, there is much room for improvement. For example, the present code will run for laminar or turbulent flow and calculate through transition, producing quite reasonable looking velocity profiles. Unfortunately, the point of transition occurs upstream (lower Reynolds number) of that observed experimentally. Little has been attempted with the present code concerning possible improvements in calculating transition.

It should be noted that this investigation was made much easier by the powerful numerical method for diffusion-type equations developed by Patankar and Spalding (Ref. 1). Effort here was expended in modeling the equations rather than in their solution. A listing of the resulting computer code is given in Appendix A.

2.1 DIMENSIONLESS BOUNDARY-LAYER EQUATIONS

The choice of the dimensionless variables was such as to recover the general form of the physical-plane equations considered by Patankar and Spalding (Ref. 1) who applied the von Mises transformation to the physical-plane equations, whereas here the von Mises transformation was applied to dimensionless equations. Dimensionless variables simplify and reduce appreciably the input required to run the program. Also some physical insight into the flow problem and its relation to other flows is gained by using dimensionless parameters and eliminating the confusion attributable to units.

In the dimensionless variables defined in the nomenclature and used in Ref. 2, the boundary-layer equations considered were

$$\frac{\partial(\bar{\rho}\,\bar{r}\,\bar{U})}{\partial\bar{x}} + \frac{\partial(\bar{\rho}\,\bar{r}\,\bar{V})}{\partial\bar{y}} = 0 \tag{1}$$

$$\bar{\rho}\,\bar{U}\,\frac{\partial\bar{U}}{\partial\bar{x}} + \bar{\rho}\,\bar{V}\,\frac{\partial\bar{U}}{\partial\bar{y}} = -\frac{d\bar{p}}{d\bar{x}} + \frac{1}{\bar{r}}\frac{\partial}{\partial\bar{y}}\left\{\bar{r}\left[\frac{(2)^{\frac{1}{2}}\bar{\mu}}{Re_{o,s}} - \frac{\bar{\rho}\overline{\langle uv\rangle}}{\partial\bar{U}/\partial\bar{y}}\right]\frac{\partial\bar{U}}{\partial\bar{y}}\right\} \tag{2}$$

9

$$\bar{\rho}\,\bar{U}\,\frac{\partial\hat{\bar{H}}}{\partial\bar{x}} + \bar{\rho}\,\bar{V}\,\frac{\partial\hat{\bar{H}}}{\partial\bar{y}} = \frac{1}{\bar{r}}\,\frac{\partial}{\partial\bar{y}}\left\{\bar{r}\left[\left(\frac{(2)^{\frac12}\bar{\mu}}{\Pr\,\mathrm{Re}_{o,s}} - \frac{\bar{\rho}\langle\overline{u\,v}\rangle}{\Pr_t\,\partial\bar{U}/\partial\bar{y}}\right)\frac{\partial\hat{\bar{H}}}{\partial\bar{y}}\right.\right.$$

$$\left.\left. + \frac{(2)^{\frac12}\bar{\mu}}{\mathrm{Re}_{o,s}}\left(1 - \frac{1}{\Pr}\right)\bar{U}\,\frac{\partial\bar{U}}{\partial\bar{y}} - \frac{\bar{\rho}\langle\overline{u\,v}\rangle}{\partial\bar{U}/\partial\bar{y}}\left(1 - \frac{1}{\Pr_t}\right)\bar{U}\,\frac{\partial\bar{U}}{\partial\bar{y}}\right]\right\} \qquad (3)$$

$$\mathrm{Re}_{o,s} = \frac{\rho_o(2H_{o,\infty})^{\frac12}s}{\mu_o} \qquad (4)$$

$$\bar{r} = \bar{r}_w \pm \bar{y}\cos\bar{\theta} \qquad (5)$$

where the plus sign in Eq. (5) is for external flow and the minus sign for internal flow. The quantity $(2)^{1/2}/\mathrm{Re}_{o,s}$ as a coefficient of $\bar{\mu}$ in Eqs. (2) and (3) is due to using $(H_{o,\infty})^{1/2}$ to nondimensionalize velocities rather than $(2H_{o,\infty})^{1/2}$, the maximum velocity. Using $(2H_{o,\infty})^{1/2}$ would introduce new coefficients for other terms, which were thought to be less convenient to handle. The $(2)^{1/2}$ was used in $\mathrm{Re}_{o,s}$ simply for convenience in order that $\mathrm{Re}_{o,s}$ be based on the maximum velocity.

In order to close this system of equations something must be done with the Reynolds stress term. Rather than introduce the usual eddy-viscosity or mixing-length concepts, the Reynolds stress was modeled here by relating it to the turbulent kinetic energy.

2.2 MODEL FOR REYNOLDS STRESS

Two forms are commonly used for modeling the Reynolds stress by relating it to the turbulent kinetic energy of the flow. The first, introduced by Townsend (Ref. 3) and refined by Lighthill (Ref. 4), written in the boundary-layer approximation, is

$$- \langle uv \rangle = ae \qquad (6)$$

and the second, introduced by Prandtl (Ref. 5), is

$$- \langle uv \rangle = b(e)^{\frac12}\ell\,\frac{\partial U}{\partial y} \qquad (7)$$

where a and b are constants and ℓ is the mixing length. Equation (6), with $a = 0.3$, was used in the present work. Both equations have been used by previous investigators. For example, Bradshaw, Ferriss and Atwell (Ref. 6) used Eq. (6) with $a = 0.3$; Ng and Spalding (Ref. 7) used Eq. (6) in equilibrium flow for evaluating a constant in the dissipation term (a effectively was 0.32); and Glushko (Ref. 8) (recently extended by

Beckwith and Bushnell (Ref. 9)) used a model which can be reduced to Eq. (7) over a portion of the boundary layer. These approaches, as well as the present one, differ primarily in the modeling of the terms in the turbulent kinetic energy equation which is required for a solution for e.

2.3 TURBULENT KINETIC ENERGY EQUATION

The derivation of the particular turbulent kinetic energy equation used here begins with the equation proposed by Kolmogoroff (Ref. 10), and used by Ng and Spalding (Ref. 7), and is written for axisymmetric flow as

$$\rho U \frac{\partial e}{\partial x} + \rho V \frac{\partial e}{\partial y} = \frac{1}{\sigma_e} \frac{1}{r} \frac{\partial}{\partial y} \left(r \rho e^{\frac{1}{2}} \ell' \frac{\partial e}{\partial y} \right) + \rho e^{\frac{1}{2}} \ell' \left(\frac{\partial U}{\partial y} \right)^2 - \left(\frac{C_D \rho e^{3/2}}{\ell'} \right) \qquad (8)$$

The terms in Eq. (8) on the left-hand side represent convection, and the first, second, and third terms on the right-hand side represent the diffusion, production, and dissipation, respectively. Glushko (Ref. 8) points out that at low Reynolds numbers the turbulent energy dissipation deviates from that specified in Eq. (8). The reason for this has to do with assumptions concerning the equilibrium of the turbulence at high wave numbers for sufficiently high Reynolds numbers as explained by Batchelor (Ref. 11). Ng and Spalding (Ref. 7) used Eq. (8) in conjunction with an additional equation in order to calculate ℓ'. However, besides the problem with the dissipation term, Ng and Spalding (Ref. 7) did not use the molecular viscosity and did not integrate completely to the wall. In an attempt to remedy these deficiencies, the following modifications were made to Eq. (8). The numerator and denominator of the dissipation term in Eq. (8) were multiplied by the integral scale length of turbulence ℓ', in order to obtain a term $e^{1/2} \ell'$ common to each term on the right-hand side of Eq. (8). Ng and Spalding (Ref. 7) used a proposal of Kolmogoroff (Ref. 10) and Prandtl (Ref. 5) to relate $e^{1/2} \ell'$ to the Reynolds stress by $e^{1/2} \ell' = - \langle uv \rangle / \partial U / \partial y$ which is the form of Eq. (7). However, in the present work the expression

$$e^{\frac{1}{2}} \ell' = - \frac{\langle uv \rangle}{(\partial U / \partial y)} + \frac{\mu}{\rho} \qquad (9)$$

is used in the diffusion and dissipation terms while retaining $e^{1/2} \ell' = - \langle uv \rangle / \partial U / \partial y$ in the production term. Equation (8) can then be written

$$\rho U \frac{\partial e}{\partial x} + \rho V \frac{\partial e}{\partial y} = \frac{1}{\sigma_e} \frac{1}{r} \frac{\partial}{\partial y} \left[r \left(\mu - \frac{\rho \langle uv \rangle}{\partial U / \partial y} \right) \frac{\partial e}{\partial y} \right] - \rho \langle uv \rangle \frac{\partial U}{\partial y} - \frac{Ce}{L^2} \left(\mu - \frac{\rho \langle uv \rangle}{\partial U / \partial y} \right) \qquad (10)$$

where L is the dissipation length and C is a constant or a function of Reynolds number. Equation (9) was not used in the production term in Eq. (8) because this term represents the production of turbulent energy and would not be zero for $e \equiv 0$ (laminar flow).

Equation (10) is the turbulent kinetic energy equation used here. It is similar in form to the equation developed by Glushko (Ref. 8). However, Glushko modeled the Reynolds stress more nearly like that given by Eq. (7), whereas in the present work the Reynolds stress is modeled by Eq. (6). Also, Glushko's modeling takes on three different explicit forms across the boundary layer, whereas here Eq. (7) was used throughout the boundary layer. This modeling was used for simplicity and can be justified only by the results obtained. In dimensionless variables the additional equations used to close the system composed of Eqs. (1) through (5) are

$$
\bar{\rho}\,\overline{U}\,\frac{\partial \bar{e}}{\partial \overline{x}} + \bar{\rho}\,\overline{V}\,\frac{\partial \bar{e}}{\partial \overline{y}} = \frac{1}{\sigma_e}\,\frac{1}{\overline{r}}\,\frac{\partial}{\partial \overline{y}}\left\{\overline{r}\left[\frac{(2)^{\frac{1}{2}}\bar{\mu}}{Re_{o,s}} - \frac{\bar{\rho}\langle\overline{uv}\rangle}{\partial\overline{U}/\partial\overline{y}}\right]\frac{\partial \bar{e}}{\partial \overline{y}}\right\}
$$

$$
-\;\bar{\rho}\,\langle\overline{uv}\rangle\,\frac{\partial \overline{U}}{\partial \overline{y}} - \frac{C\bar{e}}{\overline{L}^2}\left[\frac{(2)^{\frac{1}{2}}\bar{\mu}}{Re_{o,s}} - \frac{\bar{\rho}\langle\overline{uv}\rangle}{\partial\overline{U}/\partial\overline{y}}\right]
$$

(11)

and

$$
-\langle\overline{uv}\rangle = a\bar{e} = 0.3\,\bar{e}
$$

(12)

The expression used for C in Eq. (11) is

$$
C = 3.1 - (Re_{\infty,x})\,1.82 \times 10^{-9}
$$

(13)

with a lower bound of 2.7. The reason for this particular expression will be made clear subsequently when comparisons with experimental data are discussed.

Application of the von Mises transformation to the boundary-layer equations is given in general form by Patankar and Spalding (Ref. 1) and in the present dimensionless variables, except for the additional terms due to the Reynolds stress, in Ref. 2. Applying this transformation to the turbulent kinetic energy equation, Eq. (11), gives (the necessary partial derivative operators are given in Ref. 2)

$$
\frac{\partial \bar{e}}{\partial \overline{x}} + \frac{\omega\,(\overline{r}_E\,\dot{m}_E - \overline{r}_I\,\dot{m}_I) + \overline{r}_I\,\dot{m}_I}{\phi_E - \phi_I}\,\frac{\partial \bar{e}}{\partial \omega} = \frac{1}{\sigma_e}\,\frac{\partial}{\partial \omega}\left\{\frac{\bar{\rho}\,\overline{U}\,\overline{r}^2}{(\phi_E - \phi_I)^2}\left[\frac{(2)^{\frac{1}{2}}\bar{\mu}}{Re_{o,s}} - \frac{\bar{\rho}\langle\overline{uv}\rangle}{\partial\overline{U}/\partial\overline{y}}\right]\frac{\partial \bar{e}}{\partial \omega}\right\}
$$

$$
-\;\bar{\rho}\langle\overline{uv}\rangle\,\frac{\partial \overline{U}}{\partial \overline{y}} - \frac{C\bar{e}}{\overline{L}^2}\left[\frac{(2)^{\frac{1}{2}}\bar{\mu}}{Re_{o,s}} - \frac{\bar{\rho}\langle\overline{uv}\rangle}{\partial\overline{U}/\partial\overline{y}}\right]
$$

(14)

The boundary conditions for the governing system of equations are rather general, and are those permitted by the numerical technique of Patankar and Spalding (Ref. 1). In addition, boundary conditions on $\bar{e}$ are required which are taken as $\bar{e} = 0$ at the wall

and some prescribed free-stream turbulence level. If the turbulence is taken as $\bar{e} \equiv 0$ across the boundary layer, the governing equations describe laminar flow. If the turbulence anywhere across the boundary layer is $\bar{e} > 0$, regardless of how small, the flow is turbulent. That is, the degree of turbulence here is determined by the magnitude of $\bar{e}$, and no distinction is made between fully developed turbulent flow, transition flow, etc.

It should be pointed out that the calculation of mass flux into the boundary layer, entrainment, is not handled as suggested in Ref. 1 for turbulent flow, because the mixing-length approach is not followed. Rather, the same subroutine as utilized in Ref. 2 for laminar flow was used here for both laminar and turbulent flow. This permitted extremely small to extremely large turbulent intensities to be handled using the same entrainment calculation scheme.

2.4 COMPARISONS WITH EXPERIMENTAL DATA

For convenience, the ratio of the Reynolds number based on total conditions, Re_o, and the local unit Reynolds number, Re_∞, which is more commonly used, is given in Fig. 1 as a function of Mach number. This ratio is based on isentropic flow and assumes that $\mu \sim T^\zeta$. The assumption $\mu \sim T^\zeta$ was used in the present calculations with $\zeta = 2/3$.
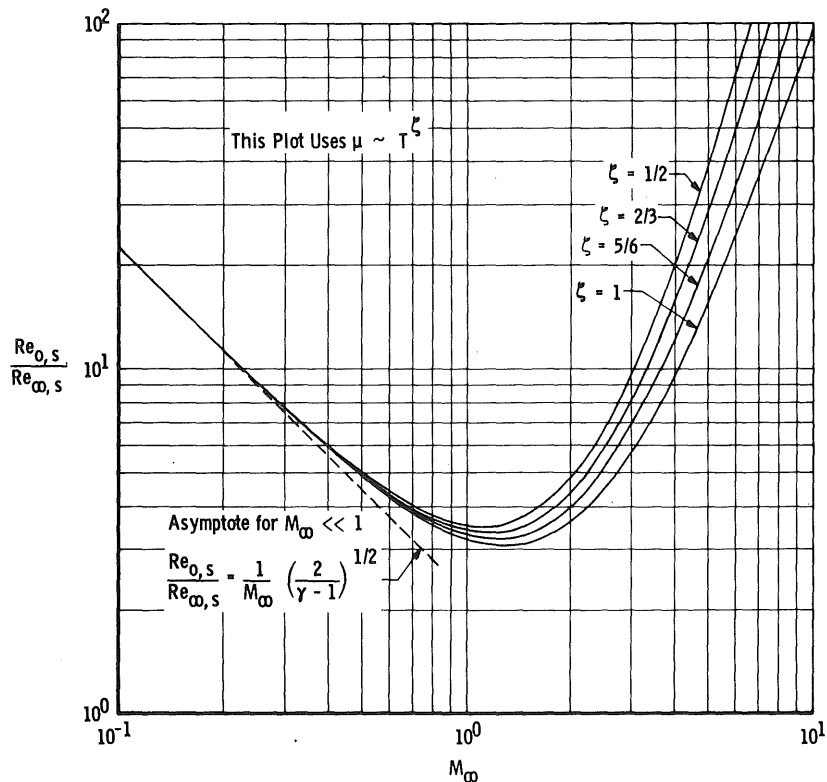
Figure 1. $Re_{o,s}/Re_{\infty,s}$ as a function of M_∞ for $\gamma = 7/5$.

13

However, it is not required, and any viscosity law can be used. Solutions presented in Ref. 2 for thick laminar boundary layers with large transverse temperature gradients indicate essentially the same results were obtained whether $\mu \sim T^\zeta$ was used or Sutherland's law was used. Therefore, it was assumed here that $\mu \sim T^\zeta$ was adequate, particularly since μ is significant only over a small portion of a turbulent boundary layer. Figure 1 is convenient for determining $Re_{o,s}$ because usually the free-stream unit Reynolds number is known for a given free-stream Mach number.

The investigation by Winter and Gaudet (Ref. 12) provides a large number of subsonic and supersonic data taken in the Royal Aircraft Establishment (R.A.E.) 8-ft by 8-ft wind tunnel. These data are particularly useful for evaluating the present work in that the development length was established and numerous detailed measurements were made at various Reynolds numbers. Winter and Gaudet's subsonic velocity profile data at $M_\infty =$ 0.2 for $16.4 \times 10^6 \leqslant Re_{\infty,x} \leqslant 224 \times 10^6$ are compared with calculated profiles in Fig. 2. These data were relied upon for determining C in Eq. (11) as given by Eq. (13). With C taken as a constant of 3.5, c_f varied from about five percent above the experimental
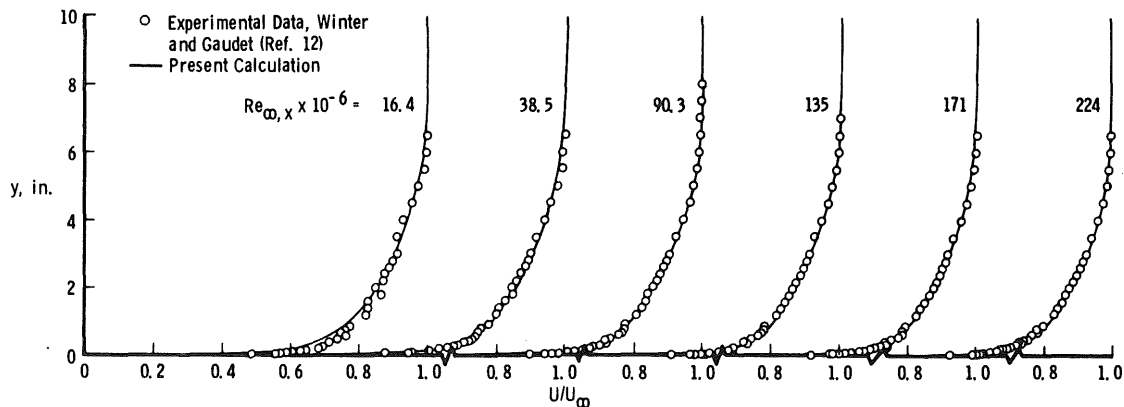
Figure 2. Theoretical and experimental velocity distributions at $M_\infty = 0.2$ and various $Re_{\infty,x}$.

skin friction data of Ref. 12 at $Re_{\infty,x} = 10^6$ to about ten percent below the experimental data at $Re_{\infty,x} = 224 \times 10^6$. Also, the calculated velocity distribution with C = 3.5 differed somewhat with the experimental velocity distribution for $Re_{\infty,x} = 224 \times 10^6$. It was found that if C were changed to about 2.7, then c_f agreed with the experimental skin friction data at $Re_{\infty,x} = 224 \times 10^6$, and the calculated velocity distribution agreed with the experimental velocity distribution. Of course, this agreement in velocities must be the case next to the wall if the skin frictions are to agree; however, not all models attempted for the various terms in Eq. (11) gave this quantitative trend. It was found that essentially the same result was obtained whether C was taken as 2.7 or concocted to be 2.7 when

$Re_{\infty,x}$ = 224 x 10^6. Therefore, C was made to take on the proper value (proper value here means giving good agreement with experimental data) at a smaller $Re_{\infty,x}$ and at $Re_{\infty,x}$ = 224 x 10^6, and Eq. (13) was used in the present calculations with a lower bound of 2.7. Actually, not a great deal of effort was expended in evaluating or improving C, and surely an improvement could be made. However, the results provided by using Eq. (13) were considered acceptable, and no further changes were made for C.

Comparisons between calculated and measured velocity distributions for the R.A.E. tunnel (Ref. 12) are presented in Fig. 3 for M_{∞} = 2.2 and 26.3 x 10^6 ≤ $Re_{\infty,x}$ ≤ 108 x 10^6. Comparisons are also made with Mach number distributions in Fig. 4 for these supersonic flow data. Considering that C was evaluated for subsonic flow, and Glushko's L came from incompressible flow, the agreement between calculated and measured data is considered good. The agreement improves as $Re_{\infty,x}$ increases, with the maximum discrepancy at $Re_{\infty,x}$ = 26.3 x 10^6.
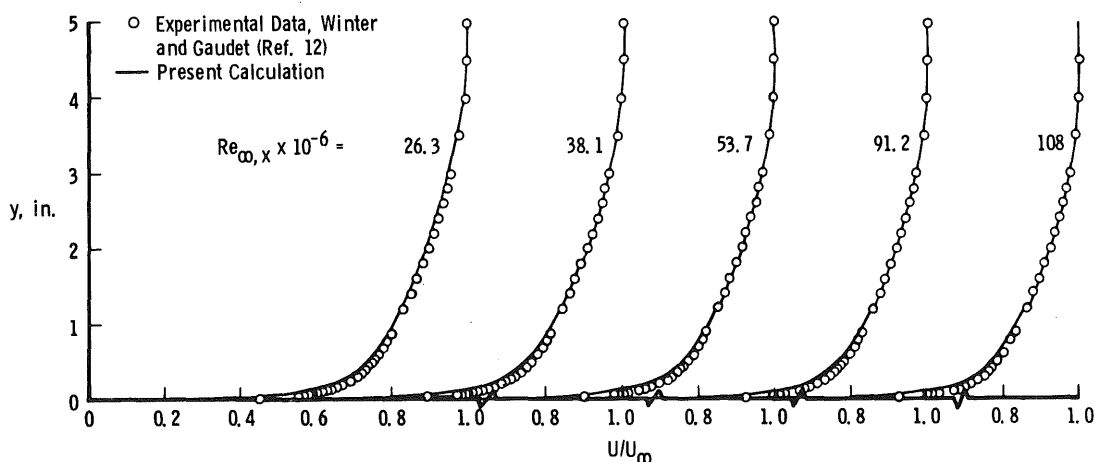
Figure 3. Theoretical and experimental velocity distributions at M_{∞} = 2.2 and various $Re_{\infty,x}$.

For comparisons at higher Mach number the experimental data of Gates (Ref. 13) at M_{∞} = 4 are considered in Figs. 5 and 6. Two inflection points are evident in each of the experimental Mach number profiles in Fig. 6. Similar inflection points exist in the calculated Mach number profiles, although the profiles at x = 4.75 ft are in best agreement. The solutions were obtained for a constant wall temperature of $T_w/T_{0,\infty}$ = 0.9 as indicated by a temperature versus distance along-the-plate plot as presented by Gates (Ref. 13). However, the tabulated profile data in Table IV of Ref. 13 indicate $T_w/T_{0,\infty}$ = 0.94 for the data at x = 2.75 ft in Figs. 5 and 6, which might cause some discrepancy. For the same reasons as mentioned in discussing the R.A.E. M_{∞} = 2.2 data of Winter and Gaudet (Ref. 12), the agreement in Figs. 5 and 6 is better than expected.

15
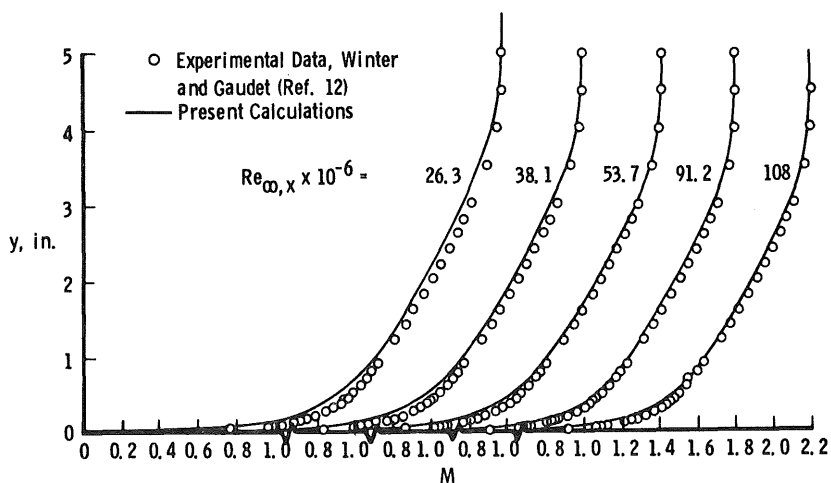
Figure 4. Theoretical and experimental Mach number distributions at $M_\infty = 2.2$ and various $Re_{\infty,x}$.
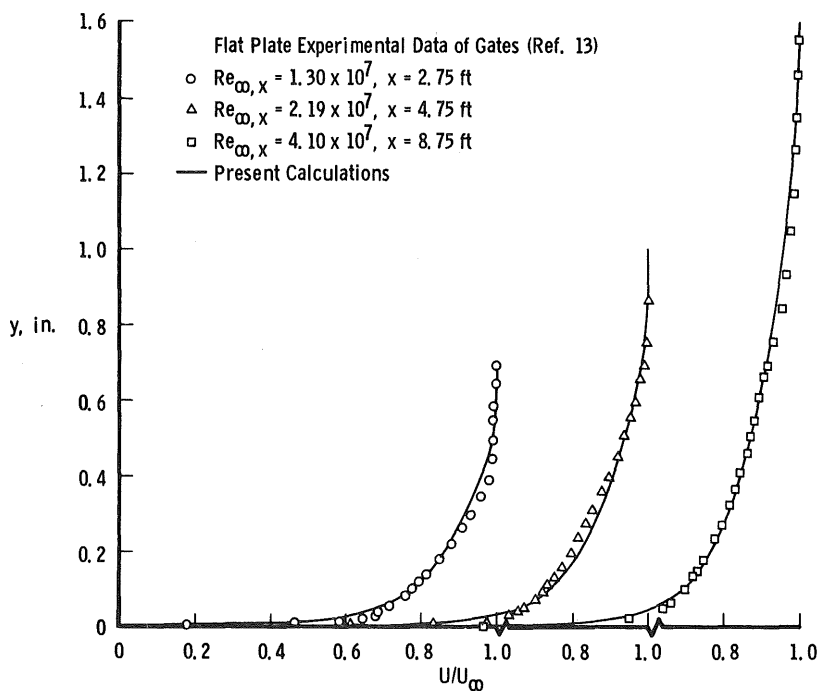
Figure 5. Theoretical and experimental velocity distributions at $M_\infty = 4$.
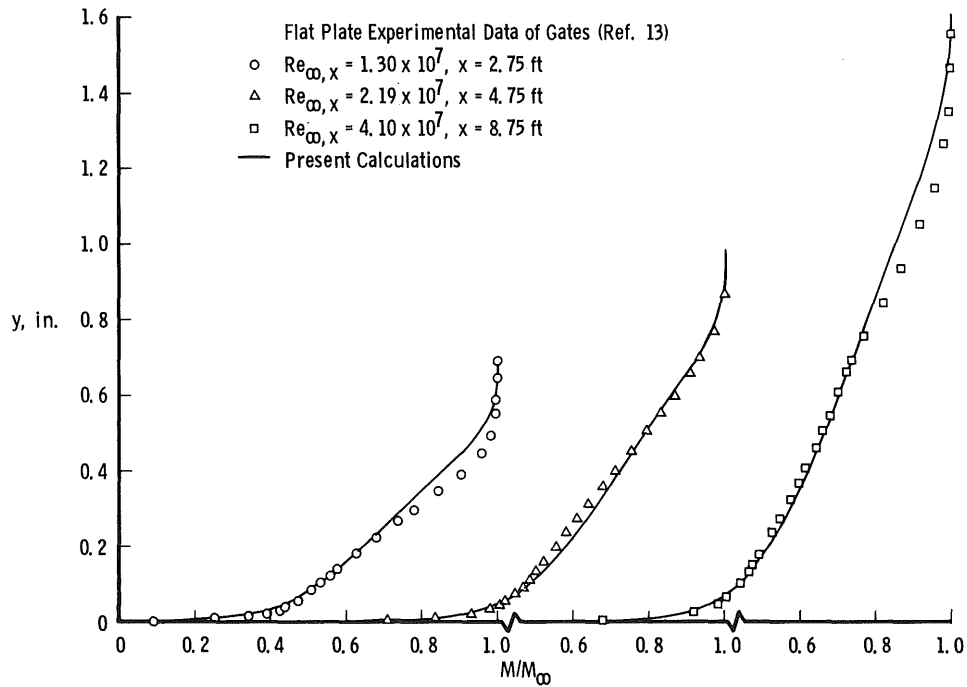
Figure 6. Theoretical and experimental Mach number distributions at $M_\infty = 4$.

3.0 ANALYTICAL RESULTS FOR TURBULENT FLOW NEAR A WALL

Of interest here is that portion of a turbulent boundary layer which extends, in a normal direction, from the wall out into the fully turbulent region. Included are the so-called viscous sublayer and buffer layer which are understood to extend over y^+ values of about 0 to 5 and 5 to 35, respectively.

This portion of the boundary layer has been investigated previously and summaries of these investigations, with the known exception of the work by Rannie (Ref. 14), are given in the books by Hinze (Ref. 15) and White (Ref. 16). The approach of these investigators included that of assuming velocity distributions in this region, developing empirical expressions for the eddy viscosity, or employing Prandtl's mixing-length hypothesis with various modifications near the wall. With the exception of simply assuming a functional form of the velocity distribution, none of the previous investigations lead to closed-form expressions for the velocity except that of Spalding (Ref. 17); the same expression was obtained later by Kleinstein (Ref. 18). Spalding (Ref. 17) developed an expression by satisfying the familiar logarithmic velocity distribution in the fully turbulent portion of the boundary layer and then matched this result to an expression, obtained by inspection, which satisfies Reichardt's (Ref. 19) requirement that the eddy viscosity vary proportionally to y raised to at least the third power as y becomes small.

Whereas Spalding's (Ref. 17) result for the velocity distribution is accurate and is in closed-form, van Driest (Ref. 20) obtained one apparently as accurate by quadrature. Surprisingly, the latter is perhaps more frequently used. This seems to be attributable to the popularity of van Driest's (Ref 20) physical development whereby he derived a damping factor for Prandtl's mixing length near a wall.

With regard to these previous investigations, the present work is of interest because (1) the approach is not founded on an eddy-viscosity or mixing-length concept; (2) the functional forms for the velocity and Reynolds stress distributions are not postulated but result from the analysis; (3) simple closed-form expressions are obtained for the velocity, Reynolds stress, turbulence production, and direct mean-flow energy dissipation; and (4) the results are in good agreement with experimental data. The approach is to model the Reynolds stress by relating it to the local turbulent kinetic energy of the flow. The momentum equation, and the turbulent kinetic energy equation developed in the previous section, are solved analytically in the region near the wall. These results are used to obtain analytical expressions for the various mean-flow turbulent quantities.

The expression used for the turbulent kinetic energy is that given by Eq. (10), and is, for two-dimensional flow

$$\rho U \frac{\partial e}{\partial x} + \rho V \frac{\partial e}{\partial y} = \frac{1}{\sigma_e} \frac{\partial}{\partial y} \left[\left(\mu - \frac{\rho <uv>}{\partial U/\partial y} \right) \frac{\partial e}{\partial y} \right] - \rho <uv> \frac{\partial U}{\partial y} - \frac{Ce}{L^2} \left(\mu - \frac{\rho <uv>}{\partial U/\partial y} \right) \tag{15}$$

Using

$$\tau = \mu \frac{\partial U}{\partial y} - \rho <uv> \tag{16}$$

Eq. (15) becomes

$$\rho U \frac{\partial e}{\partial x} + \rho V \frac{\partial e}{\partial y} = \frac{1}{\sigma_e} \frac{\partial}{\partial y} \left(\frac{\tau \, \partial e/\partial y}{\partial U/\partial y} \right) - \rho <uv> \frac{\partial U}{\partial y} - \frac{Ce}{L^2} \frac{\tau}{\partial U/\partial y} \tag{17}$$

It is hypothesized that e is an explicit function of U only. Then, Eq. (17) can be written

$$\left(\rho U \frac{\partial U}{\partial x} + \rho V \frac{\partial U}{\partial y} \right) \frac{de}{dU} = \frac{1}{\sigma_e} \frac{\partial}{\partial y} \left(\tau \frac{de}{dU} \right) - \rho <uv> \frac{\partial U}{\partial y} - \frac{Ce}{L^2} \frac{\tau}{\partial U/\partial y} \tag{18}$$

Using the zero-pressure gradient momentum equation

$$\rho U \frac{\partial U}{\partial x} + \rho V \frac{\partial U}{\partial y} = \frac{\partial \tau}{\partial y} \tag{19}$$

and taking $\sigma_e = 1$, Eq. (18) simplifies to

$$\tau \frac{d^2 e}{dU^2} - \rho \langle uv \rangle - \frac{Ce}{L^2} \frac{\tau}{(\partial U/\partial y)^2} = 0 \qquad (20)$$

The dissipation length L in the last term in Eq. (20) was taken from Glushko's report (Ref. 8). Because L was originally taken from experimental data and behaves somewhat as a mixing length (see Ref. 8), this length is eliminated by assuming it was originally related to the Reynolds stress by $-\langle uv \rangle \sim L^2 (\partial U/\partial y)^2$. Absorbing the constant of proportionality in the constant, C, Eq. (20) becomes

$$\tau \frac{d^2 e}{dU^2} - \rho \langle uv \rangle - \frac{Ce\,\tau}{-\langle u\,v \rangle} = 0 \qquad (21)$$

To obtain closure, the Reynolds stress is modeled by relating it to the turbulent kinetic energy of the flow according to Eq. (6). An exact value for the constant in Eq. (6) is not important here; rather, the significance of Eq. (6) is that the Reynolds stress is assumed proportional to the local turbulent kinetic energy. Equation (21) can then be written

$$\tau \frac{d^2 e}{dU^2} + a^2 \rho e = \beta \tau \qquad (22)$$

where a and β are constants and a^2 was written for later convenience.

Equation (22) is not restricted to the region near the wall nor to incompressible flow. However, rather simple and useful results can be obtained by making two assumptions, (1) incompressible flow and (2) τ is independent of y and is equal to τ_w. The second assumption is common and not without some justification. For example, consider Eq. (19). At the wall, with no-slip boundary conditions, one has that $\partial \tau/\partial y = 0$. Differentiating Eq. (19) one obtains

$$\frac{\partial^2 \tau}{\partial y^2} = \rho \left[U \frac{\partial^2 U}{\partial y \partial x} + V \frac{\partial^2 U}{\partial y^2} + \frac{\partial U}{\partial y} \left(\frac{\partial U}{\partial x} + \frac{\partial V}{\partial y} \right) \right] \qquad (23)$$

The first two terms on the right-hand side of Eq. (23) are zero at the wall because of the no-slip boundary conditions. The third term is zero by the continuity equation. Therefore, the first nonzero term for $\tau - \tau_w$ must be at least of order y^3, and has no y or y^2 term in zero-pressure gradient two-dimensional flow as sometimes assumed, e.g. Ref. 21. Using these two assumptions of incompressible flow and τ independent of y ($\tau = \tau_w$), Eq. (22) can be written

$$\frac{d^2 E}{du^{+2}} + a^2 E = \beta \tag{24}$$

where

$$E = \frac{e}{U_\tau^2} \tag{25}$$

and

$$u^+ = \frac{U}{U_\tau} \tag{26}$$

The boundary conditions used for Eq. (24) are $E = 0$ at $u^+ = 0$ and $dE/du^+ = 0$ at $u^+ = 0$. A boundary condition near the outer edge of the layer is not used because Eq. (24) is valid only in the vicinity of the wall because of the assumption of τ being independent of y. The boundary condition $dE/du^+ = 0$ at $u^+ = 0$ represents the behavior of the numerical solutions of the previous section near the wall, simplifies the final results, and contributed to yielding a physically reasonable turbulent kinetic energy solution across the entire boundary layer. Final justification for this boundary condition is based on the quality of the results obtained. Using these boundary conditions, the solution to Eq. (24) is

$$E = \frac{\beta}{a^2} [1 - \cos(au^+)] \tag{27}$$

With $\tau = \tau_w$, Eq. (16) can be written in dimensionless variables as

$$\frac{du^+}{dy^+} = 1 - aE \tag{28}$$

Using Eq. (27), Eq. (28) can be written

$$\frac{du^+}{dy^+} = 1 - \frac{a\beta}{a^2} [1 - \cos(au^+)] \tag{29}$$

Equation (29) can be integrated directly to give y^+ as a function of u^+ if the magnitude of the constant $a\beta/a^2$ is known, see e.g. Gradshteyn and Ryzhik (Ref. 22). To this end, consider the fact that in the fully turbulent region one has that $a\rho e_m \approx \tau_w$ (where e_m is the maximum or peak in the turbulent kinetic energy distribution). Therefore, in dimensionless variables

$$a E_m + \epsilon^2 = 1 \tag{30}$$

where ϵ^2 is a small positive quantity. That ϵ^2 is a small positive quantity is a consequence of Eq. (28) in conjunction with the fact that $E \geqslant 0$ and the physical reasoning that $du^+/dy^+ \geqslant 0$ for a smooth, impermeable wall. Then, using Eq. (27) to obtain $E_m = 2\beta/a^2$, gives

$$\frac{a\beta}{a^2} = \frac{1 - \epsilon^2}{2} \tag{31}$$

and Eq. (29) becomes

$$\frac{du^+}{dy^+} = \frac{1 + \epsilon^2}{2} + \frac{1 - \epsilon^2}{2} \cos{(au^+)} \tag{32}$$

Using the fact that $0 < \epsilon^2 < 1$, and satisfying the wall boundary condition of $u^+ = 0$ at $y^+ = 0$, Eq. (32) can be integrated (Ref. 22) to give

$$y^+ = \frac{2}{\epsilon a} \tan^{-1}\left[\epsilon \tan\left(\frac{au^+}{2}\right)\right] \tag{33}$$

Consider the limiting result of Eq. (33) for small u^+. Neglecting terms of third order in u^+, Eq. (33) gives

$$y^+ = u^+ \tag{34}$$

which is, of course, the classical sublayer result. Away from the wall, the velocity distribution depends on the values of ϵ and a. The constant a can be determined by using Eq. (27) to force the peak in the turbulent kinetic energy distribution to correspond to experimental data or to the numerical solutions of the previous section. It can also be determined by taking $\epsilon = 0$, which corresponds to the assumption of $a\rho e_m = \tau_w$, integrating Eq. (32), and then determining the value of a which gives best agreement with experimentally measured velocity distributions near the wall. Fortunately, the value of a obtained by any of these methods is about the same, and is, $a = 0.18$. With the constant a determined, ϵ can be obtained most easily by fitting Eq. (33) with experimental data at the value of u^+ where $au^+ = \pi$, in which case $\epsilon = \pi/ay^+$ according to Eq. (33) for $au^+ = \pi$. A reasonable value of ϵ appears to be $\epsilon = 1/8$. Therefore, Eq. (33) becomes

$$y^+ = \frac{8}{0.09} \tan^{-1}\left[\frac{1}{8} \tan{(0.09\,u^+)}\right] \tag{35a}$$

Note that for $u^+ > \pi/0.18$, a change of quadrants must be made, and

$$y^+ = \frac{8}{0.09}\left\{\pi + \tan^{-1}\left[\frac{1}{8} \tan{(0.09\,u^+)}\right]\right\} \text{ for } u^+ > \pi/0.18 \tag{35b}$$

The result corresponding to $\epsilon = 0$ is more simple than the expressions above and is given by

$$y^+ = \frac{1}{0.09} \tan (0.09 \, u^+) \tag{36}$$

Comparisons of the velocity distributions according to Eqs. (35) and (36) are compared with the experimental data of Lindgren (Ref. 23) in Fig. 7. Good agreement exists between Eq. (36) and the experimental data for y^+ less than about 100, and poor

Sym	Source	Ref.
△	Pipe Flow, $Re_{d,m} = 6.1 \times 10^3$	Lindgren (Ref. 23)
□	Pipe Flow, $Re_{d,m} = 1.0 \times 10^4$	Lindgren (Ref. 23)
○	Pipe Flow, $Re_{d,m} = 2.7 \times 10^4$	Lindgren (Ref. 23)
●	Pipe Flow, $Re_{d,m} = 4.9 \times 10^4$	Lindgren (Ref. 23)
——	Eq. (36)	Present
‑‑‑	Eq. (35)	Present
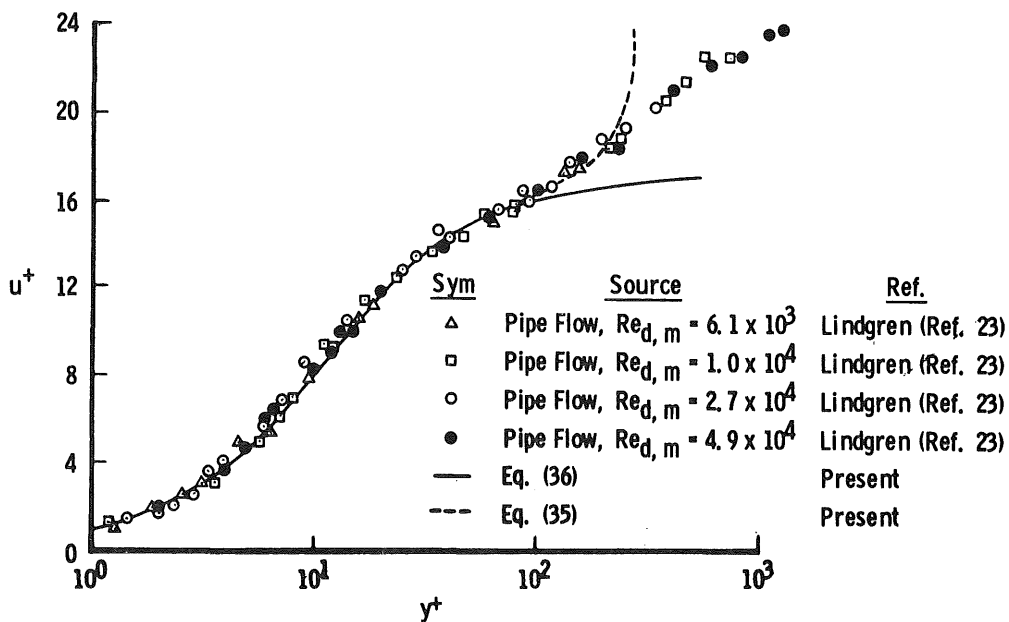
Figure 7. Velocity distributions according to Eqs. (35) and (36) and the experimental data of Lindgren (Ref. 23).

agreement exists for $y^+ > 100$. For Eq. (35), good agreement is obtained up to y^+ of approximately 200, and then poor agreement for $y^+ > 200$. Recall that Eq. (36) requires $a\rho e_m = \tau_w$, whereas Eq. (35) does not have this restriction. However, both Eqs. (35) and (36) require that τ be independent of y, which is not the case in the outer part of the boundary layer. The discrepancy between Eq. (35) and the experimental data in Fig. 7 for $y^+ > 200$ is, therefore, attributed to the assumption of $\tau = \tau_w$, and the discrepancy between Eq. (36) and the data for $y^+ > 100$ is attributed to the same assumption plus the additional restriction of requiring $a\rho e_m = \tau_w$. Equations (35) and (36) do, however, provide simple and accurate expressions for the velocity distribution throughout the viscous sublayer and buffer layer and into the fully turbulent portion of the boundary layer.

An expression for the Reynolds stress can be obtained by using Eq. (16) with τ = τ_w and either Eq. (35) or (36) for the velocity distribution. The expression resulting from using the more simple velocity distribution, Eq. (36), appears to be sufficiently accurate, and is given by

$$\frac{- <uv>}{U_\tau^2} = \sin^2 [\tan^{-1} (0.09 \, y^+)] = \frac{(0.09 \, y^+)^2}{1 + (0.09 \, y^+)^2} \qquad (37)$$

Equation (37) is compared in Fig. 8 with the experimental data of Laufer (Ref. 24) and Klebanoff (Ref. 25) and that calculated by van Driest (Ref. 20) using his damping factor concept. The low Reynolds number data of Laufer (Ref. 24) are slightly below the other data in Fig. 8 for y^+ larger than about 30. However, the agreement in Fig. 8 is considered good.
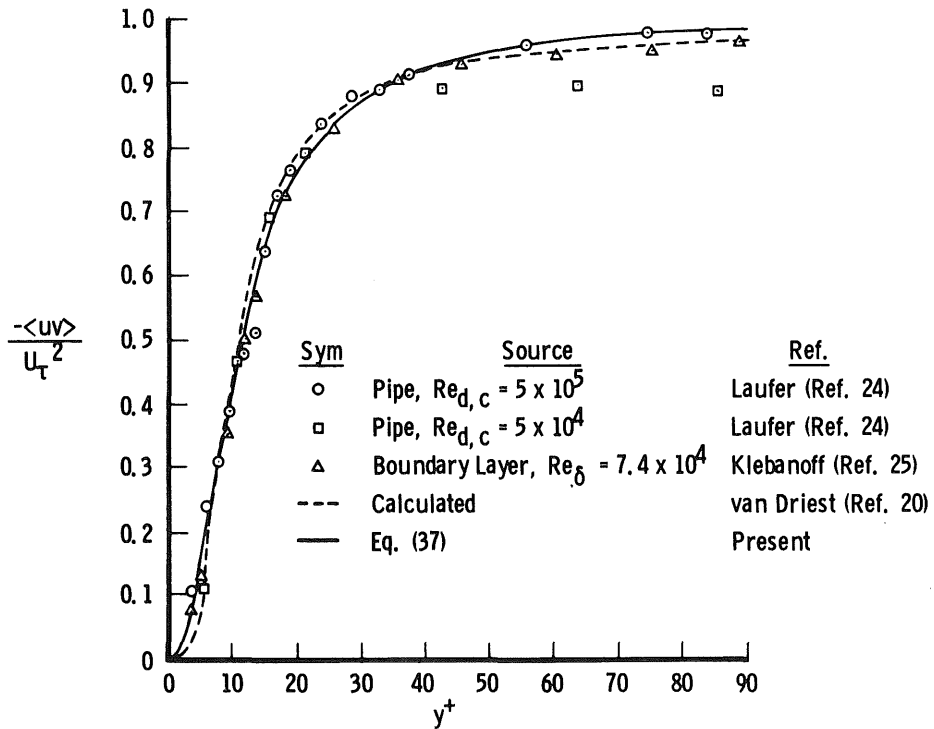
Figure 8. Reynolds stress distributions near a wall.

Schubauer (Ref. 26) considered the measurements of Laufer (Ref. 24) and Klebanoff (Ref. 25) for investigating certain turbulent processes in pipe and boundary-layer flows. Schubauer (Ref. 26) points out that the most important outcome of the investigations of Refs. 24 and 25 is the revelation that the region near the hypothetical sublayer is one of high activity for turbulence. Schubauer (Ref. 26) presents a plot of the turbulence

23

production and dissipation measurements of Laufer (Ref. 24) and Klebanoff (Ref. 25). This plot is reproduced in Fig. 9 along with the present predictions of the quantities measured using Eq. (36) for the velocity distribution. The present results for the quantities considered by Schubauer (Ref. 26) are, for the turbulence production

$$\frac{-\langle uv \rangle}{U_\tau^2} \frac{du^+}{dy^+} = \frac{1}{4} \sin^2 [2 \tan^{-1} (0.09 \, y^+)] = \left(\frac{0.09 \, y^+}{1 + (0.09y^+)^2} \right)^2 \tag{38}$$

and the direct dissipation of mean-flow energy

$$\left(\frac{du^+}{dy^+} \right)^2 = \cos^4 [\tan^{-1} (0.09 \, y^+)] = \left(\frac{1}{1 + (0.09y^+)^2} \right)^2 \tag{39}$$

Sym		Source	Ref.
o	●	Pipe Flow, $Re_{d,c} = 5 \times 10^5$	Laufer (Ref. 24)
□	■	Pipe Flow, $Re_{d,c} = 5 \times 10^4$	Laufer (Ref. 24)
△	▲	Boundary Layer, $Re_\delta = 7.4 \times 10^4$	Klebanoff (Ref. 25)
---		Eq. (38)	Present
——		Eq. (39)	Present

$\left(\dfrac{du^+}{dy^+} \right)^2$, direct dissipation of mean-flow energy

$\dfrac{-\langle uv \rangle}{U_\tau^2} \dfrac{du^+}{dy^+}$, turbulence production
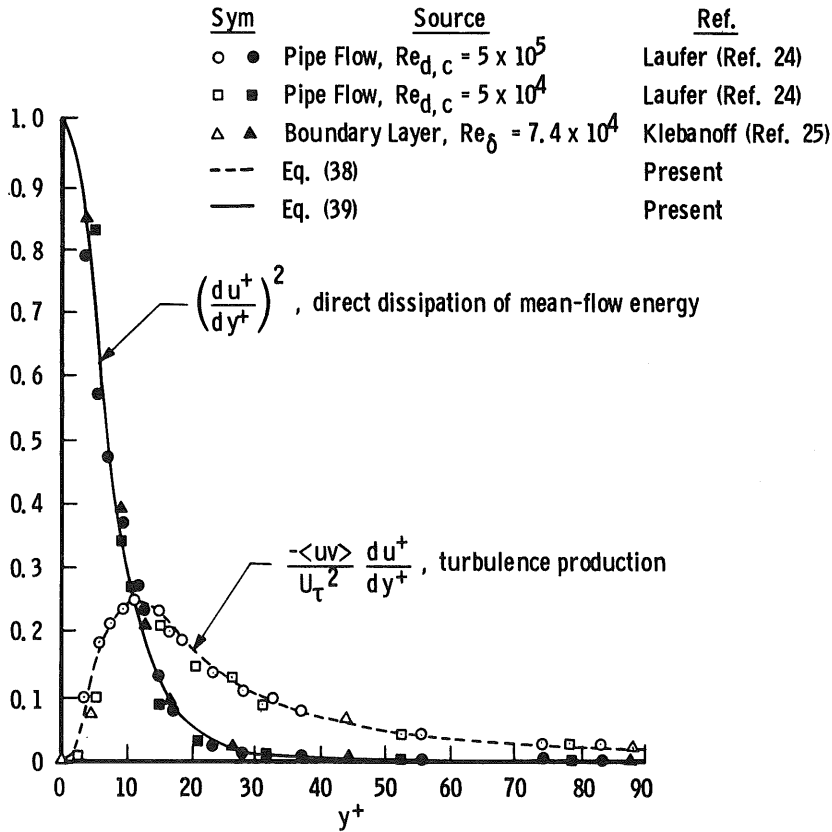
Figure 9. Distributions of turbulence production and direct dissipation
of mean-flow energy.

Schubauer (Ref. 26) points out that the maximum rate of production occurs at what is normally considered the edge of the sublayer, and that direct dissipation and turbulence production go on at the same rate at this point. According to Eq. (38), the location

of the maximum rate of production is $y^+ = 11.1$ which is approximately the edge of the sublayer. This is also the location where the direct dissipation according to Eq. (39) is equal to the production. Good agreement between Eqs. (38) and (39) and experimental measurements is demonstrated in Fig. 9.

4.0 ANALYTICAL RESULTS FOR VELOCITY-TEMPERATURE RELATIONS[*]

Relations between velocity and temperature in boundary layers were obtained in the early 1930's by Busemann (Ref. 27) and Crocco (Ref. 28). These results provide a convenient means of expressing temperature as a function of velocity, and countless applications of these early works have since been made in the study of gas dynamics. It is interesting to trace the development of the velocity-temperature relations, inasmuch as there seems to be some discrepancy among the users of these relations as to the original investigators and their specific assumptions and results.

The first relation between velocity and temperature appears to be that of Busemann (Ref. 27), who obtained the solution

$$c_p T + U^2/2 = \text{const} = c_p T_{o,\infty} \tag{40}$$

for laminar flow and $Pr = 1$. For this case, of course, one must have $T_w = T_{o,\infty}$. Shortly after this result by Busemann, Crocco (Ref. 28) presented the solution

$$c_p T + U^2/2 = aU + \text{const} \tag{41}$$

(where a is a constant) for turbulent flow and $Pr_t = 1$. It is frequently misconstrued that Crocco's (Ref. 28) result, Eq. (41), was obtained for laminar flow; however, Crocco (Ref. 28) explicitly states that his consideration is that of the equations for the turbulent boundary layer. Crocco (Ref. 28) references Busemann's (Ref. 27) work, and later Crocco (Ref. 29) states that Busemann's (Ref. 27) result was actually the particular solution portion of Eq. (41) corresponding, to what is presently called, an adiabatic wall. Later, Busemann (Ref. 30) obtained the same general result as Crocco (Ref. 28), Eq. (41), but for laminar flow and $Pr = 1$. Evaluating the constants of integration in Eq. (41) by using the wall and free-stream conditions, one obtains

$$T = T_w + (T_{o,\infty} - T_w) \bar{u} - (T_{o,\infty} - T_\infty) \bar{u}^2 \tag{42}$$

---

[*]The work in this section was done in collaboration with Dr. M. D. High, ARO, Inc.

for either laminar or turbulent flow with the appropriate Prandtl number being unity. If the wall is adiabatic, then $T_w = T_\infty + U_\infty^2/2c_p$, and Eq. (42) reduces to Eq. (40).

E. R. van Driest (Ref. 31) later investigated the problem by considering a variable Prandtl number across a turbulent boundary layer. He obtained general expressions for the temperature as a function of velocity, Reynolds analogy factor, and recovery factor. These general expressions require distributions of Prandtl number and shear stress across the boundary layer which van Driest evaluated by following von Kármán's (Ref. 32) idea of separating the boundary layer into three regions, each using different Prandtl numbers and shear stress distributions. This analysis provided quite reasonable results, illustrated the effect of Prandtl number, and showed that the local total temperature must exceed the free-stream total temperature near the edge of the boundary layer for adiabatic flat plate flow with nonunity Prandtl number.

Walz (Ref. 33) and Michel (Ref. 34) have investigated the problem along the lines of van Driest (Ref. 31). By making certain approximations to the general expressions of van Driest (Ref. 31), for example, Michel (Ref. 34) points out that if shear stress and Prandtl number were taken as constant, one obtains

$$T = T_w + (T_{aw} - T_w)\,\bar{u} - (T_{aw} - T_\infty)\,\bar{u}^2 \tag{43}$$

where the adiabatic wall temperature appears in the definition of the recovery factor

$$r = \frac{T_{aw} - T_\infty}{T_{o,\infty} - T_\infty} \tag{44}$$

It is pointed out by Schlichting (Ref. 35) and Michel (Ref. 34), for example, that Eq. (43) follows directly from Eq. (42) simply by introducing T_{aw} in place of $T_{o,\infty}$, because $T_{o,\infty}$ in Eq. (42) is actually T_{aw} for unity Prandtl number. Equation (43) is frequently referred to as the modified Crocco law, and it is the same as Eq. (15.19) in Schlichting (Ref. 35).

A parameter frequently used for presenting temperature data is $\bar{T} = (T_o - T_w)/(T_{o,\infty} - T_w)$. From Eq. (42) one obtains

$$\bar{T} = \bar{u} \tag{45}$$

Note that Eq. (45) is for unity Prandtl number because of the same restrictions on Eq. (42). For an adiabatic wall $T_w = T_{aw} = T_{o,\infty}$ and from Eq. (40) $T_o = T_{o,\infty} = T_{aw}$ and $\bar{T}$ is undefined. From Eq. (43) for an adiabatic wall, i.e., $T_{aw} = T_w$, one obtains the quadratic form

$$\overline{T} = \overline{u}^2 \qquad (46)$$

which does not require unity Prandtl number. However, Eq. (46) does not conserve energy across the boundary layer for nonunity recovery factor. This is easily seen by considering the total energy integral equation (see for example Shapiro (Ref. 36)), which for an adiabatic flat plate flow can only be satisfied if T_o takes on values in the boundary layer that are both less than and greater than $T_{o,\infty}$, i.e., there must be total-temperature "overshoot". It is clear that T_o can never be greater than $T_{o,\infty}$ according to Eq. (46) assuming $\overline{u} \leqslant 1$.

Meier (Ref. 37) recently made an interesting investigation of temperature distributions in turbulent boundary layers by considering a mixing-length hypothesis to describe a variable Prandtl number through the boundary layer. A somewhat similar analysis for the variable Prandtl number was carried out by Cebeci (Ref. 38). A variable Prandtl number approach certainly seems warranted in view of the rather extreme variations in Prandtl number which have been observed experimentally, e.g., see Refs. 39 and 40. However, Meier's (Ref. 37) approach to predicting velocity-temperature relations does not conserve momentum or energy, does not satisfy the boundary condition at the edge of the boundary layer, requires numerical solutions, and involves nine initial variables and parameters. It would appear that results obtained using, for example, Refs. 37 and 38, for a variable Prandtl number description near the wall in van Driest's (Ref. 31) general expressions for a variable Prandtl number analysis, would be more appropriate. Unfortunately, such solutions would likely need to be carried out numerically, which would limit their practical applications for such purposes as data reduction.

The objective of the present work was to obtain an analytical description of the temperature as a function of velocity throughout a turbulent boundary layer for constant but nonunity Prandtl number. The approach was to use the equation resulting from combining the boundary-layer momentum and energy equations and model the local shear stress by expressing it as a function of the local turbulent kinetic energy in the boundary layer. A second-order, nonlinear, ordinary differential equation results, for which zeroth- and first-order perturbation solutions were obtained for temperature as a function of velocity in terms of the assumed small parameter $\epsilon = 1 - Pr_m$. Crocco's (Ref. 28) result, Eq. (42), is recovered identically by the zeroth-order solution. A Reynolds analogy factor is also calculated from the present solution.

4.1 DEVELOPMENT OF THE BASIC EQUATION

The starting point of this analysis is the equation obtained by making the proposition that temperature is a function of velocity only, $T = T(U)$, and then combining the boundary-layer momentum and energy equations (see, for example, page 342 of Schlichting

(Ref. 35)). It is shown in Schlichting that the proposition is correct if (1) the pressure and wall temperature gradients are zero and the Prandtl number unity or (2) the wall is adiabatic and Prandtl number unity for nonzero pressure gradient. Because the present approach is to obtain solutions for Prandtl numbers near unity, it is assumed that the solutions are approximately correct for conditions (1) and (2) above for near unity Prandtl numbers.

The boundary-layer equations considered consisted of both the laminar and turbulent contributions to viscosity and thermal conductivity. van Driest (Ref. 31) considered these same equations, and obtained for constant mixed Prandtl number, Pr_m, the expression

$$\frac{d^2\bar{h}}{d\bar{u}^2} + (1 - Pr_m)\frac{1}{\tau}\frac{d\tau}{d\bar{u}}\frac{d\bar{h}}{d\bar{u}} + Pr_m(\gamma - 1)M_\infty^2 = 0 \tag{47}$$

Equation (47) is valid for $dp/dx = 0$, or for $Pr_m = 1$ and adiabatic wall if $dp/dx \neq 0$. The shear stress in Eq. (47) is comprised of both a laminar and turbulent portion. Again, the Reynolds stress is related to the local turbulent kinetic energy, e, in the boundary layer by Eq. (6). By fitting analytical approximations to numerical solutions and experimental data for e, for values of y larger than the y corresponding to the location in the boundary layer of maximum e (e_{max}) as predicted by the numerical solutions, the expression

$$\frac{e}{e_{max}} = \exp(-c\eta^{5/2}) \tag{48}$$

was obtained as an approximate analytical fit where $\eta = y/\delta$ and c is a constant equal to 4. An example of the quality of fit is given in Fig. 10 by comparison with the present numerical solutions and the experimental data of Klebanoff (Ref. 25). Using Eq. (48), the expression

$$\tau = U_\tau^2 \rho \exp(-c\eta^{5/2}) \tag{49}$$

was obtained for an approximation to the total (laminar and turbulent portions) shear stress distributions where $U_\tau^2 = \tau_w/\rho_w$.

Using Eq. (49) for the shear stress, and considering the terms containing τ in Eq. (47), one obtains

$$\frac{1}{\tau}\frac{d\tau}{d\bar{u}} = \frac{d}{d\bar{u}}(-c\eta^{5/2}) + \frac{1}{\rho}\frac{d\rho}{d\bar{u}} = \frac{d}{d\bar{u}}(-c\eta^{5/2}) - \frac{1}{\bar{h}}\frac{d\bar{h}}{d\bar{u}} \tag{50}$$

In order to eliminate η from Eq. (50), it was assumed that $\bar{u} = \eta^{1/m}$ for this term. This assumption is justified only by the final results (a value of m = 7 was used for the present results). Equation (50) can then be used in Eq. (47) to obtain

$$\frac{d^2\bar{h}}{d\bar{u}^2} - (1 - Pr_m)\left(\frac{5}{2} \, cm \, \bar{u}^{\frac{5}{2}m-1} + \frac{1}{\bar{h}} \frac{d\bar{h}}{d\bar{u}}\right)\frac{d\bar{h}}{d\bar{u}} + Pr_m(\gamma - 1)M_\infty^2 = 0 \qquad (51)$$
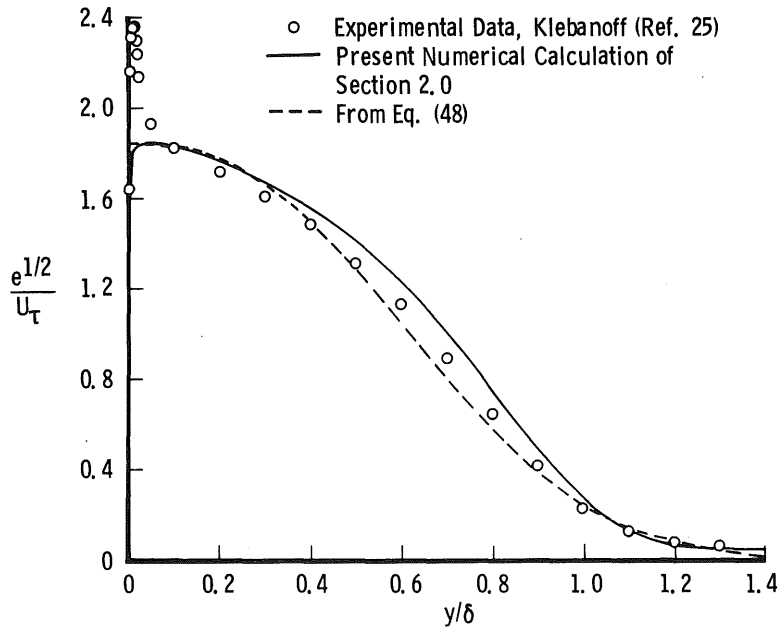
Figure 10. Theoretical and experimental turbulent kinetic energy distributions.

Introducing $\epsilon = 1 - Pr_m$ and the terms as defined in the nomenclature, Eq. (51) can be written

$$\bar{h} \frac{d^2\bar{h}}{d\bar{u}^2} - \epsilon\left(\beta \, \bar{u}^{\,a-1} \, \bar{h} + \frac{d\bar{h}}{d\bar{u}}\right)\frac{d\bar{h}}{d\bar{u}} + (1 - \epsilon)A\bar{h} = 0 \qquad (52)$$

which is the basic equation.

4.2 CONSTANT WALL TEMPERATURE SOLUTION

Equation (52) is a second-order, nonlinear, ordinary differential equation for $\bar{h}(\bar{u})$. This equation was not solved in closed form. Zeroth- and first-order perturbation solutions

were obtained in terms of the small parameter ϵ. The boundary conditions for the constant wall temperature problem are

$$\bar{h}(o) = \bar{h}_w \text{ and } \bar{h}(1) = 1 \tag{53}$$

Assuming a solution of the form

$$\bar{h}(\bar{u}) = \bar{h}_o(\bar{u}) + \epsilon\,\bar{h}_1(\bar{u}) + \cdots \tag{54}$$

one obtains to zeroth order

$$\frac{d^2\bar{h}_o}{d\bar{u}^2} = -A \tag{55}$$

and to first order

$$\frac{d^2\bar{h}_1}{d\bar{u}^2} = \beta\bar{u}^{a-1}\,\frac{d\bar{h}_o}{d\bar{u}} + \frac{1}{\bar{h}_o}\left(\frac{d\bar{h}_o}{d\bar{u}}\right)^2 + A \tag{56}$$

The boundary conditions given by Eq. (53) become

$$\bar{h}_o(o) = \bar{h}_w,\ \bar{h}_o(1) = 1 \text{ and } \bar{h}_1(o) = 0,\ \bar{h}_1(1) = 0 \tag{57}$$

The solution to Eq. (55) for the zeroth-order boundary conditions in Eq. (57) is

$$\bar{h}_o(\bar{u}) = \bar{h}_w + (\bar{H}_{o,\infty} - \bar{h}_w)\bar{u} - \frac{A}{2}\,\bar{u}^2 \tag{58}$$

Equation (58) was used in Eq. (56) to solve for $\bar{h}_1(\bar{u})$. The integration was tedious but straightforward. The first-order boundary conditions in Eq. (57) were satisfied by the two integration constants from Eq. (56), and the solution $\bar{h}_1(\bar{u})$ was included in Eq. (54) along with Eq. (58) to obtain, up to first order, the solution

$$\bar{h}(\bar{u}) = \bar{h}_w + (\bar{H}_{o,\infty} - \bar{h}_w)\bar{u} - \frac{A}{2}\,\bar{u}^2 + \epsilon\left[\frac{\beta\,A\bar{u}}{(a+1)(a+2)}\left(1 - \bar{u}^{a+1}\right)\right.$$

$$\left. - \frac{\beta(\bar{H}_{o,\infty} - \bar{h}_w)\bar{u}}{a(a+1)}(1 - \bar{u}^a) + \frac{A}{2}\,\bar{u}(1 - \bar{u}) + (1 - \bar{u})f(o) + \bar{u}f(1) - f(\bar{u})\right] \tag{59}$$

where

$$f(\bar{u}) = \frac{\Delta}{A}[(\zeta - \Delta)\ln|\zeta - \Delta| - (\zeta + \Delta)\ln|\zeta + \Delta|] \tag{60}$$

$$\zeta = \bar{H}_{o,\infty} - \bar{h}_w - A\bar{u} \tag{61}$$

and

$$\Delta = [2A\,\overline{h}_w + (H_{o,\infty} - \overline{h}_w)^2]^{\frac{1}{2}} \tag{62}$$

4.3 ADIABATIC WALL SOLUTION

The boundary conditions for the adiabatic wall problem are

$$\left.\frac{d\overline{h}}{d\overline{u}}\right|_{\overline{u}=0} = 0 \text{ and } \overline{h}(1) = 1 \tag{63}$$

Assuming again the form of the solution given by Eq. (54), the same zeroth- and first-order equations, Eqs. (55) and (56), were obtained. The appropriate boundary conditions become

$$\left.\frac{d\overline{h}_o}{d\overline{u}}\right|_{\overline{u}=0} = 0, \overline{h}_o(1) = 1 \text{ and } \left.\frac{d\overline{h}_1}{d\overline{u}}\right|_{\overline{u}=0} = 0, \overline{h}_1(1) = 0 \tag{64}$$

The solution to Eq. (55) for the zeroth-order boundary conditions in Eq. (64) is

$$\overline{h}_o(\overline{u}) = 1 + \frac{A}{2}(1 - \overline{u}^2) \tag{65}$$

As before, $\overline{h}_1(\overline{u})$ was obtained by using the solution for $\overline{h}_o(\overline{u})$, Eq. (65), in Eq. (56) and satisfying the first-order boundary conditions in Eq. (64). The complete solution, up to first order, is

$$\overline{h}(\overline{u}) = 1 + \frac{A}{2}(1 - \overline{u}^2) + \epsilon\left[\frac{\beta A}{(\alpha+1)(\alpha+2)}(1 - \overline{u}^{\alpha+2}) + \frac{A}{2}(1 - \overline{u}^2) + f(1) - f(\overline{u})\right] \tag{66}$$

where

$$f(\overline{u}) = \frac{\Delta}{A}[(\zeta - \Delta)\ln|\zeta - \Delta| - (\zeta + \Delta)\ln|\zeta + \Delta|] \tag{67}$$

$$\zeta = -A\overline{u} \tag{68}$$

and

$$\Delta = (2A\overline{H}_{o,\infty})^{\frac{1}{2}} \tag{69}$$

4.4 REYNOLDS ANALOGY

The derivation of the Reynolds analogy factor s is straightforward, and for the boundary-layer equations considered is given by (Ref. 31)

$$s \equiv \frac{c_f}{2c_h} = \frac{Pr_m \, (\overline{h}_{aw} - \overline{h}_w)}{\dfrac{d\overline{h}}{d\overline{u}}\bigg|_{\overline{u}=0}} \tag{70}$$

Values of s were obtained by using Eq. (59) for $\overline{h}(\overline{u})$ in Eq. (70). The term $d\overline{h}/d\overline{u}\big|_{\overline{u}=0}$ was found not to approach zero at the same rate as $(\overline{h}_{aw} - \overline{h}_w)$ for near-adiabatic wall conditions for all Mach numbers, and a singularity occurred at $\overline{h}_w = \overline{h}_{aw}$. However, quite reasonable values of s for $\overline{h}_w$, both greater than and less than $\overline{h}_{aw}$, were obtained and will be compared with experimental data.

4.5 COMPARISONS WITH EXPERIMENTAL DATA

To apply the analytical velocity-temperature results, it is necessary to know the Prandtl number. Specific values of the turbulent Prandtl number have been suggested by van Driest (Ref. 31) as $Pr_t = 0.86$, Bradshaw (Ref. 41) as $Pr_t = 0.91$, and Elser (Ref. 42) as $Pr_t = 0.921$. However, as mentioned, experiments (Refs. 39 and 40) indicated that Pr_t varies from above one near the wall to about 0.5 or 0.7 at large distances from the wall. These data have a relatively significant amount of scatter as might be expected due to the experimental difficulties. Because the variation in experimental recovery factors is less than in experimental Prandtl numbers, it was decided to determine Pr_m by assuming a constant r and calculating Pr_m using the adiabatic wall solution. It was assumed that the Pr_m determined by this procedure was also applicable to nonadiabatic wall conditions. This calculation was carried out by using Eq. (66) with $\overline{u} = 0$ and Eq. (44) to provide two equations for the two unknowns Pr_m and $\overline{h}_{aw}$ (or T_{aw}). The values of Pr_m determined in this way are presented in Fig. 11 for $r = 0.87$, 0.88, 0.89, and 0.90. Available values of experimental recovery factors seem to indicate a value of $r = 0.88$ as being representative, and this value was used for the present results. For $r = 0.88$, $0.800 < Pr_m < 0.914$ for all Mach numbers. For $M_\infty > 2.5$, the Pr_m from Fig. 11 for $r = 0.88$ is essentially bounded by the suggested turbulent Prandtl number values of van Driest (Ref. 31) and Bradshaw (Ref. 41).

Some of the velocity-temperature results are presented in $\overline{u}$ - $\overline{T}$ coordinates. It should be pointed out that $\overline{T}$ is a sensitive parameter. For example, for an adiabatic surface in moderate supersonic flow $\overline{T} = (T_0/T_{0,\infty} - T_{aw}/T_{0,\infty})/(1 - T_{aw}/T_{0,\infty})$, and $(1 - T_{aw}/T_{0,\infty})$ is of the order 1/10. Therefore, if a $T_0/T_{0,\infty}$ overshoot of one percent occurs, the result is a ten percent, or order of magnitude more overshoot in $\overline{T}$. The adiabatic wall solution, Eq. (66), is presented in Fig. 12 for $\gamma = 7/5$ and various M_∞ (actually, rather than γ and M_∞, $A = (\gamma-1)M_\infty^2$ is the appropriate parameter). The overshoot in $\overline{T}$ decreases as M_∞ increases, a result to be checked subsequently by comparison with experimental data.
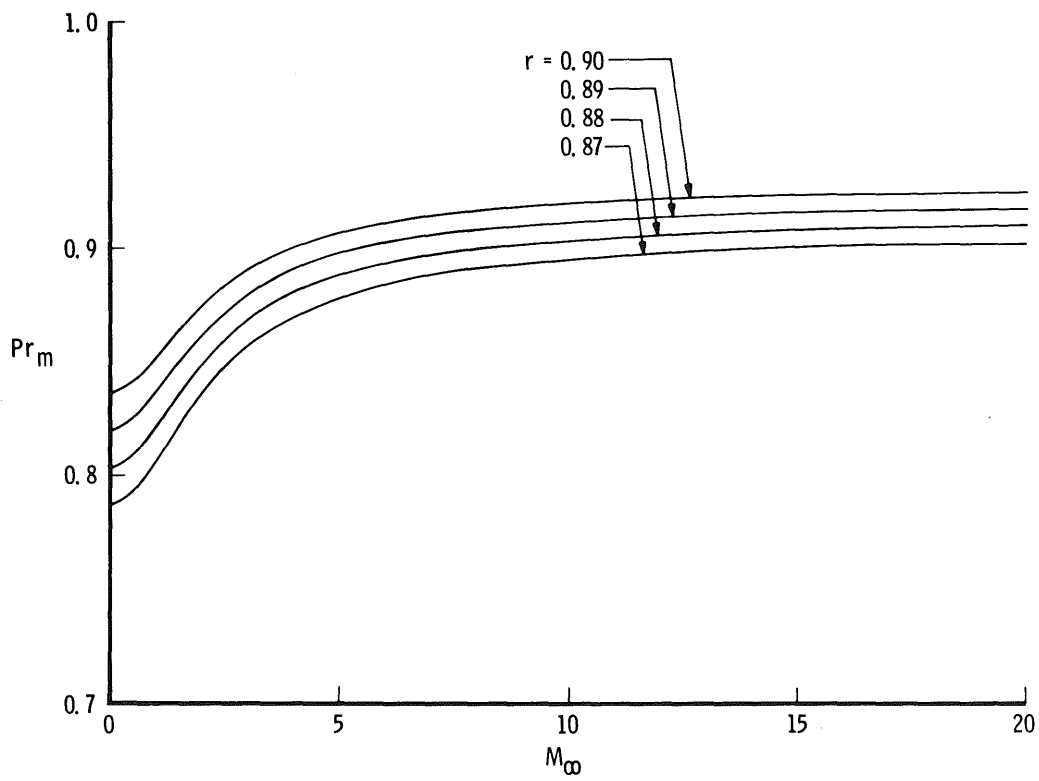
Figure 11. Mixed Prandtl number as a function of M_∞ for $\gamma = 7/5$.
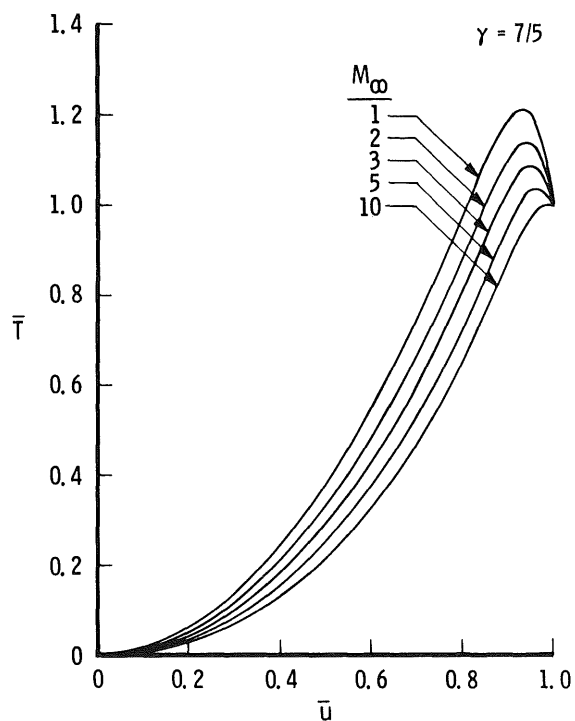
Figure 12. Velocity-temperature relations for an adiabatic wall according to Eq. (66).

Because the present result is an approximate analytical solution with constant Prandtl number, it was of interest to compare these analytical results with numerical solutions to the full boundary-layer equations including laminar and turbulent terms with variable Prandtl number. This seemed particularly warranted in view of the recent results of Meier (Ref. 37). A comparison is presented in Fig. 13 between Eq. (66) and numerical results provided by Adams (Refs. 43 and 44) for $\gamma = 7/5$, $M_\infty = 4$, and adiabatic wall, using
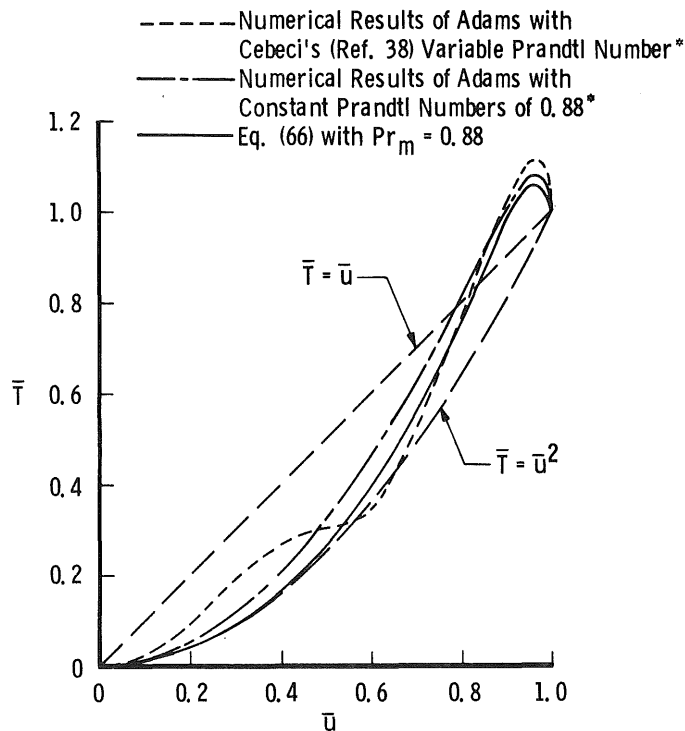
Figure 13. Velocity-temperature relations for constant and variable Prandtl number, adiabatic wall, $M_\infty = 4$, and $\gamma = 7/5$.

constant laminar and turbulent Prandtl numbers of 0.88 and also the variable turbulent Prandtl number description of Cebeci (Ref. 38) with $Pr = 0.71$. (Adams' calculation scheme was used because of its variable Prandtl number capability. The numerical scheme discussed in Section 2.0 was run for constant Prandtl numbers of 0.88 for comparison with Adams' results, and the results were essentially identical.) According to Adams*, the inflections in the numerical results for the variable Prandtl number for $\bar{u} > 0.6$ were sensitive to the modeling of the variable Prandtl number. Because of the rather significant size of the uncertainty envelope near the wall of the experimental data used to qualify the variable Prandtl number analysis of Cebeci (Ref. 38) (attributable to experimental difficulties extremely close to the wall), and because almost the entire boundary layer

---

*Unpublished data furnished by J. C. Adams, Jr., VKF, AEDC.

corresponds to $\bar{u} > 0.6$ for a turbulent boundary layer, the agreement in Fig. 13 between the more exact numerical results and the approximate analytical result, Eq. (66), is considered good. Included in Fig. 13 are the linear and quadratic results given by Eqs. (45) and (46). In addition, an analog computer solution was obtained for Eq. (52) for these conditions, and the results cannot be discerned from the result given by Eq. (66) in Fig. 13.[*]

Experimental adiabatic (or nearly so) wall data of Gates (Ref. 13) for $M_\infty \approx 4$ and Voisinet (Ref. 37) and Voisinet[**] for $M_\infty \approx 3$ are compared with Eq. (66) for $M_\infty = 3.5$ in Fig. 14. It should be pointed out that Gates' temperature data were interpolated for $\bar{u}$ less than about 0.65, but were measured for $\bar{u} > 0.65$. This limitation was due to probe size. Voisinet's data were taken with a fine-wire temperature probe (Ref. 45) and do not have this restriction. The wiggle or inflection point in these data near $\bar{u}$ of 0.6 is similar to the predictions of Meier (Ref. 37) and Adams using a variable Prandtl number through the boundary layer. According to Voisinet[**], this trend was repeatable in the experiments; however, the absolute value of the data in terms of $\bar{T}$ might not

Sym	M_∞	Ref.	Model
o	4.11	37	Flat Plate
□	3.96	37	Boundary-Layer Channel
△	2.94	Voisinet**	Boundary-Layer Channel
◇	2.90	Voisinet**	Boundary-Layer Channel
——	3.50	Eq. (66)	

Figure 14. Theoretical and experimental velocity-temperature relations for M_∞ of approximately 3 to 4 and adiabatic walls.

---
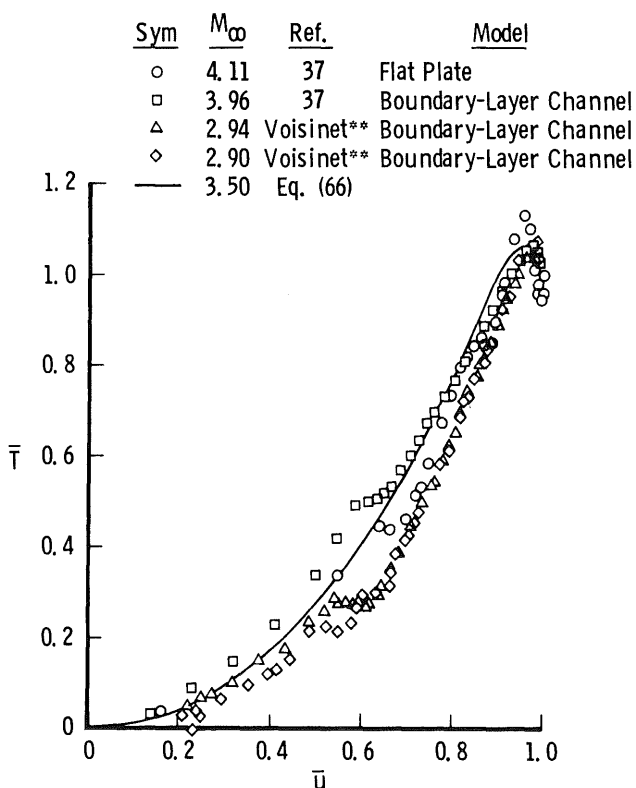
[*]This analog computer solution was provided by J. A. McClure, ARO, Inc.

[**]Unpublished data furnished by R. L. P. Voisenet, Naval Ordnance Laboratory, June 1974.

be precisely repeatable. For example, a one-Kelvin-degree change in the measured local total temperature near $\bar{u}$ = 0.6 would produce a 15-percent change in $\bar{T}$ for the conditions of these data. Such sensitivity should be kept in mind when considering data in $\bar{u}$ - $\bar{T}$ coordinates.

Experimental data similar to those in Fig. 14, except for M_∞ being approximately 5 and 6, are compared to Eq. (66) for M_∞ = 5.5 in Fig. 15. The quality of agreement between experiment and theory is about the same as obtained in Fig. 14, which is considered reasonable.

Sym	M_∞	Ref.	Model
o	4.93	46	Wind-Tunnel Nozzle
△	6.02	47	Hollow Cylinder
□	4.85	13	Boundary-Layer Channel
◇	4.96	13	Boundary-Layer Channel
—	5.50	Eq. (66)	
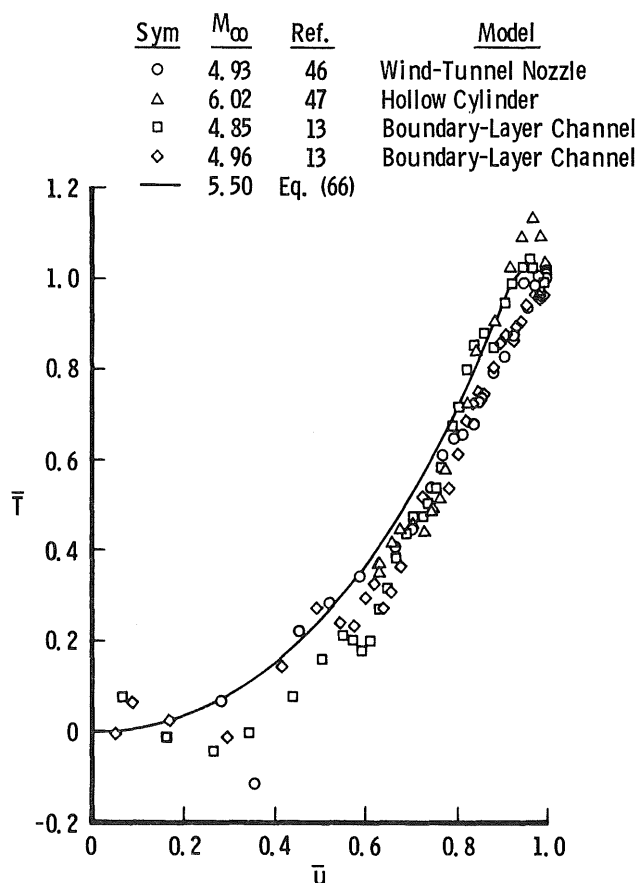
Figure 15. Theoretical and experimental velocity-temperature relations for M_∞ of approximately 5 to 6 and adiabatic walls.

Mention should be made of the data of Sturek and Danberg (Refs. 48 and 49) which were used by Meier (Ref. 37) for the selection of constants which appeared in his work. Sturek (Ref. 49) states that these measurements were made in essentially adiabatic flow after 25 to 30 minutes of run time, and no heat-transfer effects were expected to appear in the data. These data, however, were shown by Sturek (Ref. 50) to exhibit an extreme "dip" in $\bar{T}$ for $\bar{u}$ ≈ 0.6. Except for the downstream adverse pressure gradient these

measurements correspond to conditions similar to those of Voisinet, although Voisinet's measurements were made with a fine-wire probe (Ref. 45) and Sturek's (Ref 49) measurements were made with a wedge-type probe. Sturek and Danberg (Ref. 48) present temperature data to within 0.0028 in. of the wall. However, the wedge-type probe used was stated (Ref. 49) to be 0.010 to 0.015 in. thick at the tip where the measurement was made. Therefore, some of the data near the wall were interpolated or extrapolated. Moreover, the location of the dip in $\overline{T}$ corresponds to the approximate location of wall influence on probe measurements for this size probe as determined by Allen (Refs. 51 and 52). Because Sturek's data correspond to approximately the same flow conditions as Voisinet's, e.g. a Mach number of 3.5 for Sturek's data as compared to 2.9 for Voisinet's data, only the latter are considered here.

Diabatic, zero-pressure gradient data of Danberg (Ref. 53), Hopkins and Keener (Ref. 54), and measurements made by Adcock and Peterson and reported by Bertram and Neal (Ref. 55), are compared with Eq. (59) in Fig. 16. The cold-wall results, both calculated and measured, tend to be more linear in $\overline{u}$ - $\overline{T}$ coordinates and have less or no $\overline{T}$ overshoot. The calculated curves in Fig. 16, for the two conditions indicated, essentially bound the curves which would correspond to the conditions of the other data in Fig. 16.

Sym	M_∞	$T_w/T_{0,\infty}$	Ref.	Model
o	6.37	0.515	53	Flat Plate
□	6.34	0.782	53	Flat Plate
◇	6.50	0.268	54	Flat Plate
▷	6.50	0.446	54	Flat Plate
△	6.00	0.38	55	Hollow Cylinder
○	6.00	0.49	55	Hollow Cylinder
———	6.50	0.268	Eq. (59)	
--------	6.34	0.782	Eq. (59)	

Figure 16. Theoretical and experimental velocity-temperature relations for M_∞ of 6.0 to 6.5, nonadiabatic walls, and zero pressure gradient.
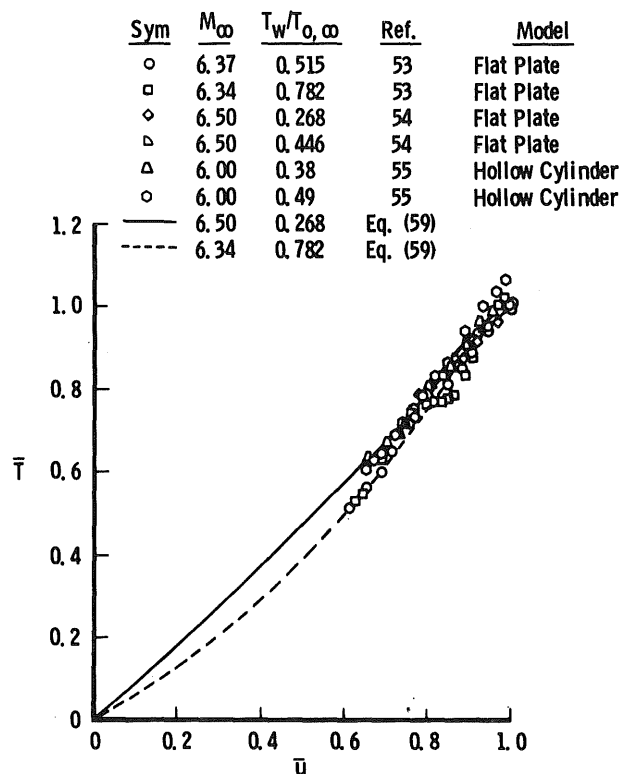
As alluded to, increasing $\bar{T}$ overshoot for the same $\bar{u}$ is predicted by the present results for decreasing M_∞ and adiabatic wall. This result is qualitatively supported by the data of Winter and Gaudet (Ref. 12) as shown in Fig. 17.
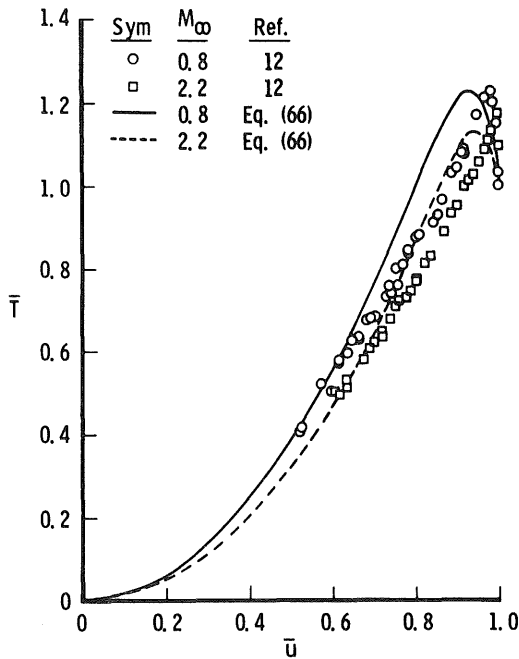
Figure 17. Theoretical and experimental velocity-temperature relations for M_∞ of 0.8 and 2.2 and adiabatic walls.

An interesting comparison between predicted and measured temperature distributions as a function of Mach number is presented in Fig. 18. These data were used by Winter and Gaudet (Ref. 12) to obtain a reliable relation between local temperature and Mach number for $2.2 \leqslant M_\infty \leqslant 6.0$. The present analytical result for $M_\infty = 2.2$ is shown in Fig. 18. There is an effect of M_∞ on the present result, causing it to move toward the modified Crocco result (the linear curve) as M_∞ increases. However, this effect is slight over the M_∞ range of the data in Fig. 18, and the $M_\infty = 2.2$ result provides a lower bound and yet is in relatively good agreement with the experimental data.

Some results on Reynolds analogy according to Eq. (70) are given in Fig. 19. The singularity which occurs in Eq. (70) at $T_w/T_{aw} = 1$ appears to influence the solution only in a region near $T_w/T_{aw} = 1$. This observation is based on the fact that if the region near $T_w/T_{aw} = 1$ is excluded, then a smooth curve can be faired through this region which asymptotically joins the results for $T_w/T_{aw} < 1$ and $T_w/T_{aw} > 1$. However, the results for small values of T_w/T_{aw} are of primary interest here, because this particular distribution does not appear to have been previously predicted.
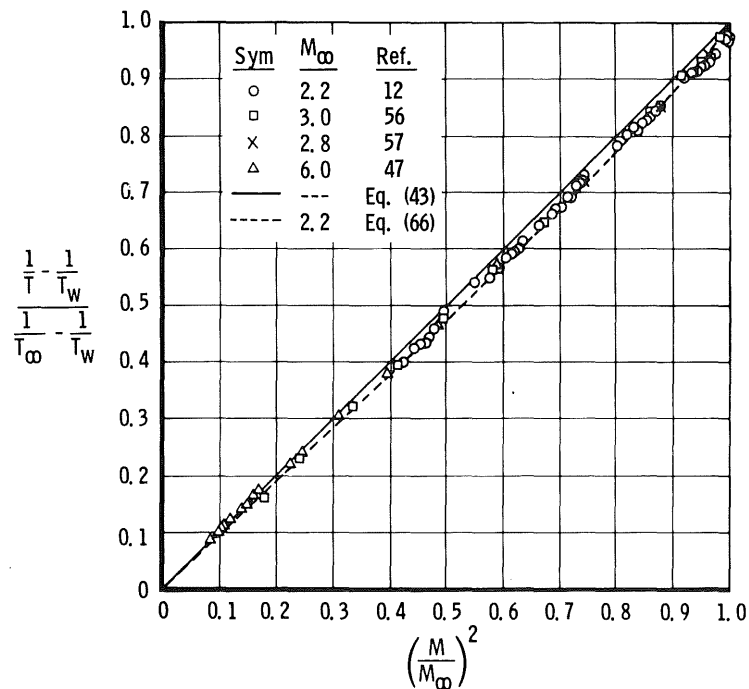
Figure 18. Theoretical and experimental Mach number-
temperature relations for adiabatic walls.

Figure 19. Reynolds analogy as a function
of wall temperature according
to Eq. (70).
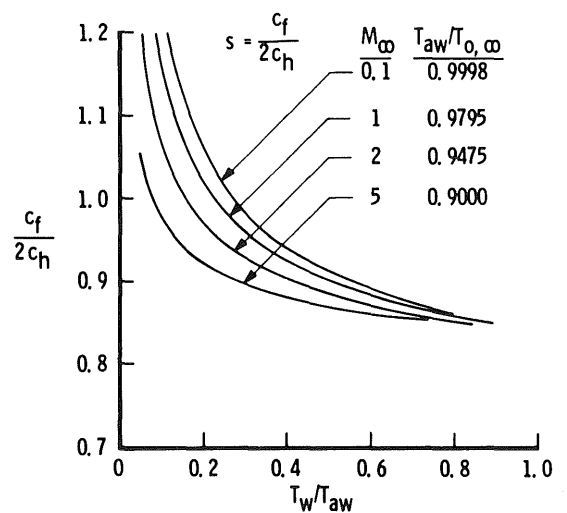
A comparison of Eq. (70) with experimental data is presented in Fig. 20. The solid curve in Fig. 20 is Eq. (70), and the dashed extension is the limiting result of Eq. (70) for large T_w/T_{aw}. With the exceptions of Eq. (70) and the data of Wilson (Ref. 69), Fig. 20 was taken from the report of Cary (Ref. 70). Note that Cary plots $2c_h/c_f$ rather

than the inverse as plotted in Fig. 19. Of particular interest here is the behavior of $2c_h/c_f$ for small values of $h_w/H_{o,\infty}$. Cary states that there is an indication from the experimental data that decreasing the ratio of $h_w/H_{o,\infty}$ decreases $2c_h/c_f$, an observation predicted by

Sym	M_∞	Ref.
□	4.0	55
◇	2.5	58
○	6.8	59
◔	7.4	60
◓	6.8	60
◇	8.8	61, 62, and 63
◇	7.4	
△	4.6	
▽	7.6	
▽	8.1	

Sym	M_∞	Ref.
▽	7.0	61, 62, and 63
▽	6.4	
◇	5.4	
▽	5.8	
◁	7.1	
◁	11.3	
◇	11.7	
◇	7.2	
◁	4.9	64
▨	1.5 to 4.0	65
■	0 to 0.3	65
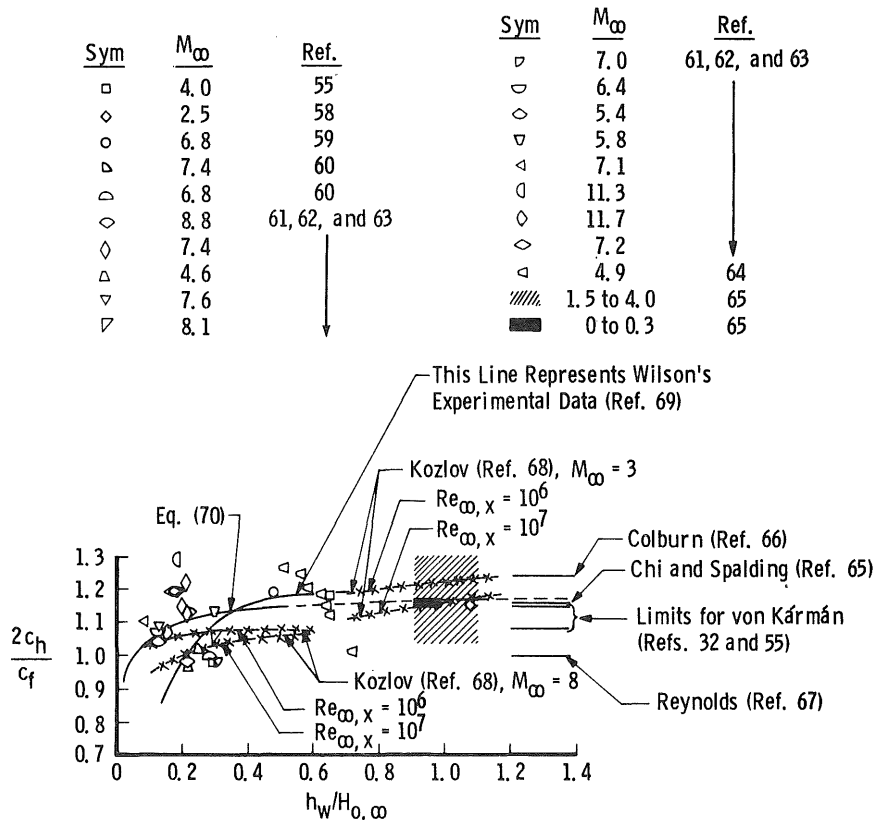
Figure 20. Theoretical and experimental Reynolds analogy data.

the present result. This observation is further substantiated by the results of Kozlov (Ref. 68) and Wilson (Ref. 69), both of which are presented in Fig. 20. Kozlov's (Ref. 68) results are empirical expressions for the local skin-friction coefficient and Stanton number which were derived independently from fits with experimental data. Wilson (Ref. 69) states that the theoretical prediction of decreasing $2c_h/c_f$ with decreasing $h_w/H_{o,\infty}$ has not been reported. For larger values of $h_w/H_{o,\infty}$, the present result is seen in Fig. 20 to be about a compromise of the results of previous investigators.

5.0 DATA REDUCTION OF PITOT PRESSURE MEASUREMENTS

The results of the previous two sections, and the work of Allen and Tudor (Ref. 71) in determining skin friction from pitot pressure measurements, are incorporated in this section in a data reduction computer program. Input includes spatial measurements

of pitot pressure taken normal to a wall, and output includes Mach number distribution, velocity distribution, temperature distribution, various boundary-layer parameters, and skin friction.

The calculation of Mach number distribution is, of course, not new and is included only to be complete. Further usefulness of pitot pressure data follows if the temperature distribution is measured or some relation between velocity and temperature is used. It is assumed here that only pitot pressure data are available, and a relation between velocity and temperature is required. Commonly used relations are either the Crocco (Eq. (42)) or modified Crocco (Eq. (43)) result. Crocco's relation is essentially the assumption of a constant total temperature across the boundary layer with the requirement that the wall temperature be equal to the free-stream total temperature. The modified Crocco result does not require a constant total temperature; however, it does not properly predict the total-temperature distribution for an adiabatic wall (as discussed in Section 4.). The velocity-temperature relations used here are those obtained in the previous section. Using a velocity-temperature relation, it is possible to calculate velocity and temperature distributions, boundary-layer parameters, and skin friction. A listing of the computer program is given in Appendix B.

5.1 MACH NUMBER, VELOCITY, AND TEMPERATURE DISTRIBUTIONS

The data reduction program was written such that if the free-stream flow is subsonic, then the static pressure (which is usually measured to determine M_∞) is input for the $y = 0$ point (at the wall) and M_∞ is calculated from the perfect gas, isentropic relation (Ref. 72)

$$\frac{P_\infty}{P_{0,\infty}} = \frac{1}{\left(1 + \frac{\gamma - 1}{2} M_\infty^2\right)^{\frac{\gamma}{\gamma-1}}} \tag{71}$$

If the free-stream is supersonic, then M_∞ is obtained by solving the adiabatic, perfect gas equation (Ref. 72)

$$\frac{P'_{0,\infty}}{P_{0,\infty}} = \left[\frac{(\gamma + 1)M_\infty^2}{(\gamma - 1)M_\infty^2 + 2}\right]^{\frac{\gamma}{\gamma-1}} \left[\frac{\gamma + 1}{2\gamma M_\infty^2 - (\gamma - 1)}\right]^{\frac{1}{\gamma-1}} \tag{72}$$

for M_∞ by the Newton-Raphson method (Ref. 73).

The Mach number distribution across the boundary layer is obtained by solving the Rayleigh pitot equation (Ref. 72)

41

$$\frac{P_o'}{P_\infty} = \left[\frac{(\gamma + 1)M^2}{2}\right]^{\frac{\gamma}{\gamma-1}} \left[\frac{\gamma + 1}{2\gamma M^2 - (\gamma - 1)}\right]^{\frac{1}{\gamma-1}} \tag{73}$$

for M for

$$\frac{P_o'}{P_\infty} > ((\gamma + 1)/2)^{\gamma/(\gamma-1)}$$

and

$$\frac{P_\infty}{P_o'} = \frac{1}{\left(1 + \frac{\gamma - 1}{2} M^2\right)^{\frac{\gamma}{\gamma-1}}} \tag{74}$$

for M for $p_o'/p_\infty \leq ((\gamma + 1)/2)^{\gamma/(\gamma-1)}$. The static pressure is assumed constant across the boundary layer, and is input for $M_\infty \leq 1$ and calculated from Eq. (71) for $M_\infty > 1$. Equation (73) is solved for M by the Newton-Raphson method (Ref. 73).

The Mach number distribution provides one equation for velocity and temperature at each measured point (spatial position) in the boundary layer according to the expression

$$\frac{M}{M_\infty} = \frac{U}{U_\infty} \left(\frac{T_\infty}{T}\right)^{\frac{1}{2}} \tag{75}$$

which, of course, is a consequence of the definition of Mach number. The left-hand side of Eq. (75) is known from the Mach number distribution, and therefore, U/U_∞ and T/T_∞ can be determined if another independent equation is available to provide two equations for the two unknowns, U/U_∞ and T/T_∞. The expression used for this equation is that given by Eq. (59) or (66). Equation (75) and Eq. (59) or (66), whichever is appropriate, are solved simultaneously for the velocity and temperature.

Having calculated spatial distributions of velocity and temperature, and using ρ/ρ_∞ = T_∞/T because of the assumption that the static pressure in the transverse direction is constant, various boundary-layer parameters such as displacement and momentum thickness can be calculated by numerical integration. Because of experimental difficulties associated with making measurements extremely close to a wall, Eq. (35) of Section 3.0 is used to describe the velocity distribution (from which temperature is determined using the results of Section 4.0) for $y^+ < 140$.

5.2 SKIN FRICTION

The skin friction is determined by the technique discussed by Allen and Tudor (Ref. 71). Allen and Tudor present plots of U/U_∞ versus $(\mu_\infty/\mu_w)\,Re_{\infty,y}$ with several curves, each for constant c_f. Each plot is for different M_∞. These plots are based on the compressible law-of-the-wall as presented by Fenter and Stalmach (Ref. 74). This equation is given by

$$\frac{\sin^{-1}\left(\sigma^{\frac{1}{2}}\,\frac{U}{U_\infty}\right)}{\left(\sigma\,\frac{c_f}{2}\,\frac{T_w}{T_\infty}\right)^{\frac{1}{2}}} = 5.75\,\log_{10}\left[Re_{\infty,y}\,\frac{\mu_\infty}{\mu_w}\left(\frac{c_f}{2}\,\frac{T_\infty}{T_w}\right)^{\frac{1}{2}}\right] + 5.1 \tag{76}$$

The technique of Allen and Tudor (Ref. 71), which is an idea first proposed and used by Clauser (Ref. 75) for incompressible flow, is to plot U/U_∞ versus $(\mu_\infty/\mu_w)\,Re_{\infty,y}$ on transparent paper and overlay it on the plot in their report for the appropriate M_∞, and determine c_f by the curve in best agreement with the experimental data. Agreement cannot be expected all the way across the boundary layer, i.e. for all values of $(\mu_\infty/\mu_w)\,Re_{\infty,y}$. This is because the law-of-the-wall expression is only valid in a particular region near the wall. The reader is referred to Ref. 76 for an example of the agreement sufficient to determine c_f by this method. The trend is for the experimental data to follow a curve which is parallel to a constant c_f curve. The value of c_f which corresponds to the curve fit that passes through the experimental data in this portion of the curve is the appropriate value of c_f for the experimental data. That is, there are data points in a profile set which have the same values of c_f. This technique has the important practical advantage of not requiring data from the sublayer.

In lieu of plotting the data, skin friction is determined in the present data reduction program by solving Eq. (76) for c_f by the Newton-Raphson method (Ref. 73) at each point across the boundary layer. Assuming the viscosity is proportional to temperature to some power, everything in Eq. (76) is known except c_f. The power law $\mu \sim T^{0.768}$ was used in the present data reduction because it was that used by Allen (Ref. 76). For the experimental data considered thus far, the constant values of c_f for each set of data (i.e. the data for each profile set) have also been equal to the minimum c_f in a profile set. Equal here means within the scatter of the data. This facilitates the selection of the appropriate c_f in the computed set of c_f's.

It was pointed out by Allen and Tudor (Ref. 71) that the law-of-the-wall given in Ref. 74 has only been verified for an adiabatic or near-adiabatic wall. Also, Allen and Tudor further state that the surface should be smooth in the aerodynamic sense, and caution should be employed in using the technique in flows with large pressure gradients.

Verification of this technique was investigated by considering the experimental data of Winter and Gaudet (Ref. 12). Winter and Gaudet measured skin friction using a balance. They also made boundary-layer pitot surveys which were used to determine U/U_∞ which in turn were used to determine c_f by the present data reduction program for comparison with c_f as determined by the balance measurements. These results are presented in Fig. 21 and good agreement is obtained between these two methods of determining c_f.
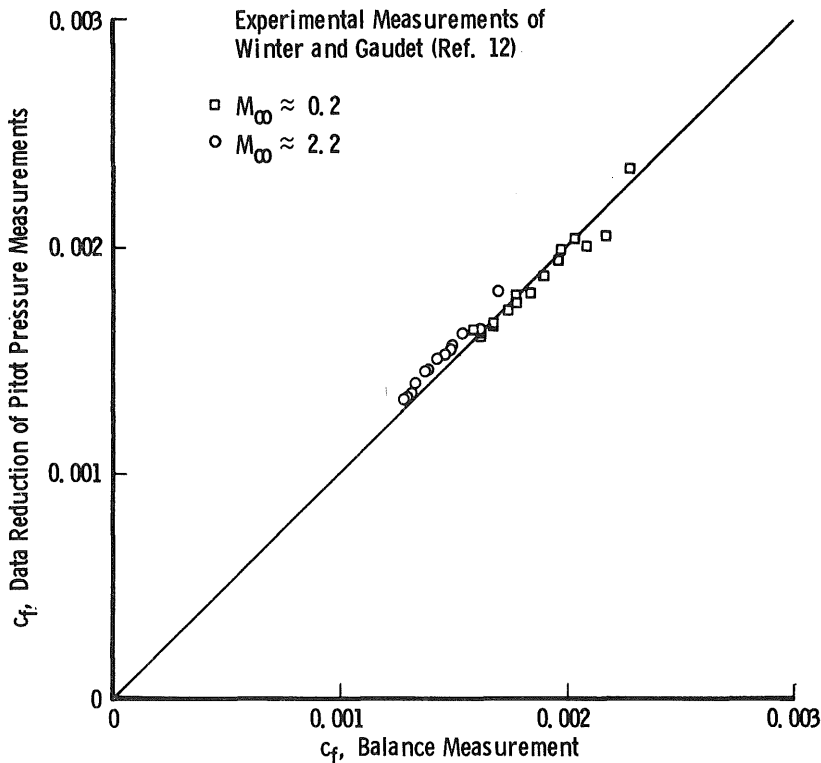
Figure 21. Skin-friction coefficients as determined by balance measurements and data reduction of boundary-layer pitot pressure measurements.

6.0 TURBULENT BOUNDARY-LAYER MEASUREMENTS FROM TUNNELS 16S, 16T, AND ART

6.1 MACH NUMBER, VELOCITY, AND TEMPERATURE DISTRIBUTIONS

Boundary-layer measurements have been made on the walls, ceiling, and floor of the 16-ft Supersonic Wind Tunnel (16S) in PWT by Baker and Pate (Ref. 77) and Maxwell and Hartley (Ref. 78). These measurements were made using a pitot pressure rake where the spacing between probe centers was 0.5 in. near the wall and 1.0 in. away from the wall. Recently, measurements have been made of the floor boundary layer in 16S using a traversing probe mechanism to make pitot pressure and total-temperature measurements

simultaneously. Results from the pitot pressure measurements are presented in Figs. 22 through 24. These results are for Station -2.9 which is 61.6 ft (axial distance) downstream of the geometric nozzle throat. The numerical solutions were started at the nozzle throat and the pressure gradient corresponding to that appropriate for the flexible sidewalls rather than the straight floor or ceiling wall was used because it was known from the nozzle design criteria. The initial conditions used to begin the numerical computations at the throat were estimated by obtaining solutions (beginning about 75 ft upstream of the throat) through the converging portion of the nozzle using the pressure distribution from assuming one-dimensional flow through the geometric area distribution. The numerical results for Station -2.9 were relatively insensitive to the initial conditions, so long as the initial boundary-layer displacement thickness did not exceed that predicted by the numerical solutions up to throat.

Sym	M_∞	Re_∞/ft	Probe Size, in.	Source
o	1.60	0.738×10^6	0.035	16S Data
□	1.60	0.738×10^6	0.032	16S Data
◊	1.60	1.105×10^6	0.035	16S Data
▷	1.60	1.361×10^6	0.035	16S Data
△	1.60	1.602×10^6	0.035	16S Data
o	1.60	1.614×10^6	0.035	16S Data
△	1.60	1.602×10^6	0.032	16S Data
---	1.60	0.700×10^6	---	Present Calculation
——	1.60	1.600×10^6	---	Present Calculation

All Results for Sta -2.9 on the Floor Centerline
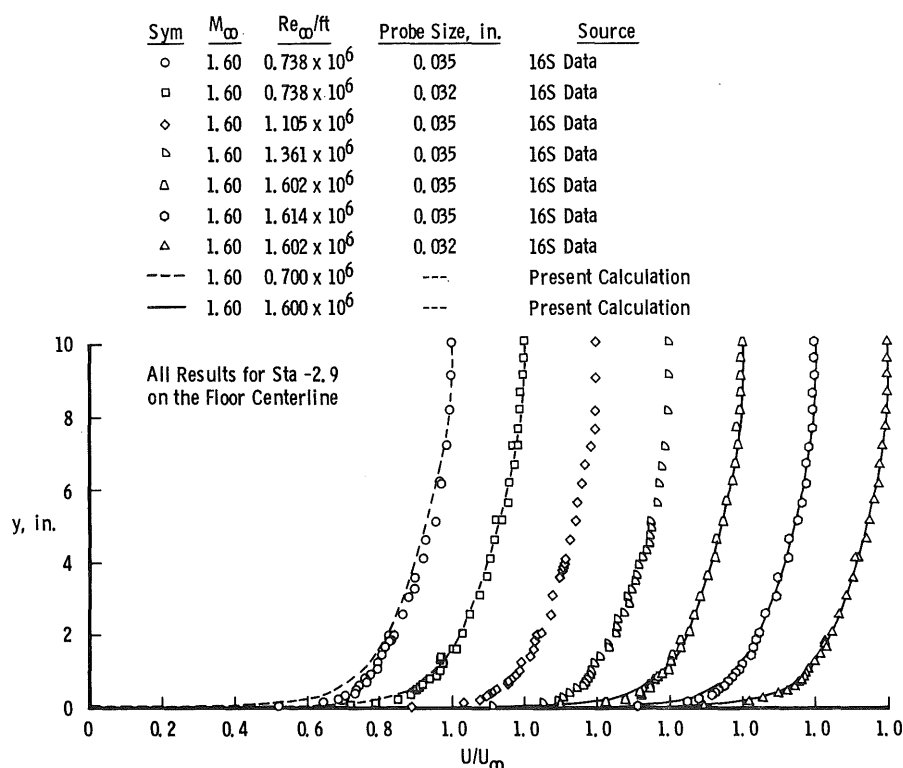
Figure 22. Theoretical and experimental velocity distributions in Tunnel 16S for $M_\infty = 1.6$.

The agreement between calculations and experimental data in Figs. 22 through 24 is considered good. The maximum discrepancy occurs for one of the lowest Reynolds number, $M_\infty = 1.6$ profiles in Fig. 22 indicated by the circle symbols. This profile

Sym	M_∞	Re_∞/ft	Probe Size, in.	Source
○	2.20	0.739×10^6	0.062	16S Data
□	2.20	0.718×10^6	0.032	16S Data
◇	2.20	1.210×10^6	0.062	16S Data
�ু	2.20	1.679×10^6	0.062	16S Data
△	2.20	1.679×10^6	0.032	16S Data
---	2.20	0.700×10^6	---	Present Calculation
——	2.20	1.700×10^6	---	Present Calculation

All Results for Sta -2.9
on the Floor Centerline

y, in.

U/U_∞
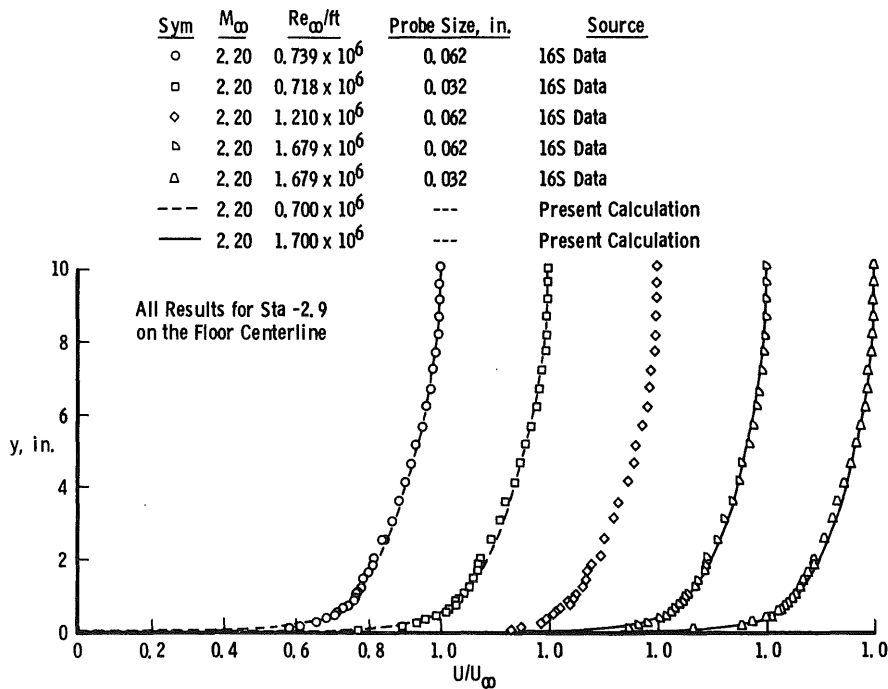
Figure 23. Theoretical and experimental velocity distributions in Tunnel 16S for M_∞ = 2.2.

Sym	M_∞	Re_∞/ft	Probe Size, in.	Source
△	1.60	1.602×10^6	0.032	16S Data
△	2.20	1.679×10^6	0.032	16S Data
---	1.60	1.600×10^6	---	Present Calculation
——	2.20	1.700×10^6	---	Present Calculation

All Results for Sta -2.9
on the Floor Centerline

y, in.

M/M_∞

M/M_∞
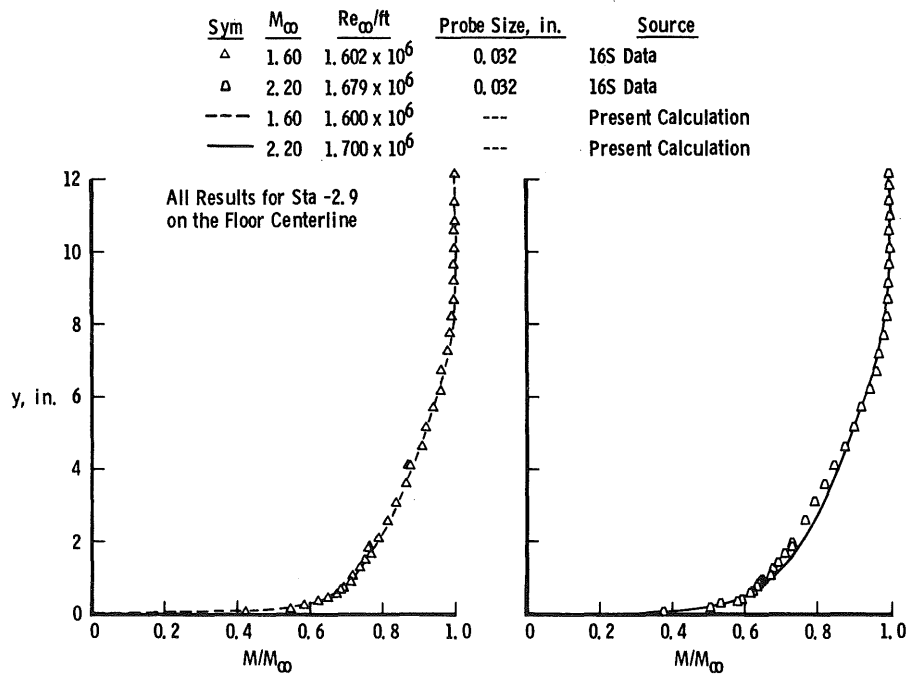
Figure 24. Theoretical and experimental Mach number distributions in Tunnel 16S for M_∞ = 1.6 and 2.2.

46

measurement was repeated one week later using a different pitot probe, and better agreement was obtained as indicated by the square symbols in Fig. 22. Although the digital voltmeter output of the pitot pressure was not stable while the circle symbol profile was taken, the discrepancy is not necessarily attributed to probe vibration or transducer problems. Maxwell and Hartley (Ref. 78) observed some time ago that at low Mach number the boundary layer varied with time. This anomaly was not resolved in their work and it is not resolved herein.

Boundary-layer measurements have recently been made on the floor and east side wall of the 16-ft Transonic Wind Tunnel (16T) in PWT using this same traversing probe mechanism. These measurements were made at Station -8 on the solid walls between the first upstream hole patterns at the beginning of the transition region which separates the solid and porous tunnel walls. Measurements on the floor centerline were made first and compared with the present numerical solutions. The pressure gradient used for the calculations was obtained from static pressure measurements extending 32 ft upstream of the point of measurement, and the pressure distribution upstream of the static measurements was obtained from solutions using the Potential Flow Computer Program (Ref. 79) and were provided by Palko, Todd, and Lutz of AEDC. Examples of these boundary-layer results are presented in Fig. 25. All measured boundary layers were thinner than predicted. The results from the potential flow solution for $M_\infty = 0.6$ and 0.8 indicated a pressure difference between floor (or top) and sidewall due to the difference in contraction of the top and bottom and the sidewalls. (The top and bottom wall contraction is the same and each sidewall contraction is the same.) The sidewall pressure was larger than the top or bottom wall pressure upstream of Station -60, and then the bottom and top wall pressure was larger than the sidewall pressure downstream of Station -60, with all pressures becoming equal at Station 0. Considering the possibility that mass flow from the floor boundary layer could be taking place because of this pressure difference downstream of Station -60, the probe was moved to two feet below the east wall centerline at Station -8 and further measurements were made. Examples of these results are given in Figs. 26 and 27. The predicted boundary layers are only slightly thicker than the measured and better agreement is obtained than with the floor data.

To investigate flow behavior further in 16T, the east half of the floor and bottom half of the east wall were coated with oil to visually study flow direction near the wall for a $M_\infty = 0.7$ flow condition. Two primary results of this investigation should be noted. First, oil streaks downstream of Station -60 and upstream of Station -8 definitely indicated a flow direction across the bottom wall, away from the centerline, and up the sidewall. Secondly, although no pumping is applied to the porous walls at $M_\infty = 0.7$, oil streaks indicated that some of the holes were actually pumping in the transition region, and also some streaks indicated the flow was influenced by this local pumping a few feet

(approximately two to three) upstream of the transition region. Therefore, in addition to mass being moved from the floor to the sidewall, it could also be removed from the solid wall region existing between the sawtooth pattern of holes at the beginning of the porous wall transition region, thereby thinning the boundary layer.

Sym	M_∞	Re_∞/ft	δ^*, in.	θ, in.	H	Source
o	0.6	2.44×10^6	0.511	0.359	1.423	16T Data
——	0.6	2.50×10^6	0.676	0.484	1.397	Present Calculation
□	0.8	5.00×10^6	0.481	0.310	1.550	16T Data
----	0.8	5.10×10^6	0.619	0.418	1.483	Present Calculation
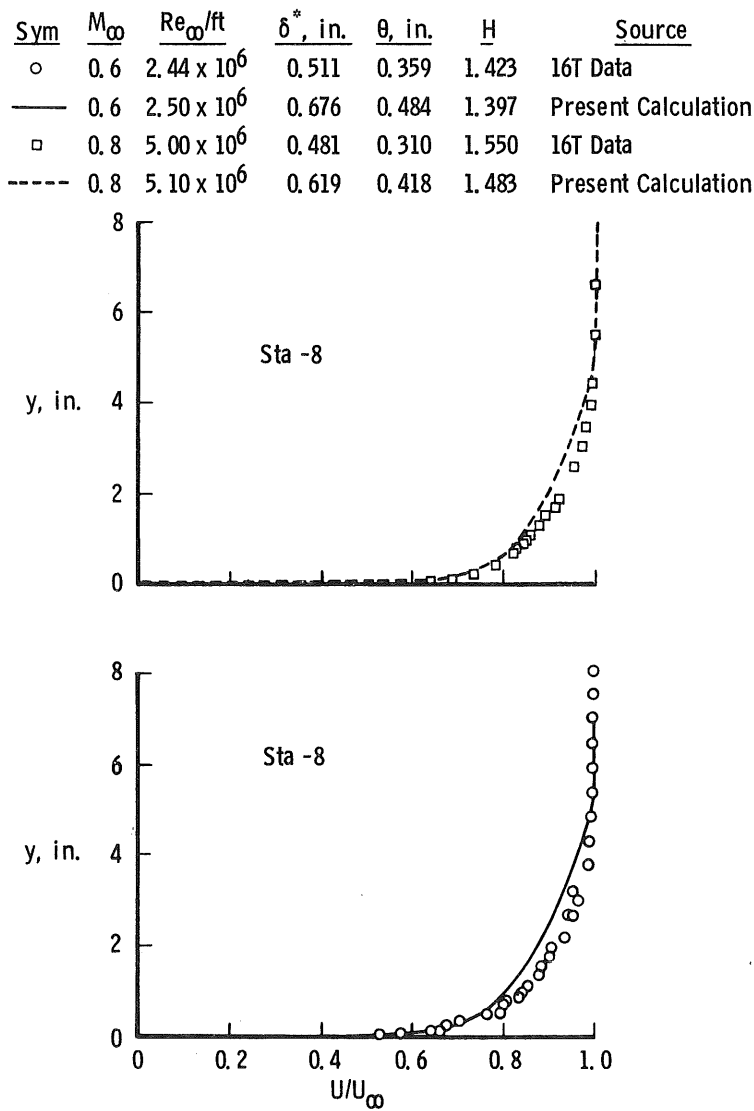
Figure 25. Theoretical and experimental velocity distributions on the floor centerline in Tunnel 16T for M_∞ = 0.6 and 0.8.

Results from the total-temperature measurements which were made simultaneously with the pitot pressure in 16S are presented in Figs. 28 and 29 in $\bar{u} - \bar{T}$ coordinates. One set of the M_∞ = 2.2 data is presented in Fig. 30 in terms of T/T_∞ versus U/U_∞.

Also presented in Fig. 30 are the present results according to Eq. (59) and Crocco's result, Eq. (42), which assumes constant total temperature across the boundary layer and is frequently used to reduce pitot pressure data. The sensitivity of the $\bar{u}$ - $\bar{T}$ coordinates is again made clear by the fact that although the trend of the present analytical results is in agreement with the experimental data in Figs. 28 and 29, the absolute value is not in agreement for all U/U_∞ for these particular data. However, good absolute value agreement is obtained in Fig. 30 in terms of static temperature. Fortunately, for data reduction purposes, it is the agreement in static temperature as a function of velocity that is important.

Sym	Re_∞/ft	δ^*, in.	θ, in.	H	Source
o	4.741×10^6	0.586	0.364	1.610	16T Data
—	4.741×10^6	0.613	0.429	1.429	Present Calculation
□	3.885×10^6	0.583	0.393	1.483	16T Data
—	3.885×10^6	0.630	0.439	1.435	Present Calculation
◇	2.210×10^6	0.636	0.423	1.504	16T Data
—	2.210×10^6	0.682	0.470	1.451	Present Calculation
△	0.435×10^6	0.833	0.559	1.490	16T Data
—	0.435×10^6	0.923	0.611	1.511	Present Calculation
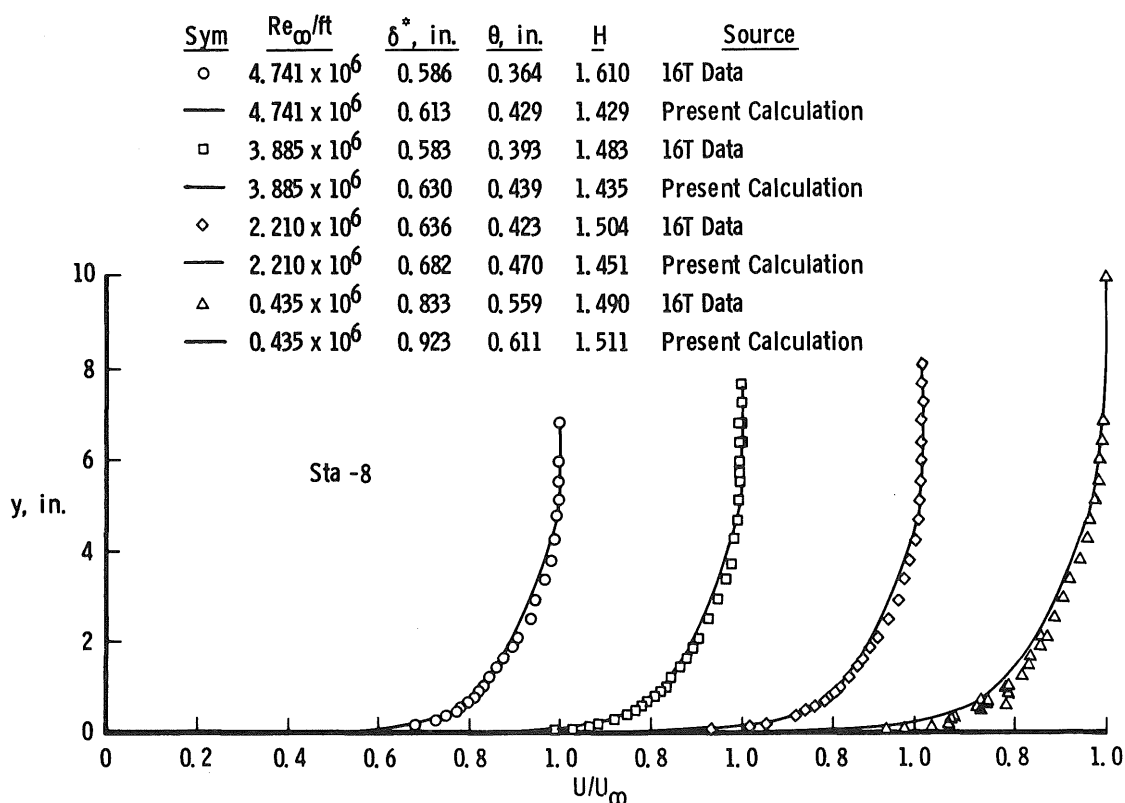
Figure 26. Theoretical and experimental velocity distributions 2 ft below east-wall centerline in Tunnel 16T for M_∞ = 0.7.

Comparisons between experimental data and the numerical calculations of Section 2.0 are presented in Fig. 31 for M_∞ = 1.6 and 2.2. The agreement is considered reasonable.

The total-temperature probe used to obtain the temperature results in Figs. 28 through 31 was 0.046 in. in diameter and constructed according to the description given in Ref. 80. The center of the total-temperature probe was positioned to be the same distance from the wall as the center of the pitot pressure probe and was traversed simultaneously

with the pitot probe. The probe recovery factor was determined by relating the measured probe temperature outside the boundary layer to the tunnel total temperature as measured upstream in the stagnation chamber. Tunnel stratification was neglected. The wall temperature was measured by determining the surface temperature of two 0.25-in. Gardon gages (Ref. 81) located on the tunnel floor near the total-temperature probe. These two measured wall temperatures were within 0.2°F.

Sym	Re_∞/ft	δ^*, in.	θ, in.	H	Source
o	1.983×10^6	0.606	0.366	1.654	16T Data
---	1.967×10^6	0.682	0.431	1.581	Present Calculation
□	3.447×10^6	0.600	0.366	1.639	16T Data
——	3.447×10^6	0.628	0.402	1.561	Present Calculation
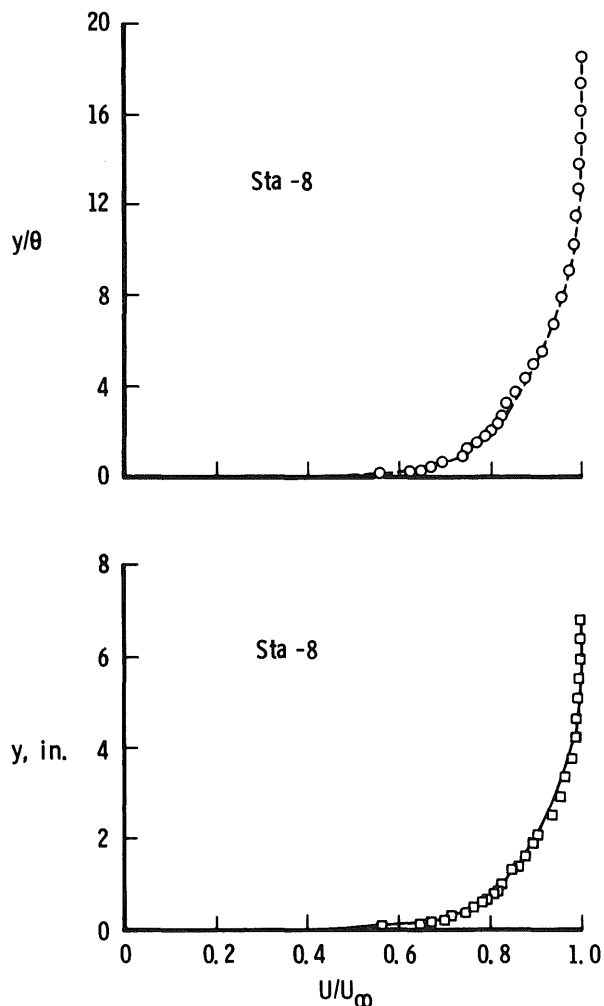
Figure 27. Theoretical and experimental velocity distributions 2 ft below east-wall centerline in Tunnel 16T for M_∞ = 0.9.

Sym	M_∞	$T_w/T_{0,\infty}$	Re_∞/ft	Source
o	1.632	0.949	1.61×10^6	16S Data
□	1.617	0.937	0.74×10^6	16S Data
—	1.600	0.937	---	Eq. (59)

All Results for Sta -2.9
on the Floor Centerline

Figure 28. Theoretical and experimental velocity-temperature relations in Tunnel 16S for M_∞ = 1.6.

Sym	M_∞	$T_w/T_{0,\infty}$	Re_∞/ft	Source
o	2.219	0.929	1.68×10^6	16S Data
□	2.203	0.934	0.72×10^6	16S Data
—	2.200	0.929	---	Eq. (59)

All Results for Sta -2.9
on the Floor Centerline
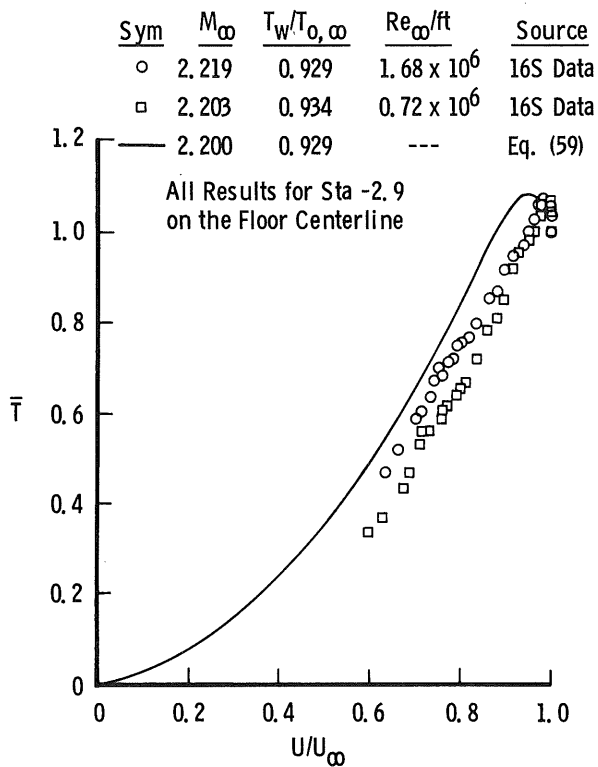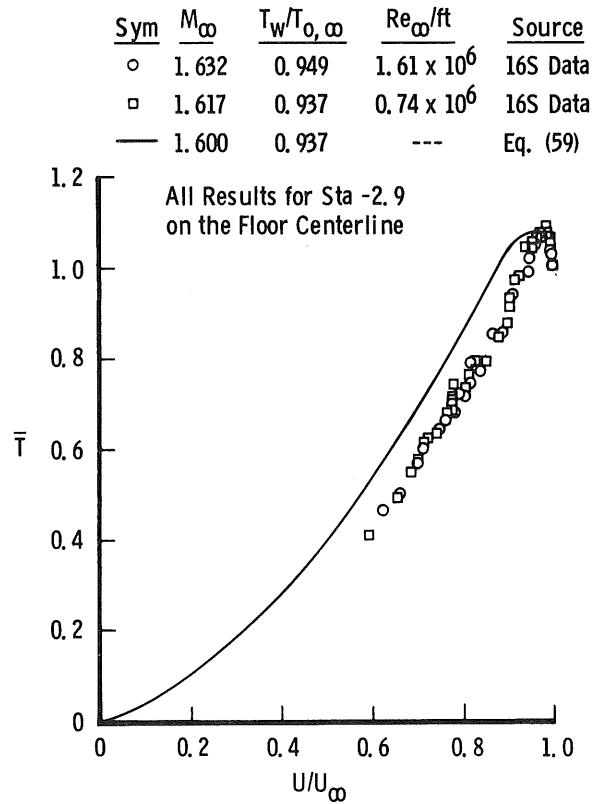
Figure 29. Theoretical and experimental velocity-temperature relations in Tunnel 16S for M_∞ = 2.2.

51

Sym	M_∞	$T_w/T_{0,\infty}$	Source
o	2.219	0.929	16S Data $(Re_\infty/ft = 1.68 \times 10^6)$
——	2.219	0.929	Eq. (59)
----	2.219	1.0	Eq. (42), Crocco Result

Experimental Data Are Same as
Circle Symbols on Fig. 29

Figure 30. Theoretical and experimental static temperature results in Tunnel 16S for M_∞ = 2.2.

Sym	M_∞	$T_w/T_{0,\infty}$	Re_∞/ft	Source
o	2.219	0.929	1.68×10^6	16S Data
——	2.200	0.941	1.70×10^6	Present Calculation
□	1.632	0.940	1.61×10^6	16S Data
----	1.600	0.960	1.60×10^6	Present Calculation
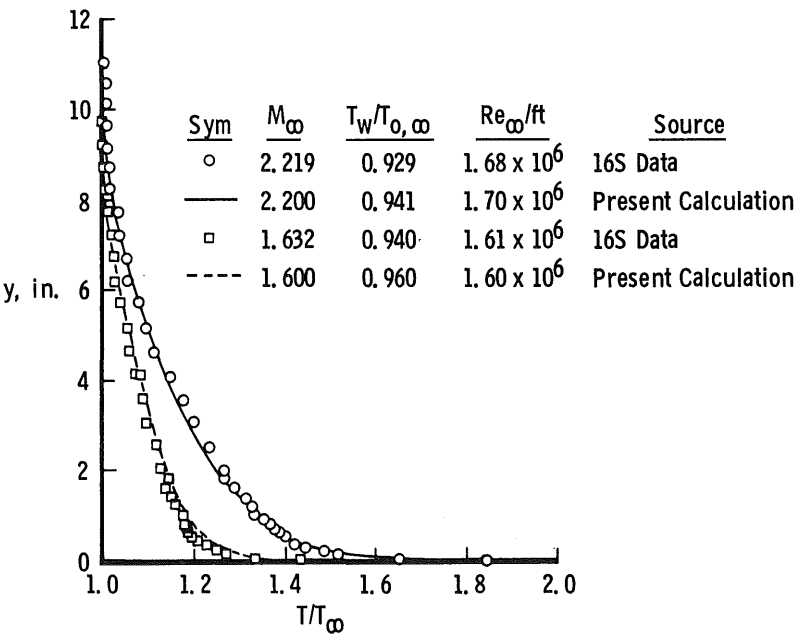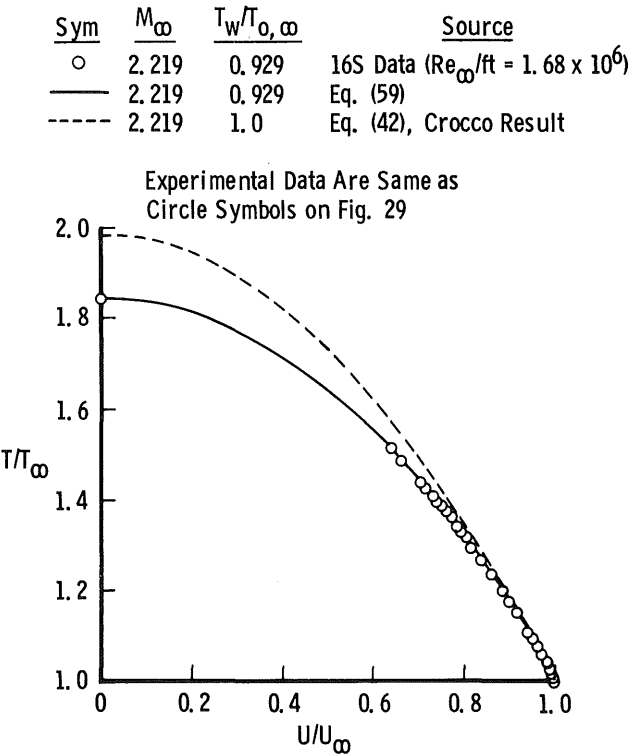
Figure 31. Theoretical and experimental spatial distributions of static temperature in Tunnel 16S for M_∞ = 1.6 and 2.2.

6.2 SKIN FRICTION

Of particular interest here are the tunnel wall skin-friction coefficients in 16S. Tunnel wall skin-friction coefficients are required in the boundary-layer transition correlation method of Pate and Schueler (Ref. 82). Boundary-layer pitot pressure measurements were made by Baker and Pate (Ref. 77) on the ceiling and east wall of 16S at Station 5.4. These measurements were used to determine c_f and δ^* which were used in the correlation of the boundary-layer transition measurements made on a 12-in.-diam hollow cylinder located in the 16S test section. Skin friction was determined for use in Ref. 82 by the expression $c_f = 2\theta/\ell_r$ where ℓ_r was taken as the axial distance from the nozzle throat to the point of measurement. Baker's measurements (Ref. 77) have been reduced using the present data reduction technique, and these results are presented in Fig. 32. Also presented in Fig. 32 are measurements at Station -2.9 corresponding to the 16S data already presented.

The skin-friction coefficients used by Pate and Schueler (Ref. 82) (they used M_∞ = 3 data only) were those determined from Baker's ceiling (straight wall) measurements using $c_f = 2\theta/\ell_r$. These results are about 25 percent larger than the M_∞ = 3 ceiling data in Fig. 32 using the present data reduction technique. Also, there is considerably more scatter than in the data of Fig. 32. Using $c_f = 2\theta/\ell_r$, the ceiling data (Ref. 77) produce larger c_f's than the east-wall data. However, the east-wall data have larger skin frictions than the ceiling data using the present technique as shown in Fig. 32. The skin frictions used by Pate and Schueler were about 10 percent larger than the east wall results in Fig. 32. The difference in c_f between ceiling and east wall data for the same Mach number is attributed to the difference in upstream pressure gradients.

Skin-friction measurements (i.e. deduced from pitot pressure measurements using the present data reduction technique) have also been made in the Acoustic Research Tunnel (ART) and Tunnel 16T in PWT. These data, along with those from 16S, are presented in Fig. 33 using the correlation technique of Winter and Gaudet (Ref. 12). These data cover the Mach number range from 0.5 to 3.0. The east wall (Tunnel 16S) data at Station 5.4 are slightly high in $F_c\, c_f$ and/or $F_\delta\, Re_\theta$. This deviation is within the scatter of the data used by Winter and Gaudet (Ref. 12), and the correlation is considered reasonable. Skin frictions obtained by using $c_f = 2\theta/\ell_r$ would have larger values of $F_c\, c_f$ than the Tunnel 16S data in Fig. 33, and acceptable correlation would not be obtained.

In practice, skin frictions are frequently required for axial stations or flow conditions where data are not available. To obtain c_f for different axial locations and flow conditions, the following suggestions are given. A program is available to calculate c_f according to the theory of White and Christoph (Ref. 83). It gives reasonable results (Fig. 32) and

can be used to predict the trend and hence extrapolate or interpolate quite accurately. The same can be said of the present finite-difference calculations, of which some comparisons with data are given in Fig. 32. Sufficiently accurate interpolations or extrapolations might be made using c_f proportional to some power of Reynolds number,

Sym	M_∞	Station	Source
o	1.6	-2.9	Experimental Floor Data
□	2.2	-2.9	Experimental Floor Data
——	As Indicated	-2.9	Theoretical (Ref. 83)
———	As Indicated	-2.9	Theoretical (Present Calculations)
◇	2.0	5.4	Experimental Ceiling Data
◆	2.0		Experimental East-Wall Data
◺	2.5		Experimental Ceiling Data
◣	2.5		Experimental East-Wall Data
△	3.0		Experimental Ceiling Data
▲	3.0		Experimental East-Wall Data
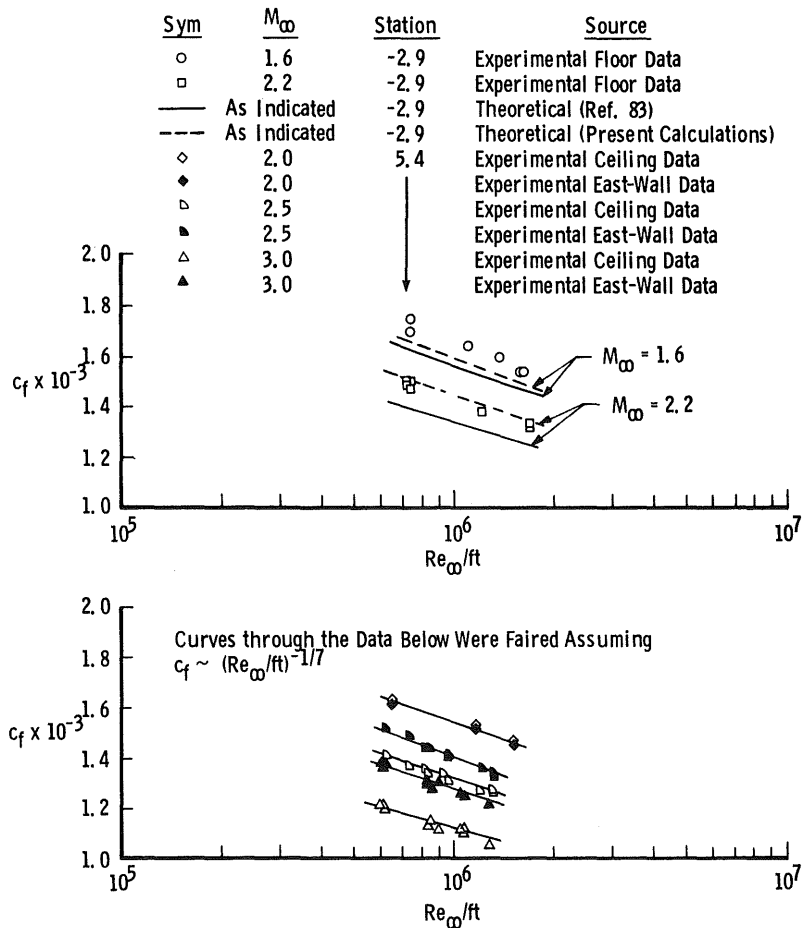
Figure 32. Tunnel wall skin-friction coefficients
in Tunnel 16S for M_∞ of 1.6 to 3.0.

such as the faired curves in Fig. 32. Another possibility is to use the correlations of Winter and Gaudet (Ref. 12). Besides F_c c_f versus $F_\delta Re_\theta$, they also present F_c c_f versus $(F_\delta/F_c)Re_x$. These two plots provide a direct relation between Re_θ and Re_x and hence interpolations or extrapolations can be made graphically.

Sym	M_∞	Tunnel	Location
◇	0.5	ART	Test Section, Floor Centerline
◇	0.6	16T	Sta -8, Floor Centerline
◻	0.7	16T	Sta -8, 2 ft below East-Wall Centerline
▽	0.8	16T	Sta -8, Floor Centerline
◇	0.85	16T	Sta -8, 2 ft below East-Wall Centerline
◻	0.9	16T	Sta -8, 2 ft below East-Wall Centerline
▽	1.6	16S	Sta -2.9, Floor Centerline
○	2.0	16S	Sta 5.4, Ceiling Centerline
△	2.0	16S	Sta 5.4, East-Wall Centerline
☆	2.2	16S	Sta -2.9, Floor Centerline
◇	2.5	16S	Sta 5.4, Ceiling Centerline
○	2.5	16S	Sta 5.4, East-Wall Centerline
◇	3.0	16S	Sta 5.4, Ceiling Centerline
◅	3.0	16S	Sta 5.4, East-Wall Centerline

— Correlation of Winter and Gaudet, Eq. (22) of Ref. 12

$$F_c = \left(1 + 0.2 M_\infty^2\right)^{1/2}$$
$$F_\delta = 1 + 0.056 M_\infty^2$$

Figure 33. Correlation of tunnel wall skin-friction data from three tunnels in PWT.

6.3 BOUNDARY-LAYER PARAMETERS

The frequently used boundary-layer parameters of displacement thickness, δ^*, momentum thickness, θ, and shape factor, $H = \delta^*/\theta$, are presented in Fig. 34 for Tunnel 16T at Station -8. These data indicate, as did the velocity data, that the floor boundary layer is thinner than the east wall boundary layer. For example, the $M_\infty = 0.6$ and 0.8 floor data have a δ^* of about 0.47 in. at Re_∞/ft of approximately 4.5 x 10^6, whereas the $M_\infty = 0.7$ east wall data show δ^* to be 0.57 in., or about 20 percent larger. Although the calculated shape factors are in agreement with measured shape factors for both floor and east wall data, only relatively good agreement with δ^* and θ is obtained with the east wall data. Plausible explanations for the difference in floor and east wall boundary layers have been given when the velocity distributions were considered.

Boundary-layer parameters in Tunnel 16S at Station -2.9 are considered in Fig. 35. Good agreement between calculated and measured data is obtained. Results for one of the low Reynolds number, $M_\infty = 1.6$ condition, are shown to be low as compared to

55

the other data in Fig. 35. This anomaly was also discussed earlier when the velocity data were considered. Repeat measurements of this flow condition provided results in better agreement with the calculations and the other data as shown in Fig. 35. Boundary-layer parameters from the measurements of Baker can be found in Ref. 77. Boundary-layer parameters for a wider range of Mach numbers have been measured and reported by Maxwell and Hartley (Ref. 78).
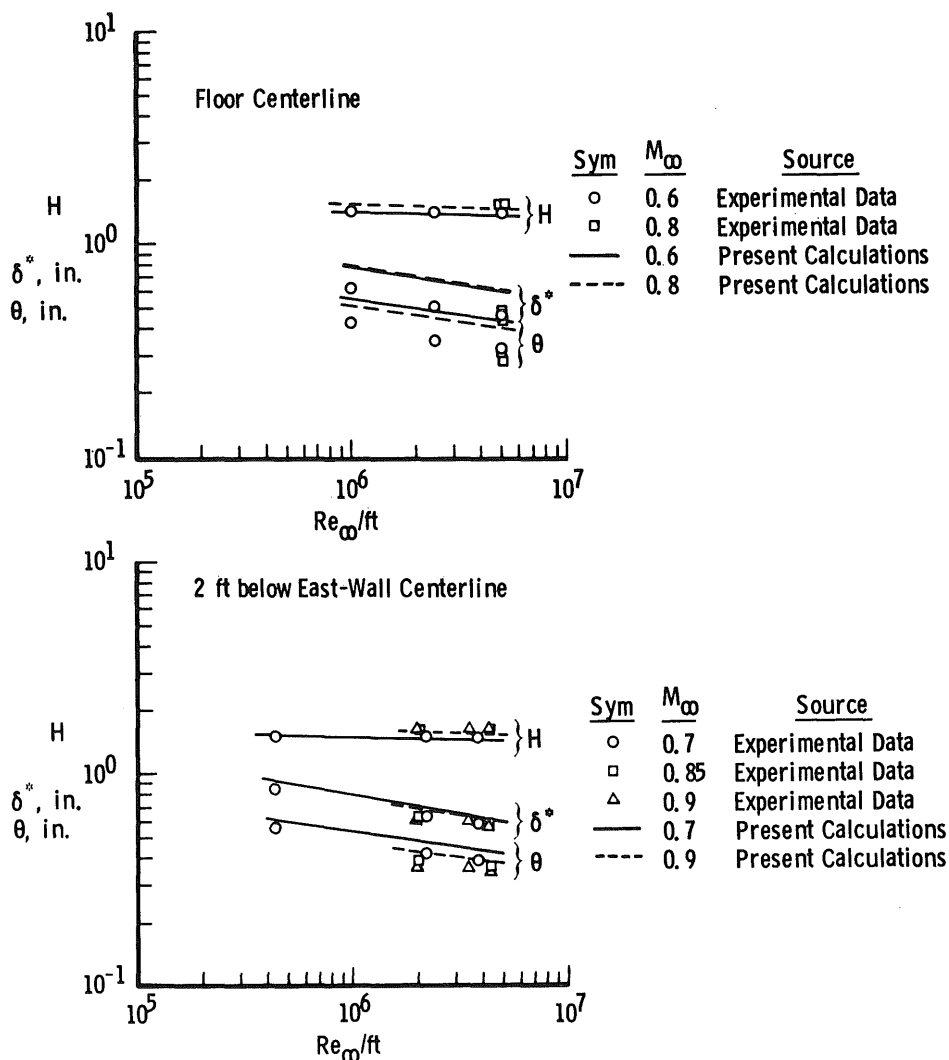
Figure 34. Boundary-layer parameters in Tunnel 16T for Station -8.
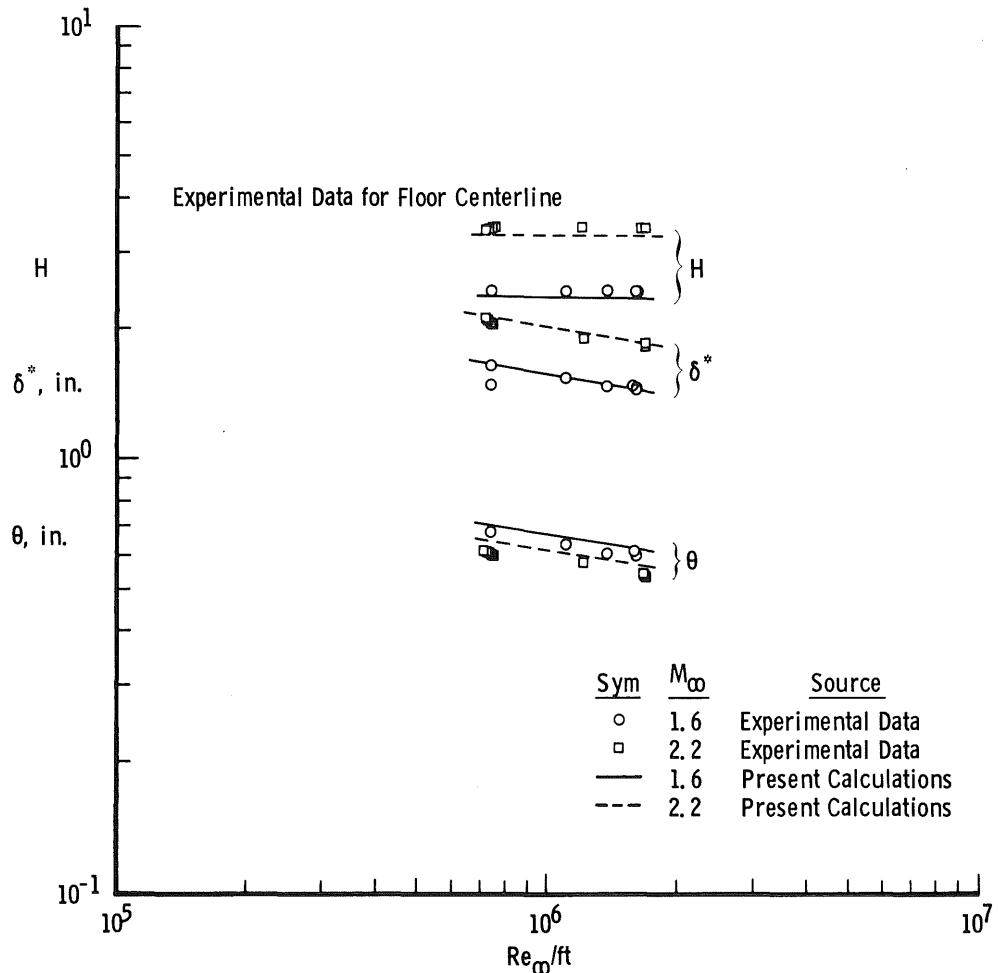
Figure 35. Boundary-layer parameters in Tunnel 16S for Station -2.9.

7.0 CONCLUSIONS AND COMMENTS

The numerical boundary-layer computations described in Section 2.0 have provided a useful tool for estimates of boundary-layer problems associated with various research, test, and test facility development projects conducted in PWT. Of primary importance in this work was the assessment of the modeling for the Reynolds stress and the calculation of the turbulent kinetic energy. Although the particular modeling of the Reynolds stress used here has been used by previous investigators, the particular modeling of the turbulent kinetic energy equation (on which the Reynolds stress depended) has not been used. The approach followed permitted the use of the natural turbulent kinetic energy boundary conditions and the computation of e throughout the boundary layer without having to handle such regions as the laminar sublayer, buffer layer, logarithmic, and wake regions separately.

The analytical investigation of turbulence near a wall (Section 3.0) provides convenient expressions of describing the flow in this region. Of interest is the fact that these results were obtained without the use of mixing-length theory, in which the approach appears to be unique. This was made possible by the form of the turbulent kinetic energy equation developed in Section 2.0.

The analytical results obtained in Section 4.0, for temperature as a function of velocity throughout the boundary layer, were shown to be improvements over previously used results. The application of these results to the calculation of the quantity $2c_h/c_f$, indicated that $2c_h/c_f$ decreased for small decreasing values of $h_w/H_{o,\infty}$. This prediction was substantiated by comparisons with experimental data.

The analytical results of Sections 3.0 and 4.0 were used in Section 5.0 in a computer program for the data reduction of pitot pressure measurements made in turbulent boundary layers. In addition to Mach number, velocity, temperature, and various boundary-layer parameters, skin friction is determined from the pitot pressure measurements. The technique used to determine c_f has the important practical advantage of not requiring measurements near the wall in the sub- or buffer layers and hence eases experimental requirements.

The recent pitot pressure and total-temperature measurements made in Tunnel 16S were in good agreement with the present theoretical results. However, this was not the case with regard to the solid wall pitot pressure measurements made in Tunnel 16T. The calculated boundary layer was consistently thicker than the measured boundary layer, particularly the floor boundary layer. Potential flow solutions indicate, however, that the flow near the tunnel wall experiences a pressure drop from the floor toward the sidewall, and oil streak experiments conducted in the lower east quadrant for 60 ft upstream of the test section at $M_\infty = 0.7$ indicated that a crossflow did occur from the floor toward the east wall. The oil streak experiments further indicated that crossflow was induced over the solid wall between some of the upstream holes in the transition section, which extends 10 ft upstream of the test section, thereby effecting the measured boundary layer.

The skin-friction coefficients obtained by using the present data reduction program to reduce the measurements of Baker and Pate (Ref. 77) were not in agreement with those obtained by Pate and Schueler (Ref. 82) and used to correlate the Tunnel 16S boundary-layer transition data. However, preliminary results indicate that the effect of using the present skin-friction coefficients in the correlation of Pate and Schueler (Ref. 82) is not necessarily to invalidate the correlation of the Tunnel 16S data as it is to extend the correlation below the original lower Mach number bound of three to include the remainder of the Tunnel 16S transition data (Ref. 77) (which include Mach numbers down to two) not correlated by Pate and Schueler (Ref. 82).

An effort was made to make the present computer results readily available for engineering applications. The boundary-layer computer program given in Appendix A has simple input, and unless desired, no dimensional variables or properties are input and no units are involved. The pitot pressure data reduction computer program given in Appendix B is essentially self-contained and has been used for online and offline data reduction.

REFERENCES

1. Patankar, S. V. and Spalding, D. B. Heat and Mass Transfer in Boundary Layers. Morgan-Grampian: London 1967.

2. Whitfield, D. L. "Viscous Effects in Low-Density Nozzle Flows." AEDC-TR-73-52 (AD761489), June 1973.

3. Townsend, A. A. The Structure of Turbulent Shear Flow. Cambridge University Press, Cambridge, 1956.

4. Lighthill, M. J. Review of A. A. Townsend's book, "The Structure of Turbulent Shear Flow." Journal of Fluid Mechanics, Vol. 1, Part 5, November 1956, pp. 554-560.

5. Prandtl, L. "On a New Representation of Fully Developed Turbulence." JPL Publication No. 13, 1952, Translation by D. Coles.

6. Bradshaw, P., Ferriss, D. H., and Atwell, N. P. "Calculation of Boundary-Layer Development Using the Turbulent Energy Equation." Journal of Fluid Mechanics, Vol. 28, Pt. 3, May 1967. pp. 593-616.

7. Ng, K. H. and Spalding, D. B. "Turbulence Model for Boundary Layers near Walls." The Physics of Fluids, Vol. 15, No. 1, January 1972, pp. 20-30.

8. Glushko, G. S. "Turbulent Boundary-Layer on a Flat Plate in an Incompressible Fluid." NASA TT F-10,080, Translation from Izvestiya Akademii Nank SSSR, Seriya Mekhanika, No. 4, pp. 13-23.

9. Beckwith, I. E. and Bushnell, D. M. "Calculation of Mean and Fluctuating Properties of the Incompressible Turbulent Boundary Layer." Proceedings of the AFOSR-IFR-Standford Conference on Computation of Turbulent Boundary Layers, 1968, pp. 275-299.

10. Kolmogoroff, A. N. Izv. Akad. Nank SSSR Ser. Fiz. 6, 56, 1942 (Imperial College Mech. Eng. Dept. ON/6, 1968).

11. Batchelor, G. K. The Theory of Homogeneous Turbulence. Cambridge University Press, Cambridge, 1953, Chapter VI.

12. Winter, K. G. and Gaudet, L. "Turbulent Boundary-Layer Studies at High Reynolds Numbers at Mach Numbers Between 0.2 and 2.8." Aeronautical Research Council, London, Reports and Memoranda No. 3712, December 1970.

13. Gates, D. F. "Measurements of Upstream History Effects in Compressible Turbulent Boundary Layers." NOLTR 73-152, July 1973.

14. Rannie, W. D. "Heat Transfer in Turbulent Shear Flow." Journal of the Aeronautical Sciences, Vol. 23, No. 5, May 5, 1956, pp. 485-489.

15. Hinze, J. O. Turbulence; An Introduction to Its Mechanism and Theory. McGraw-Hill Book Company, New York, N. Y., 1959, pp. 471-473.

16. White, F. M. Viscous Fluid Flow. McGraw-Hill Book Company, New York, N. Y., 1974, pp. 474-477.

17. Spalding, D. B. "A Single Formula for the "Law of the Wall"." Journal of Applied Mechanics, Transactions of the ASME, Series E., Vol. 28, September 1961, pp. 455-458.

18. Kleinstein, G. "Generalized Law of the Wall and Eddy-Viscosity Model for Wall Boundary Layers." AIAA Journal, Vol. 5, No. 8, August 1967, pp. 1402-1407.

19. Reichardt, Von. H. "Vollständige Darstellung der turbulenten Geschwindigkeits-verteilung in glatten Leitungen." Z. angew. Math. Mech., Vol. 31, No. 7, July 1951, pp. 208-219.

20. van Driest, E. R. "On Turbulent Flow Near a Wall." Journal of the Aeronautical Sciences, Vol. 23, 1956, pp. 1007-1011.

21. Kutaleladze, S. S. and Leont'ev, A. I. Turbulent Boundary Layers in Compressible Gases. Translated by D. B. Spalding, Academic Press, Inc., New York, N. Y., 1964, p. 24.

22. Gradshteyn, I. S. and Ryzhik, I. M. Table of Integrals, Series, and Products. Translated by A. Jeffrey, Academic Press, Inc., New York, N. Y., 1965, p. 148.

23. Lindgren, E. R. "Experimental Study on Turbulent Pipe Flows of Distilled Water." Department of Civil Engineering, Oklahoma State University, Report 1, AD621071, 1965.

24. Laufer, J. "The Structure of Turbulence in Fully Developed Pipe Flow." NACA Report 1174, 1954.

25. Klebanoff, P. S. "Characteristics of Turbulence in a Boundary Layer with Zero Pressure Gradient." NACA Report 1247, 1955.

26. Schubauer, G. B. "Turbulent Processes as Observed in Boundary Layer and Pipe." Journal of Applied Physics, Vol. 25, No. 2, February 1954, pp. 188-196.

27. Busemann, A. "Gasdynamik." in Handbuch der Experimentalphysik, Band 4, 1. Teil, Akademische Verlagsgesellschaft M.B.H., Leipzig, 1931, p. 366.

28. Crocco, L. "Sulla Transmissiene del Calore da una Lamina piana a un fluide Scorrente ad alta Velocita." L'Aerotechnica, Vol. XII, No. 2, February 1932, pp. 181-197. (Transmission of Heat from a Flat Plate to a Fluid Flowing at a High Velocity, NACA Technical Memorandum No. 690, October 1932.)

29. Crocco, L. "Lo Strato Limite Laminare nei Gas." Monografie Scientifiche di Aeronautica, No. 3, Ministero della Difesa-Aeronautica, Roma, December 1946. (Translation in North American Aviation Aerophysics Lab., Rep. AL-684, July 15, 1948.)

30. Busemann, A. "Gasstromung mit laminarer Grenzschicht entlang einer Platte." in Zeitschrift fur Angewandte Mathematik und Mechanik, Ingenieurwissenschaftliche Forschungsarbeitm, Berlin, 1935, pp. 23-25.

31. van Driest, E. R. "The Turbulent Boundary Layer with Variable Prandtl Number." in 50 Jahre Grenzschichtferschung, Friedr. Vieweg & Sohn, Braunschweig, 1955, pp. 257-271.

32. von Kármán, T. "The Analogy Between Fluid Friction and Heat Transfer." Trans., A.S.M.E., Vol. 61, No. 11, November 1939, pp. 705-710.

33. Walz, A. "Compressible Turbulent Boundary Layers." International Symposium on the Mechanics of Turbulence, Marseilles, France, August 28 - September 2, 1961, Centre National de la Reserche Scientifique, N. Y. Gordon and Breach, 1964, pp. 299-350.

34. Michel, R. "Thermal Characteristics of the Boundary Layers and Practical Calculation of Heat Transfer in Hypersonic Flow." Progress in Aeronautical Sciences, Vol. 9, ONERA T.P. No. 432, 1966.

35. Schlichting, H. Boundary Layer Theory. Fourth Edition, McGraw-Hill Book Company, New York, N. Y., 1960, pp. 342 and 346.

36. Shapiro, A. H. The Dynamics and Thermodynamics of Compressible Fluid Flow. Vol. II. The Ronald Press Company, New York, 1954, p. 1063.

37. Meier, H. N., Voisinet, R.L.P., and Gates, D. F. "Temperature Distributions Using the Law of the Wall for Compressible Flow with Variable Turbulent Prandtl Numbers." AIAA Paper No. 74-596, June 1974.

38. Cebeci, T. "A Model for Eddy Conductivity and Turbulent Prandtl Number." Transactions of the ASME, Series C, Journal of Heat Transfer, Vol. 95, No. 2, May 1973, pp. 227-234.

39. Simpson, R. L., Whitten, D. G., and Moffat, R. J. "An Experimental Study of the Turbulent Prandtl Number of Air with Injection and Suction." International Journal of Heat and Mass Transfer, Vol. 13, 1970, pp. 125-143.

40. Kestin, J. and Richardson, P. D. "Heat Transfer Across Turbulent, Incompressible Boundary Layers." International Journal of Heat and Mass Transfer, Vol. 6, 1963, pp. 147-189.

41. Bradshaw, P. "Comments on Temperature Laws for a Turbulent Boundary Layer with Injection and Heat Transfer." AIAA Journal, Vol. 8, No. 7, July 1970, pp. 1375-1376.

42. Elser, K. "Reibungstemperaturfelder in turbulenten Grenzschichten." Mitt 1. a.d. Inst. f. Thermodyn. und Verbr. Mot. ETH Zurich, Ber. Nr. 8, Verlag Leeman, Zurich.

43. Adams, J. C., Jr. and Martindale, W. R. "Hypersonic Lifting Body Windward Surface Flow-Field Analysis for High Angles of Incidence." AEDC-TR-73-2 (AD756499), February 1973.

44. Adams, J. C., Jr. "Numerical Calculation of the Subsonic and Transonic Turbulent Boundary Layer on an Infinite Yawed Airfoil." AEDC-TR-73-112 (AD763730), July 1973.

45. Yanta, W. J. "A Fine-Wire Stagnation Temperature Probe." NOLTR-70-81, June 1970.

46. Lobb, K. R., Winkler, E. M., and Persh, J. "NOL Hypersonic Tunnel No. 4 Results VII: Experimental Investigation of Turbulent Boundary Layers in Hypersonic Flow." NAVORD Report 3880, March 1955.

47. Adcock, J. B., Peterson, J. B., Jr., and McRee, D. I. "Experimental Investigation of a Turbulent Boundary Layer at Mach 6, High Reynolds Number, and Zero Heat Transfer." NASA TN D-2907, July 1965.

48. Sturek, W. B. and Danberg, J. E. "Supersonic Turbulent Boundary Layer in an Adverse Pressure Gradient, Data Tabulation." The University of Delaware, Technical Report No. 141, November 1971.

49. Sturek, W. B. "An Experimental Investigation of the Supersonic Turbulent Boundary Layer in a Moderate Adverse Pressure Gradient, Part I. A Detailed Description of the Experiment and Data Tabulation." BRL R 1506, October 1970.

50. Sturek, W. B. "An Experimental Investigation of the Supersonic Turbulent Boundary Layer in a Moderate Adverse Pressure Gradient, Part II. Analysis of the Experimental Data." BRL R 1543, June 1971.

51. Allen, J. M. "Pitot-Probe Displacement in a Supersonic Turbulent Boundary Layer." NASA TN D-6759, April 1972.

52. Allen, J. M. "Effects of Mach Number on Pitot-Probe Displacement in a Turbulent Boundary Layer." NASA TN D-7466, June 1974.

53. Danberg, J. E. "Characteristics of the Turbulent Boundary Layer with Heat and Mass Transfer at M = 6.7." NOL TR-64-99, October 1964.

54. Hopkins, E. J. and Keener, E. R. "Pressure-Gradient Effects on Hypersonic Turbulent Skin-Friction and Boundary-Layer Profiles." AIAA Journal, Vol. 10, No. 9, September 1972, pp. 1141-1142.

55. Bertram, M. H. and Neal, L., Jr. "Recent Experiments in Hypersonic Turbulent Boundary Layers." Paper presented at AGARD Specialist Meeting on Recent Developments in Boundary Layer Research, Naples, Italy, May 10-14, 1965.

56. Nothwang, W. S. "An Evaluation of Four Experimental Methods for Measuring Mean Properties of a Supersonic Turbulent Boundary Layer." NACA TR-1320, 1957.

57. Bradfield, W. S. "Conical Turbulent Boundary Layer Experiments and a Correlation with Flat Plate Data." Transactions of the ASME, Series C, Journal of Heat Transfer, May 1960, pp. 94-100.

58. Fallis, W. B. "Heat Transfer in the Transitional and Turbulent Boundary Layers of a Flat Plate at Supersonic Speeds." UTIA Report No. 19, Institute of Aerophysics, University of Toronto, May 1952.

59. Neal, L., Jr. "A Study of the Pressure, Heat Transfer, and Skin Friction on Sharp and Blunt Flat Plates at Mach 6.8." NASA TN D-3312, April 1966.

60. Hopkins, E. J., Rubesin, M. W., Inouye, M., Keener, E. R., Mateer, G. C., and Polek, T. E. "Summary and Correlation of Skin-Friction and Heat-Transfer Data for a Hypersonic Turbulent Boundary Layer on Simple Shapes." NASA TN D-5089, June 1969.

61. Hironimus, G. A. "Hypersonic Shock Tunnel Experiments on the W7 Flat Plate Model - Expansion Side, Turbulent Flow and Leading Edge Transpiration Data." CAL Rep. No. AA-1952-Y-2, Cornell Aeronautical Laboratory, Inc., February 1966.

62. Wallace, J. E. "Hypersonic Turbulent Boundary Layer Studies at Cold Wall Conditions." Proceedings of the 1967 Heat Transfer and Fluid Mechanics Institute, P. A. Libby, D. B. Olfe, and C. W. Van Atta, Editors, Stanford University Press, 1967, pp. 427-451.

63. Bertram, M. H., Cary, A. M., Jr., and Whitehead, A. H., Jr. "Experiments with Hypersonic Turbulent Boundary Layers on Flat Plates and Delta Wings." Hypersonic Boundary Layers and Flow Fields, AGARD CP No. 30, May 1968.

64. Young, F. L. "Experimental Investigation of the Effects of Surface Roughness on Compressible Turbulent Boundary Layer Skin Friction and Heat Transfer." DRL-532, CR-21, Defense Research Laboratory, University of Texas, May 1965.

65. Chi, S. W. and Spalding, D. B. "Influence of Temperature Ratio on Heat Transfer to a Flat Plate Through a Turbulent Boundary Layer in Air." Proceedings of the Third International Heat Transfer Conference - Vol. II, Am. Inst. Chem. Eng., c. 1966, pp. 41-49.

66. Colburn, A. P. "A Method of Correlating Forced Convection Heat-Transfer Data and a Comparison with Fluid Friction." Trans. Am. Inst. Chem. Eng., Vol. XXIX, 1933, pp. 174-210.

67. Reynolds O. "On the Extent and Action of the Heating Surface for Steam Boilers." Proceedings of the Manchester Literary and Philosophical Society, Manchester, England, Vol. 14, 1975, pp. 7-12.

68. Kozlov, L. V. "Connection of Aerodynamic Heat with Skin Friction." FTD-TT-64-377/142, U. S. Air Force, December 1964. Available from DDC as AD609788.

69. Wilson, D. M. "A Correlation of Heat-Transfer and Skin-Friction Data and an Experimental Reynolds Analogy Factor for Highly Cooled Turbulent Boundary Layers at Mach 5.0." NOL TR 69-51, March 1969.

70. Cary, A. M., Jr. "Summary of Available Information on Reynolds Analogy for Zero-Pressure-Gradient, Compressible, Turbulent-Boundary-Layer Flow." NASA TN D-5560, January 1970.

71. Allen, J. M. and Tudor, D. H. "Charts for Interpolation of Local Skin Friction from Experimental Turbulent Velocity Profiles." NASA SP-3048, 1969.

72. Ames Research Staff. "Equations, Tables, and Charts for Compressible Flow." NACA Report 1135, 1953.

73. Nielsen, K. L. Methods in Numerical Analysis. Second Edition, the MacMillan Company, New York, 1964, p. 175.

74. Fenter, F. W. and Stalmach, C. J., Jr. "The Measurements of Local Turbulent Skin Friction at Supersonic Speeds by Means of Surface Impact Pressure Probes." DRL 392, CM-878, University of Texas, October 1957.

75. Clauser, F. H. "Turbulent Boundary Layers in Adverse Pressure Gradients." Journal of the Aeronautical Sciences, Vol. 21, No. 2, February 1954, pp. 91-108.

76. Allen, J. M. "Use of Baronti-Libby Transformation and Preston Tube Calibrations to Determine Skin Friction from Turbulent Velocity Profiles." NASA TN D-4853, November 1968.

77. Baker, W. B., Jr. and Pate, S. R. "Measurement of the Transition Reynolds Number in the AEDC 16-ft, Supersonic, Propulsion Wind Tunnel." AEDC-TR-67-144 (AD817165), July 1967.

78. Maxwell, H. and Hartley, M. S. "Aerodynamic Calibration Results for the AEDC-PWT 16-ft Supersonic Tunnel at Mach Numbers from 1.50 to 4.75." AEDC-TR-69-102 (AD852942), May 1969.

79. Todd, D. C. and Palko, R. L. "The AEDC Three-Dimensional, Potential Flow Computer Program, Vols. I and II." AEDC-TR-75-75, February 1976.

80. Bontrager, P. J. "Development of Thermocouple Type Total Temperature Probes in the Hypersonic Flow Regime." M.S. Thesis, University of Tennessee, March 1968, also AEDC-TR-69-25 (AD681489), January 1969.

81. Trimmer, L. L., Matthews, R. K., and Buchanan, T. D. "Measurement of Aerodynamic Heat Rates at the von Kármán Facility." International Congress on Instrumentation in Aerospace Simulation Facilities, 1973, pp. 35-44.

82. Pate, S. R. and Schueler, C. J. "Effects of Radiated Aerodynamic Noise on Model Boundary-Layer Transition in Supersonic and Hypersonic Wind Tunnels." AEDC-TR-67-236 (AD666644), March 1968.

83. White, F. M. and Christoph, G. H. "A Simple Theory for the Two-Dimensional Compressible Turbulent Boundary Layer," Journal of Basic Engineering, Transactions of the ASME, September 1972, pp. 636-642.

APPENDIX A
BOUNDARY-LAYER COMPUTER CODE

Improvements to this code that have to do primarily with the region near the wall were made subsequent to its submission for publication. These improvements hardly produce discernible changes from the results given herein. The code used for the computations in this report is listed here and the new version is available on request.

MAIN

```
C      MAIN                                                              A   2
       IMPLICIT REAL*8(A-H,O-Z)
       COMMON /GEN/ PEI,AMI,AME,DPDX,PREF(2),PR(2),P(2),DEN,AMU,XU,XD,XP, A   3
      1XL,DX,XSTEP,CSALFA,ALPHA,XR,REORS,GAM,ZETA,PPO,TWIO,YSTART,USUP,ID  A   4
      2IMEN,IHEAT,Z,TO,INTG/I/N,NP1,NP2,NP3,NEQ,NPH,KEX,KIN,KASE,KRAD/B/B  A   5
      3ETA,GAMA(2),TAUI,TAUE,AJI(2),AJE(2),INDI(2),INDE(2)/V/U(200),F(2,2  A   6
      400),R(200),RHO(200),OM(200),Y(200)/C/SC(200),AU(200),BU(200),CU(20  A   7
      50),A(2,200),B(2,200),C(2,200)/D/YR(200),UR(200),RR(200),HR(200),XM  A   8
      6(200),PITOT(200),TEMP(200)/E/DSTAR(300),XRS(300),RWRS(300),COSAL(3  A   9
      700)                                                               A  10
      1/F/ITURB,IPRINT,TURBIN,TURBFS,IDELY
       COMMON /L/ AK,ALMG                                                 A  11
       CALLERRSET(207,256,-1,1)
       CALLERRSET(208,256,-1,1)
       CALLERRSET(209,256,-1,1)
       CALLERRSET(251,256,-1,1)
       CALLERRSET(253,256,-1,1)
       CALLERRSET(261,256,-1,1)
1      CONTINUE                                                           A  12
       AK=1.D+0                                                           A  13
       INTG=0                                                             A  14
       CALL BEGIN                                                         A  15
       AMI=0.D+0                                                          A  18
       AME=0.D+0                                                          A  19
       DX=XSTEP*YSTART
       XD=XU+DX
       GO TO 3                                                            A  20
2      CALL READY                                                         A  21
C      THE FOLLOWING STATEMENT IS TO KILL SHOT IF PROBLEMS (LIKE MERGING) A  22
C      OCCUR IN SUBROUTINE READY                                         A  23
       IF (XD.GT.XL) GO TO 13                                            A  24
3      CONTINUE                                                           A  25
       DO 5 M=1,NP3
       IF(U(NP3-M)/U(NP3).LT.0.99D+0)GO TO 4
5      CONTINUE
4      L=NP3-M
       DELTA=Y(L)+(0.99D+0-U(L)/U(NP3))*(Y(L+1)-Y(L))/((U(L+1)-U(L))/U(NP
      *3))
       DSTAR(300)=DELTA
       INTG=INTG+1                                                        A  26
       XD=XU+DX
       CALL PRE (XD,DPDX)                                                 A  39
       CALL ENTRN                                                         A  40
       CALL PRE (XU,DPDX)                                                 A  41
C      CHOICE OF FORWARD STEP                                            A  27
       DX=0.05D+0*PEI/(R(1)*AMI-R(NP3)*AME)
       DX=DABS(DX)
       IF(DX.GT.XSTEP*Y(NP3))DX=XSTEP*Y(NP3)
       XD=XU+DX                                                           A  29
       IF (KASE.EQ.2) GO TO 6                                            A  42
       IF (KIN.EQ.1) CALL MASS (XU,XD,AMI)                               A  43
       IF (KEX.EQ.1) CALL MASS (XU,XD,AME)                               A  44
       CALL WALL                                                          A  45
6      CALL OUTPUT                                                        A  46
       CALL PRE (XD,DPDX)                                                 A  47
       CALL COEFF                                                         A  48
```

MAIN

```
C      SETTING UP VELOCITIES AT A FREE BOUNDARY                              A   49
C      MODIFIED FOLLOWING STATEMENT FOR INTERNAL CORE FLOW                   A   50
       IF (KEX.EQ.2) U(NP3)=DSQRT(2.D+0)*DSQRT(1.D+0-PPO**((GAM-1.D+0)/GA    A   51
     *M))
       IF (KIN.EQ.2) U(1)=DSQRT(U(1)*U(1)-2.D+0*(XD-XU)*DPDX/RHO(1))         A   52
       CALL SOLVE (AU,BU,CU,U,NP3)                                          A   53
C      SETTING UP VELOCITIES AT A SYMMETRY LINE                             A   54
       IF (KIN.NE.3) GO TO 7                                                A   55
       U(1)=U(2)                                                            A   56
       IF (KRAD.EQ.0) U(1)=.75D+0*U(2)+.25D+0*U(3)                          A   57
7      IF (KEX.EQ.3) U(NP3)=.75D+0*U(NP2)+.25D+0*U(NP1)                     A   58
       IF (NEQ.EQ.1) GO TO 14                                               A   59
       DO 13 J=1,NPH                                                        A   60
       DO 8 I=2,NP2                                                         A   61
       AU(I)=A(J,I)                                                         A   62
       BU(I)=B(J,I)                                                         A   63
8      CU(I)=C(J,I)                                                         A   64
       DO 9 I=1,NP3                                                         A   65
9      SC(I)=F(J,I)                                                         A   66
       CALL SOLVE (AU,BU,CU,SC,NP3)                                         A   67
       DO 10 I=1,NP3                                                        A   68
10     F(J,I)=SC(I)                                                         A   69
       IF (KASE.EQ.2) GO TO 11                                              A   70
C      SETTING UP WALL VALUES OF F                                          A   71
       IF (KIN.EQ.1.AND.INDI(J).EQ.2) F(J,1)=((1.D+0+BETA+GAMA(J))*F(J,2)   A   72
     1-(1.D+0+BETA-GAMA(J))*F(J,3))*.5D+0/GAMA(J)                           A   73
       IF (KEX.EQ.1.AND.INDE(J).EQ.2) F(J,NP3)=((1.D+0+BETA+GAMA(J))*F(J,   A   74
     1NP2)-(1.D+0+BETA-GAMA(J))*F(J,NP1))*.5D+0/GAMA(J)                     A   75
C      SETTING UP SYMMETRY-LINE VALUES OF F                                 A   76
11     IF (KIN.NE.3) GO TO 12                                               A   77
       F(J,1)=F(J,2)                                                        A   78
       IF (KRAD.EQ.0) F(J,1)=.75D+0*F(J,2)+.25D+0*F(J,3)                    A   79
12     IF (KEX.EQ.3) F(J,NP3)=.75D+0*F(J,NP2)+.25D+0*F(J,NP1)              A   80
13     CONTINUE                                                             A   81
14     XP=XU                                                                A   82
       XU=XD                                                                A   86
       PEI=PEI+DX*(R(1)*AMI-R(NP3)*AME)                                     A   87
C      THE TERMINATION CONDITION                                            A   88
       IF (XU.LT.XL) GO TO 2                                                A   89
       IPRINT=INTG-1
       CALL READY
       CALL WALL
       CALL OUTPUT
       STOP                                                                 A   91
       END                                                                  A   92-
```

BEGIN

```
      SUBROUTINE BEGIN                                                    C    1
      IMPLICIT REAL*8(A-H,O-Z)
      COMMON /GEN/ PEI,AMI,AME,DPDX,PREF(2),PR(2),P(2),DEN,AMU,XU,XD,XP,   C    2
     1XL,DX,XSTEP,CSALFA,ALPHA,XR,REORS,GAM,ZETA,PPO,TWTO,YSTART,USUP,ID   A    4
     2IMEN,IHEAT,Z,TO,INTG/I/N,NP1,NP2,NP3,NEQ,NPH,KEX,KIN,KASE,KRAD/B/B   C    4
     3ETA,GAMA(2),TAUI,TAUE,AJI(2),AJE(2),INDI(2),INDE(2)/V/U(200),F(2,2   C    5
     400),R(200),RHO(200),OM(200),Y(200)                                  C    6
     1/F/ITURB,IPRINT,TURBIN,TURBFS,IDELY
C     PROBLEM SPECIFICATION                                               C    7
      READ(5,28)KRAD,IDIMEN,NEQ,KEX,KIN,IHEAT,ITURB,IDELY,IPRINT,N
      READ (5,29) REORS,ZETA,PR(1),GAM,ALPHA,XR,XL,USUP,YSTART,TWTO,XSTE   C    9
     1P,PR(2),TURBIN,TURBFS
C     IDIMEN=0 FOR PLANAR FLOW AND IDIMEN=1 FOR AXISYMMETRIC FLOW          C   11
C     INITIAL EDGE OF BOUNDARY LAYER IS YSTART                            C   12
      PREF(1)=PR(1)                                                       C   13
      PREF(2)=PR(2)
C     APPROXIMATE CALCULATION OF UEDGE FROM ONE DIMENSION FLOW RELATIONS   C   14
      XU=0.D+0                                                            C   20
      CALL PRE (XU,DPDX)
      UEDGE=DSQRT(2.D+0*(1.D+0-PPO**((GAM-1.D+0)/GAM)))
      KASE=2                                                              C   18
      IF (KIN.EQ.1.OR.KEX.EQ.1) KASE=1                                    C   19
      NPH=NEQ-1                                                           C   21
      NP1=N+1                                                             C   22
      NP2=N+2                                                             C   23
      NP3=N+3                                                             C   24
C     INITIAL VELOCITY PROFILE                                            C   25
      Y(1)=0.0D+0                                                         C   26
      U(1)=0.0D+0                                                         C   27
      DELU=UEDGE/DFLOAT(NP2)
      DO 1 I=2,NP3                                                        C   30
      U(I)=U(I-1)+DELU
      Y(I)=YSTART*(U(I)/UEDGE)**IDELY
1     CONTINUE                                                            C   34
      IF(ITURB.EQ.1)GO TO 30
      DO 30 I=2,NP3
      ETA=Y(I)/YSTART
      U(I)=(2.D+0*ETA-ETA*ETA)*UEDGE
30    CONTINUE
C     CALCULATION OF SLIP VELOCITIES AND DISTANCES                        C   35
      BETA=1.D+0
      GO TO (2,3,4), KIN                                                  C   37
2     U(2)=U(3)/(1.D+0+2.D+0*BETA)                                        C   38
      Y(2)=Y(3)*BETA/(2.D+0+BETA)                                         C   39
      GO TO 6                                                             C   40
3     U11=U(1)*U(1)                                                       C   41
      U13=U(1)*U(3)                                                       C   42
      U33=U(3)*U(3)                                                       C   43
      SQ=84.D+0*U11-12.D+0*U13+9.D+0*U33                                  C   44
      U(2)=(16.D+0*U11-4.D+0*U13+U33)/(2.D+0*(U(1)+U(3))+DSQRT(SQ))        C   45
      Y(2)=Y(3)*(U(2)+U(3)-2.D+0*U(1))**.5D+0/(U(2)+U(3)+U(1))            C   46
      GO TO 6                                                             C   47
4     IF (KRAD.NE.0) GO TO 5                                              C   48
      U(2)=(4.D+0*U(1)-U(3))/3.D+0                                        C   49
      Y(2)=0.D+0                                                          C   50
      GO TO 6                                                             C   51
```

```
                              BEGIN

5          U(2)=U(1)                                                         C  52
           Y(2)=Y(3)/3.D+0                                                   C  53
6          GO TO (7,8,9), KEX                                               C  54
7          U(NP2)=U(NP1)/(1.D+0+2.D+0*BETA)                                 C  55
           Y(NP2)=Y(NP3)-(Y(NP3)-Y(NP1))*BETA/(2.D+0+BETA)                  C  56
           GO TO 10                                                         C  57
8          U11=U(NP1)*U(NP1)                                                C  58
           U13=U(NP1)*U(NP3)                                                C  59
           U33=U(NP3)*U(NP3)                                                C  60
           SQ=84.D+0*U33-12.D+0*U13+9.D+0*U11                               C  61
           U(NP2)=(16.D+0*U33-4.D+0*U13+U11)/(2.D+0*(U(NP1)+U(NP3))+DSQRT(SQ)  C  62
          *)
           Y(NP2)=Y(NP3)-(Y(NP3)-Y(NP1))*(U(NP2)+U(NP1)-2.D+0*U(NP3))*.5D+0/(  C  63
          1U(NP2)+U(NP1)+U(NP3))                                            C  64
           GO TO 10                                                         C  65
9          U(NP2)=(4.D+0*U(NP3)-U(NP1))/3.D+0                               C  66
           Y(NP2)=Y(NP3)                                                    C  67
10         CONTINUE                                                         C  68
           IF (NEQ.EQ.1) GO TO 20                                           C  69
           DO 19 J=1,NPH                                                    C  70
C          INITIAL PROFILES OF OTHER DEPENDENT VARIABLES                    C  71
           CONST=UEDGE*UEDGE*TURBIN
           CONSFS=UEDGE*UEDGE*TURBFS
           TEDGE=1.D+0-UEDGE**2/2.D+0
           TAWTO=0.88D+0*(1.D+0-TEDGE)+TEDGE
           IF(IHEAT.EQ.0)TWTO=TAWTO
           DO 11 I=1,NP3                                                    C  72
           ETA=Y(I)/YSTART
           IF(J.EQ.1)F(J,I)=TWTO+(TAWTO-TWTO)*(U(I)/UEDGE)+(1.D+0-TAWTO)*
          1    (U(I)/UEDGE)**2
           IF(J.EQ.2.AND.ETA.LT.0.03D+0)F(J,I)=CONST*DERF(72.3D+0*ETA)
           IF(J.EQ.2.AND.ETA.GE.0.03D+0)F(J,I)=CONST*(1.D+0+DCOS(3.14159265D+
          10*ETA))/2.D+0+CONSFS*(ETA-0.03D+0)
           IF(J.EQ.2.AND.I.EQ.1)F(J,I)=0.D+0
11         CONTINUE                                                         C  75
C          CALCULATION OF CORRESPONDING SLIP VALUES                         C  76
           GAMA(J)=1.D+0
           GO TO (12,13,14), KIN                                           C  78
12         F(J,2)=F(J,1)+(F(J,3)-F(J,1))*(1.D+0+BETA-GAMA(J))/(1.D+0+BETA+GAM  C  79
          *A(J))
           GO TO 15                                                         C  80
13         G=(U(2)+U(3)-8.D+0*U(1))/(5.D+0*(U(2)+U(3))+8.D+0*U(1))          C  81
           GF=(1.D+0-PREF(J))/(1.D+0+PREF(J))                              C  82
           GF=(G+GF)/(1.D+0+G*GF)                                          C  83
           F(J,2)=F(J,3)*GF+(1.D+0-GF)*F(J,1)                             C  84
           GO TO 15                                                         C  85
14         F(J,2)=F(J,1)                                                    C  86
           IF (KRAD.EQ.0) F(J,2)=(4.D+0*F(J,1)-F(J,3))/3.D+0               C  87
15         GO TO (16,17,18), KEX                                           C  88
16         F(J,NP2)=F(J,NP3)+(F(J,NP1)-F(J,NP3))*(1.D+0+BETA-GAMA(J))/(1.D+0+  C  89
          1BETA+GAMA(J))                                                    C  90
           GO TO 19                                                         C  91
17         G=(U(NP2)+U(NP1)-8.D+0*U(NP3))/(5.D+0*(U(NP2)+U(NP1))+8.D+0*U(NP3)  C  92
          *)
           GF=(1.D+0-PREF(J))/(1.D+0+PREF(J))                              C  93
           GF=(G+GF)/(1.D+0+G*GF)                                          C  94
```

BEGIN

```
       F(J,NP2)=F(J,NP1)*GF+(1.D+0-GF)*F(J,NP3)                        C   95
       GO TO 19                                                        C   96
18     F(J,NP2)=(4.D+0*F(J,NP3)-F(J,NP1))/3.D+0                        C   97
19     CONTINUE                                                        C   98
20     CONTINUE                                                        C   99
       CALL DENSTY                                                     C  100
C      CALCULATION OF RADII                                            C  101
       CALL RAD (XU,R(1),CSALFA)                                       C  102
       IF (CSALFA.EQ.0.D+0.OR.KRAD.EQ.0) GO TO 22                      C  103
       DO 21 I=2,NP3                                                   C  104
21     R(I)=R(1)-Y(I)*CSALFA                                           C  105
C      CHANGE MADE IN STATEMENT NUMBER 28 FOR INTERNAL FLOW            C  106
       GO TO 24                                                        C  107
22     DO 23 I=2,NP3                                                   C  108
23     R(I)=R(1)                                                       C  109
24     CONTINUE                                                        C  110
C      CALCULATION OF OMEGA VALUES                                     C  111
       OM(1)=0.D+0                                                     C  112
       OM(2)=0.D+0                                                     C  113
       DO 25 I=3,NP2                                                   C  114
25     OM(I)=OM(I-1)+.5D+0*(RHO(I)*U(I)*R(I)+RHO(I-1)*U(I-1)*R(I-1))*(Y(I C  115
      1)-Y(I-1))                                                       C  116
       PEI=OM(NP2)                                                     C  117
       DO 26 I=3,NP1                                                   C  118
26     OM(I)=OM(I)/PEI                                                 C  119
       OM(NP2)=1.D+0                                                   C  120
       OM(NP3)=1.D+0                                                   C  121
       IF (NEQ.EQ.1) RETURN                                           C  122
       DO 27 J=1,NPH                                                   C  123
       IF (KEX.EQ.1) INDE(J)=1                                         C  124
       IF (KIN.EQ.1) INDI(J)=1                                         C  125
27     CONTINUE                                                        C  126
       RETURN                                                          C  127
C                                                                      C  128
28     FORMAT(8I1,2I3)                                                 C
29     FORMAT (8E10.0)                                                 C  130
       END                                                            C  131-
```

OUTPUT

```
      SUBROUTINE OUTPUT                                               J    1
      IMPLICIT REAL*8(A-H,O-Z)
      COMMON /GEN/ PEI,AMI,AME,DPDX,PREF(2),PR(2),P(2),DEN,AMU,XU,XO,XP,  J    2
     1XL,DX,XSTEP,CSALFA,ALPHA,XR,REORS,GAM,ZETA,PPO,TWTO,YSTART,USUP,ID  A    4
     2IMEN,IHEAT,Z,TO,INTG/V/U(200),F(2,200),R(200),RHO(200),OM(200),Y(2  J    4
     300)/C/SC(200),AU(200),BU(200),CU(200),A(2,200),B(2,200),C(2,200)/D  J    5
     4/YR(200),UR(200),RR(200),HR(200),XM(200),PITOT(200),TEMP(200)/E/DS  J    6
     5TAR(300),XRS(300),RWRS(300),COSAL(300)/I/N,NP1,NP2,NP3,NEQ,NPH,KEX  J    7
     6,KIN,KASE,KRAD/B/BETA,GAMA(2),TAUI,TAUE,AJI(2),AJE(2),INDI(2),INDE  J    8
     7(2)                                                                J    9
     1/F/ITURB,IPRINT,TURBIN,TURBFS,IDELY
      IF (INTG.NE.1) GO TO 1                                            J   10
      DO 14 I=1,NP3
  14  YR(I)=0.D+0
      AL=ALPHA*180.D+0/3.14159265D+0                                   J   11
      WRITE (6,7) (OM(I),I=1,NP3)                                      J   12
      WRITE(6,6)KRAD,IDIMEN,NEQ,KEX,KIN,IHEAT,ITURB,IDELY,IPRINT,N
      XRS(300)=0.D+0
   1  CONTINUE                                                         J   14
      IF(DFLOAT(INTG-1)/DFLOAT(IPRINT).NE.DFLOAT((INTG-1)/IPRINT))RETURN
      DPDXG=DPDX*GAM/(GAM-1.D+0)                                       J   15
      IF (KRAD.EQ.0) DS        =Y(NP3)=PEI/(R(1)*RHO(NP3)*U(NP3))
      IF (KRAD.EQ.0) GO TO 2                                           J   17
      DS        =R(1)-DSQRT(R(1)**2-2.D+0*CSALFA*(R(1)*Y(NP3)-0.5D+0*CS
     1ALFA*Y(NP3)**2-PEI/(RHO(NP3)*U(NP3))))                           J   19
      IF (CSALFA.NE.0.0D+0) DS        =DSTAR(INTG)/CSALFA
   2  CONTINUE                                                         J   21
      DO 3 I=1,NP3                                                     J   23
      TEMP(I)=F(1,I)-U(I)**2/2.D+0                                     J   24
      XM(I)=U(I)/DSQRT((GAM-1.D+0)*TEMP(I))                            J   25
      XSQ=XM(I)**2                                                     J   26
      IF (XM(I).LE.1.0D+0) PITOT(I)=(1.D+0+(GAM-1.D+0)*XSQ/2.D+0)**(GAM/  J   27
     *(GAM-1.D+0))
      IF (XM(I).LE.1.0D+0) GO TO 3                                     J   28
      PITOT(I)=((GAM+1.D+0)*XSQ/2.D+0)**(GAM/(GAM-1.D+0))              J   29
      PITOT(I)=PITOT(I)*((GAM+1.D+0)/(2.D+0*GAM*XSQ-GAM+1.D+0))**(1.D+0/  J   30
     *(GAM-1.D+0))
   3  CONTINUE                                                         J   31
      SQ2=DSQRT(2.D+0)                                                 J   32
      DO 4 I=1,NP3                                                     J   33
      PITOT(I)=PITOT(I)/PITOT(NP3)                                     J   34
      UR(I)=U(I)/U(NP3)                                                J   36
      RR(I)=F(2,I)
      HR(I)=U(I)/SQ2                                                   J   38
   4  CONTINUE                                                         J   39
      THETA=0.D+0
      DO 15 KL=3,N
  15  THETA=THETA+(TEMP(NP3)/TEMP(KL)*UR(KL)*(1.D+0-UR(KL))+
     1    TEMP(NP3)/TEMP(KL+1)*UR(KL+1)*(1.D+0-UR(KL+1)))/2.D+0*(Y(KL+1)-
     *Y(KL))
      THETA=THETA+TEMP(NP3)/TEMP(3)*UR(3)*(1.D+0-UR(3))/2.D+0*Y(3)+
     1    TEMP(NP3)/TEMP(NP1)*UR(NP1)*(1.D+0-UR(NP1))/2.D+0*(Y(NP3)-Y(
     *NP1))
      CF=TAUI/(HR(NP3)**2*RHO(NP3))
      WRITE (6,8)                                                      J   40
      WRITE(6,12)INTG,XU,Z,REORS,GAM,PR(1),ZETA,TURBIN,TURBFS,
```

OUTPUT

```
      1 USTAR(300),XL
        WRITE (6,13) AJI(1),DS           ,PEI,AME,DPDXG,DX,XRS(300),USUP,PPO,
      1 CF,THETA
        WRITE (6,9)                                                         J  44
        DO 5 I=1,NP3,2                                                       J  45
        WRITE (6,11) (Y(I),F(1,I),UR(I),HR(I),R(I),RHO(I),YR(I),XM(I),TEMP   J  46
      1(I),RR(I),PITOT(I))                                                   J  47
5       CUNTINUE                                                            J  48
        WRITE (6,10) (Y(NP3),F(1,NP3),UR(NP3),HR(NP3),R(NP3),RHO(NP3),YR(N   J  49
      1P3),XM(NP3),TEMP(NP3),RR(NP3),PITOT(NP3))                            J  50
        WRITE (6,9)                                                         J  51
        RETURN                                                              J  52
C                                                                           J  53
6       FORMAT(/////////,20X,'THE INPUT FLAGS ARE',///,25X,'KRAD   = ',I1,  J  54
      1//,25X,'IDIMEN = ',I1,//,25X,'NEQ    = ',I1,//,25X,'KEX    = ',I1,   J  55
      2//,25X,'KIN    = ',I1,//,25X,'IHEAT  = ',I1,//,25X,'ITURB  = ',I1,
      *//,25X,'IDELY  = ',I1,
      3//,25X,'IPRINT = ',I3,//25X,'N      = ',I3)
7       FORMAT(24H1THE VALUES OF OMEGA ARE/(1P10E11.4))                     J  57
8       FORMAT(1H1,4X,'INTG',9X,'XU',11X,'Z',9X,'REOHS',7X,'GAMMA',8X,'PR'  J  58
      1,9X,'ZETA',8X,'TURBI',7X,'TURBE',6X,'DELTA',9X,
      1                                  'XL'/,6X,  'QW',9X,'DS
      2TAR',8X,'PEI',9X,'AME',8X,'DP/DX',8X,'DX',8X,' REX  ',7X,'USUP',8X
      3,'P/PO',9X,'CF',8X,'THETA'/)
9       FORMAT(6X,'Y',9X,'H/HO',9X,'U/UE',8X,'U/UM',9X,'R',10X,'RHO',10X,   J  62
      1'YL ',9X,'M',11X,'T',10X,'E/HO',7X,'PITOT'/)
10      FORMAT(1P11E12.5,/)                                                 J  64
11      FORMAT(1P11E12.5)                                                   J  65
12      FORMAT(I8,4X,1P10E12.4)                                            J  66
13      FORMAT(      1P11E12.4,//)
        END                                                                 J  68-
```

75

SOURCE

```
      SUBROUTINE SOURCE (J,I,CS,DS)
      IMPLICIT REAL*8(A-H,O-Z)
      COMMON /GEN/ PEI,AMI,AME,DPDX,PREF(2),PR(2),P(2),DEN,AMU,XU,XD,XP,     A    3
     1XL,DX,XSTEP,CSALFA,ALPHA,XR,REORS,GAM,ZETA,PPO,TWTO,YSTART,USUP,ID      A    4
     2IMEN,IHEAT,Z,TO,INTG/I/N,NP1,NP2,NP3,NEQ,NPH,KEX,KIN,KASE,KRAD/B/B      A    5
     3ETA,GAMA(2),TAUI,TAUE,AJI(2),AJE(2),INDI(2),INDE(2)/V/U(200),F(2,2      A    6
     400),R(200),RHO(200),OM(200),Y(200)/C/SC(200),AU(200),BU(200),CU(20     A    7
     50),A(2,200),B(2,200),C(2,200)/D/YR(200),UR(200),RR(200),HR(200),XM     A    8
     6(200),PITOT(200),TEMP(200)/E/DSTAR(300),XRS(300),RWRS(300),COSAL(3     A    9
     700)                                                                    A   10
      IF (J.GT.1) GO TO 1
      CS=SC(I)*(U(I+1)*U(I+1)-U(I)*U(I))/(OM(I+1)-OM(I))
      CS=CS-SC(I-1)*(U(I)*U(I)-U(I-1)*U(I-1))/(OM(I)-OM(I-1))
      CS=(1.D+0-1.D+0/PREF(J))*CS/(OM(I+1)-OM(I-1))
      DS=0.D+0
      RETURN
1     CONTINUE
      IF(I.GT.3)GO TO 3
      REX=DSQRT(PPO**((1.D+0-GAM)/GAM)-1.D+0)*PPO**((GAM+1.D+0)/(2.D+0*G
     1AM)-         ZETA*(GAM-1.D+0)/GAM)
      REX=REORS*XD*REX
      XRS(300)=REX
      CON=3.10D+0-1.82D-09*REX
      IF(CON.LT.2.7D+0)CON=2.7D+0
3     CONTINUE
      DELTA=DSTAR(300)
      ETA=Y(I)/DELTA
      IF(ETA.LE.0.2D+0)YL=Y(I)
      IF(ETA.GT.0.2D+0.AND.ETA.LE.0.4D+0)YL=Y(I)/2.D+0+0.1D+0*DELTA
      IF(ETA.GT.0.4D+0.AND.ETA.LE.0.5D+0)YL=0.3D+0*Y(I)+0.18D+0*DELTA
      IF(ETA.GT.0.5D+0.AND.ETA.LE.0.6D+0)YL=-0.1D+0*Y(I)+0.38D+0*DELTA
      IF(ETA.GT.0.6D+0.AND.ETA.LE.0.7D+0)YL=-0.2D+0*Y(I)+0.44D+0*DELTA
      IF(ETA.GT.0.7D+0.AND.ETA.LE.0.8D+0)YL=-0.4D+0*Y(I)+0.58D+0*DELTA
      IF(ETA.GT.0.8D+0)YL=(-Y(I)+1.424D+0*DELTA) /2.4D+0
      YR(I)=YL
      IF (I.EQ.1.OR.I.EQ.NP3) CS=0.D+0
      IF (I.EQ.1.OR.I.EQ.NP3) GO TO 2
      CALL VEFF(I,I+1,EMU)
      CS= (U(I+1)-U(I-1))/(OM(I+1)-OM(I-1))*R(I)/PEI
      CS=CS*0.32D+0*RHO(I)*F(2,I)
      CS=CS-EMU*F(2,I)/(RHO(I)*U(I)*YL*YL)*CON
2     CONTINUE
      EEE=.32D+0*PEI/(U(I)*R(I))*((U(I+1)-U(I-1))/(OM(I+1)-OM(I-1)))
      EEE=EEE*CON*F(2,I)/(YL*YL*RHO(I)*U(I))
      DS=CS/F(2,I)-EEE
      RETURN
      END
```

READY

```
      SUBROUTINE READY                                                  E    1
      IMPLICIT REAL*8(A-H,O-Z)
      COMMON /GEN/ PEI,AMI,AME,DPDX,PREF(2),PR(2),P(2),DEN,AMU,XU,XD,XP, E    2
     1XL,DX,XSTEP,CSALFA,ALPHA,XR,REORS,GAM,ZETA,PPO,TWIO,YSTART,USUP,ID  A    4
     2IMEN,IHEAT,Z,TO,INTG/V/U(200),F(2,200),R(200),RHO(200),OM(200),Y(2  E    4
     300)/I/N,NP1,NP2,NP3,NEQ,NPH,KEX,KIN,KASE,KRAD/B/BETA,GAMA(2),TAUI,  E    5
     4TAUE,AJI(2),AJE(2),INDI(2),INDE(2)                                  E    6
      CALL DENSTY                                                        E    7
      CALL RAD (XU,R(1),CSALFA)                                          E    8
C     Y NEAR THE I BOUNDARY                                             E    9
      GO TO (1,2,3), KIN                                                 E   10
    1 Y(2)=(1.D+0+BETA)*OM(3)*4.D+0/((3.D+0*RHO(2)+RHO(3))*(U(2)+U(3)))  E   11
      GO TO 4                                                            E   12
    2 Y(2)=12.D+0*OM(3)/((3.D+0*RHO(2)+RHO(3))*(U(2)+U(3)+4.D+0*U(1)))   E   13
      GO TO 4                                                            E   14
    3 Y(2)=.5D+0*OM(3)/(RHO(1)*U(1))                                     E   15
    4 Y(3)=Y(2)+.25D+0*OM(3)*(1.D+0/(RHO(3)*U(3))+2.D+0/(RHO(3)*U(3)+RHO E   16
     1(2)*U(2)))                                                         E   17
C     Y 'S FOR INTERMEDIATE GRID POINTS                                 E   18
      DO 5 I=4,NP1                                                       E   19
    5 Y(I)=Y(I-1)+.5D+0*(OM(I)-OM(I-1))*(1.D+0/(RHO(I)*U(I))+1.D+0/(RHO( E   20
     1I-1)*U(I-1)))                                                      E   21
C     Y NEAR THE E BOUNDARY                                             E   22
      Y(NP2)=Y(NP1)+.25D+0*(OM(NP2)-OM(NP1))*(1.D+0/(RHO(NP1)*U(NP1))+2. E   23
     1D+0/(RHO(NP1)*U(NP1)+RHO(NP2)*U(NP2)))                             E   24
      GO TO (6,7,8), KEX                                                 E   25
    6 Y(NP3)=Y(NP2)+(1.D+0+BETA)*(OM(NP2)-OM(NP1))*4.D+0/((RHO(NP1)+3.D+ E   26
     10*RHO(NP2))*(U(NP1)+U(NP2)))                                       E   27
      GO TO 9                                                            E   28
    7 Y(NP3)=Y(NP2)+12.D+0*(OM(NP2)-OM(NP1))/((RHO(NP1)+3.D+0*RHO(NP2))* E   29
     1(U(NP2)+U(NP1)+4.D+0*U(NP3)))                                      E   30
      GO TO 9                                                            E   31
    8 Y(NP3)=Y(NP2)+.5D+0*(OM(NP2)-OM(NP1))/(RHO(NP3)*U(NP3))            E   32
    9 IF (CSALFA.EQ.0.D+0.OR.KRAD.EQ.0) GO TO 11                         E   33
C     XXX IS USED TO KILL SHOT IF NECESSARY                             E   34
      DO 10 I=2,NP3                                                      E   35
      XXX=R(1)*R(1)-2.D+0*Y(I)*PEI*CSALFA                               E   36
      IF (XXX.LT.0.0D+0) XD=2.D+0*XL                                     E   37
      IF (XXX.LT.0.0D+0) GO TO 14                                        E   38
   10 Y(I)=2.D+0*Y(I)*PEI/(R(1)+DSQRT(R(1)*R(1)-2.D+0*Y(I)*PEI*CSALFA))  E   39
C     CHANGED SIGN OF 2 IN THE DENOMINATOR OF ABOVE FOR INTERNAL FLOW    E   40
      GO TO 13                                                           E   41
   11 DO 12 I=2,NP3                                                      E   42
   12 Y(I)=PEI*Y(I)/R(1)                                                 E   43
   13 Y(2)=2.D+0*Y(2)-Y(3)                                               E   44
      Y(NP2)=2.D+0*Y(NP2)-Y(NP1)                                         E   45
C     CALCULATION OF RADII                                              E   46
      DO 14 I=2,NP3                                                      E   47
      IF (KRAD.EQ.0) R(I)=R(1)                                           E   48
      IF (KRAD.NE.0) R(I)=R(1)-Y(I)*CSALFA                               E   49
C     CHANGED SIGN IN EXPRESSION ABOVE FOR INTERNAL FLOW                E   50
   14 CONTINUE                                                           E   51
      IF (R(NP3).LE.0.0D+0) XD=2.D+0*XL                                  E   52
      IF (Y(NP3).LT.0.0D+0) XD=2.D+0*XL                                  E   53
      RETURN                                                            E   54
      END                                                               E   55-
```

VEFF

```
      SUBROUTINE VEFF (I,IP1,EMU)                                      P    1
      IMPLICIT REAL*8(A-H,O-Z)
      COMMON /GEN/ PEI,AMI,AME,DPDX,PREF(2),PR(2),P(2),DEN,AMU,XU,XD,XP, P    2
     1XL,DX,XSTEP,CSALFA,ALPHA,XR,REORS,GAM,ZETA,PPO,TWTO,YSTART,USUP,ID   A    4
     2IMEN,IHEAT,Z,TO,INTG/V/U(200),F(2,200),R(200),RHO(200),OM(200),Y(2  P    4
     300)/I/N,NP1,NP2,NP3,NEQ,NPH,KEX,KIN,KASE,KRAD                       P    5
      T=F(1,I)-U(I)**2/2.D+0                                             P    6
      TT=F(1,IP1)-U(IP1)**2/2.D+0                                        P    7
      T=(T+TT)/2.D+0                                                     P    8
      EMU=T**ZETA/(REORS/DSQRT(2.D+0))                                  P    9
      IF (I.EQ.1.OR.I.EQ.NP3) RETURN
      EE=0.3D+0*RHO(I)*F(2,I)*PEI
      EE=EE/(RHO(I)*U(I)*R(I)*(U(I+1)-U(I-1))/(OM(I+1)-OM(I-1)))
      EMU=EMU+EE
      RETURN                                                            P   10
      END                                                               P   11-
```

VISCO

```
      FUNCTION VISCO (I)                                                Q    1
      IMPLICIT REAL*8(A-H,O-Z)
      COMMON /GEN/ PEI,AMI,AME,DPDX,PREF(2),PR(2),P(2),DEN,AMU,XU,XD,XP, Q    2
     1XL,DX,XSTEP,CSALFA,ALPHA,XR,REORS,GAM,ZETA,PPO,TWTO,YSTART,USUP,ID   A    4
     2IMEN,IHEAT,Z,TO,INTG/V/U(200),F(2,200),R(200),RHO(200),OM(200),Y(2  Q    4
     300)/I/N,NP1,NP2,NP3,NEQ,NPH,KEX,KIN,KASE,KRAD                       Q    5
      T=F(1,I)-U(I)**2/2.D+0                                             Q    6
      VISCO=T**ZETA/(REORS/DSQRT(2.D+0))                                Q    7
      IF (I.EQ.1.OR.I.EQ.NP3) RETURN
      EE=0.3D+0*RHO(I)*F(2,I)*PEI
      EE=EE/(RHO(I)*U(I)*R(I)*(U(I+1)-U(I-1))/(OM(I+1)-OM(I-1)))
      VISCO=VISCO+EE
      RETURN                                                            Q    8
      END                                                               Q    9-
```

FBC

```
      SUBROUTINE FBC (X,J,IND,AJFS)                                      H    1
      IMPLICIT REAL*8(A-H,O-Z)
      COMMON /GEN/ PEI,AMI,AME,DPDX,PREF(2),PR(2),P(2),DEN,AMU,XU,XD,XP, H    2
     1XL,DX,XSTEP,CSALFA,ALPHA,XR,REORS,GAM,ZETA,PPO,TWTO,YSTART,USUP,ID   A    4
     2IMEN,IHEAT,Z,TO,INTG/V/U(200),F(2,200),R(200),RHO(200),OM(200),Y(2  J    4
     300)
C     TW IS PRESCRIBED IF IHEAT = 1 -- QDOT IS PRESCRIBED IF NOT 1       H    5
      IND=1                                                             H    6
      AJFS=TWTO                                                         H    7
      IF (IHEAT.EQ.1) GO TO 1                                           H    8
      IND=2                                                             H    9
      AJFS=0.0D+0                                                       H   10
    1 CONTINUE                                                          H   11
      IF (J.EQ.1) RETURN
      IND=1
      AJFS=F(J,1)
      RETURN                                                            H   12
      END                                                               H   13-
```

COEFF

```
      SUBROUTINE COEFF                                               D    1
      IMPLICIT REAL*8(A-H,O-Z)                                       D    2
      COMMON /GEN/ PEI,AMI,AME,DPDX,PREF(2),PR(2),P(2),DEN,AMU,XU,XD,XP,  D    2
     1XL,DX,XSTEP,CSALFA,ALPHA,XR,REORS,GAM,ZETA,PPO,TWTO,YSTART,USUP,ID   A    4
     2IMEN,IHEAT,Z,TO,INTG/I/N,NP1,NP2,NP3,NEQ,NPH,KEX,KIN,KASE,KRAD/B/B   D    4
     3ETA,GAMA(2),TAUI,TAUE,AJI(2),AJE(2),INDI(2),INDE(2)/V/U(200),F(2,2   D    5
     400),R(200),RHO(200),OM(200),Y(200)/C/SC(200),AU(200),BU(200),CU(20   D    6
     50),A(2,200),B(2,200),C(2,200)                                  D    7
      COMMON /L/ AK,ALMG                                             D    8
      DIMENSION G1(200), G2(200), G3(200), D(2,200), S1(200), S2(200), S   D    9
     13(200)                                                        D   10
C     CALCULATION OF SMALL C 'S                                     D   11
      DO 1 I=2,NP1                                                  D   12
      RA=.5D+0*(R(I+1)+R(I))                                        D   13
      RH=.5D+0*(RHO(I+1)+RHO(I))                                    D   14
      UM=.5D+0*(U(I+1)+U(I))                                        D   15
      CALL VEFF (I,I+1,EMU)                                         D   16
1     SC(I)=RA*RA*RH*UM*EMU/(PEI*PEI)                               D   17
C     THE CONVECTION TERM                                          D   18
      SA=R(1)*AMI/PEI                                               D   19
      SB=(R(NP3)*AME-R(1)*AMI)/PEI                                  D   20
      DX=XD-XU                                                      D   21
      DO 4 I=3,NP1                                                  D   22
      OMD=OM(I+1)-OM(I-1)                                           D   23
      P2=.25D+0/DX                                                  D   24
      P3=P2/OMD                                                     D   25
      P1=(OM(I+1)-OM(I))*P3                                         D   26
      P3=(OM(I)-OM(I-1))*P3                                         D   27
      P2=3.D+0*P2                                                   D   28
      Q=SA/OMD                                                      D   29
      R2=-SB*.25D+0                                                 D   30
      R3=R2/OMD                                                     D   31
      R1=-(OM(I+1)+3.D+0*OM(I))*R3                                  D   32
      R3=(OM(I-1)+3.D+0*OM(I))*R3                                   D   33
      G1(I)=P1+Q+R1                                                 D   34
      G2(I)=P2+R2                                                   D   35
      G3(I)=P3-Q+R3                                                 D   36
      CU(I)=-P1*U(I+1)-P2*U(I)-P3*U(I-1)                            D   37
C     THE DIFFUSION TERM                                           D   38
      AU(I)=2.D+0/OMD                                              D   39
      BU(I)=SC(I-1)*AU(I)/(OM(I)-OM(I-1))                           D   40
      AU(I)=SC(I)*AU(I)/(OM(I+1)-OM(I))                             D   41
      IF (NEQ.EQ.1) GO TO 3                                         D   42
      DO 2 J=1,NPH                                                  D   43
      C(J,I)=-P1*F(J,I+1)-P2*F(J,I)-P3*F(J,I-1)                     D   44
      CALL SOURCE (J,I,CS,D(J,I))                                   D   45
      C(J,I)=-C(J,I)+CS-F(J,I)*D(J,I)                               D   46
      A(J,I)=AU(I)/PREF(J)                                          D   47
      B(J,I)=BU(I)/PREF(J)                                          D   48
2     CONTINUE                                                      D   49
C     SOURCE TERM FOR VELOCITY EQUATION                            D   50
3     S1(I)=DPDX*DX                                                 D   51
      S2(I)=P2*S1(I)/(RHO(I)*U(I))                                  D   52
      S3(I)=P3*S1(I)/(RHO(I-1)*U(I-1))                              D   53
      S1(I)=P1*S1(I)/(RHO(I+1)*U(I+1))                              D   54
      CU(I)=-CU(I)-2.D+0*(S1(I)+S2(I)+S3(I))                        D   55
```

COEFF

```
       S1(I)=S1(I)/U(I+1)                                        D   56
       S2(I)=S2(I)/U(I)                                          D   57
       S3(I)=S3(I)/U(I-1)                                        D   58
4      CONTINUE                                                  D   59
C      COEFFICIENTS IN THE FINAL FORM                            D   60
       DO 5 I=3,NP1                                              D   61
       RL=1.D+0/(G2(I)+AU(I)*BU(I)-S2(I))                        D   62
       AU(I)=(AU(I)+S1(I)-G1(I))*RL                              D   63
       BU(I)=(BU(I)+S3(I)-G3(I))*RL                              D   64
5      CU(I)=CU(I)*RL                                            D   65
       IF (NEQ.EQ.1) GO TO 7                                     D   66
       DO 6 J=1,NPH                                              D   67
       DO 6 I=3,NP1                                              D   68
       RL=1.D+0/(G2(I)+A(J,I)*B(J,I)-D(J,I))                     D   69
       A(J,I)=(A(J,I)-G1(I))*RL                                  D   70
       B(J,I)=(B(J,I)-G3(I))*RL                                  D   71
6      C(J,I)=C(J,I)*RL                                          D   72
7      CALL SLIP                                                 D   73
       RETURN                                                    D   74
       END                                                       D   75-
```

DENSTY

```
       SUBROUTINE DENSTY                                         F    1
       IMPLICIT REAL*8(A-H,O-Z)                                  F    2
       COMMON /GEN/ PEI,AMI,AME,DPDX,PREF(2),PR(2),P(2),DEN,AMU,XU,XD,XP,   F    2
      1XL,DX,XSTEP,CSALFA,ALPHA,XR,REQRS,GAM,ZETA,PPO,TWTO,YSTART,USUP,ID    A    4
      2IMEN,IHEAT,Z,TO,INTG/V/U(200),F(2,200),R(200),RHO(200),OM(200),Y(2   F    4
      300)/I/N,NP1,NP2,NP3,NEQ,NPH,KEX,KIN,KASE,KRAD              F    5
       TNP3=F(1,NP3)-U(NP3)**2/2.D+0                             F    6
       RHONP3=TNP3**(1.D+0/(GAM-1.D+0))                          F    7
       DO 1 I=1,NP3                                              F    8
       T=F(1,I)-U(I)**2/2.D+0                                    F    9
1      RHO(I)=RHONP3*TNP3/T                                      F   10
       RETURN                                                    F   11
       END                                                       F   12-
```

80

ENTRN

```
          SUBROUTINE ENTRN                                          G    1
          IMPLICIT REAL*8(A-H,O-Z)
          COMMON /GEN/ PEI,AMI,AME,DPDX,PREF(2),PR(2),P(2),DEN,AMU,XU,XD,XP,   G    2
         1XL,DX,XSTEP,CSALFA,ALPHA,XR,REORS,GAM,ZETA,PPO,TWTO,YSTART,USUP,ID   A    4
         2IMEN,IHEAT,Z,TO,INTG/V/U(200),F(2,200),R(200),RHO(200),OM(200),Y(2   G    4
         300)/I/N,NP1,NP2,NP3,NEQ,NPH,KEX,KIN,KASE,KRAD                        G    5
    1     GO TO (2,3,6), KEX                                       G    6
    2     RETURN                                                   G    7
    3     CONTINUE                                                 G    8
    C     THE FOLLOWING AME IS FOR LAMINAR FLOW                    G    9
          IF (INTG.NE.1) GO TO 5                                   G   10
          DO 4 I=1,NP3                                             G   11
          IF (OM(I).GT.0.9D+0) N9=I                                G   12
          IF (OM(I).GT.0.9D+0) I=NP3                               G   13
    4     CONTINUE                                                 G   14
          DOM=OM(N9)-OM(N9-1)                                      G   15
          DOM9=OM(N9)-0.9D+0                                       G   16
    5     CONTINUE                                                 G   17
          U9=U(N9)-DOM9/DOM*(U(N9)-U(N9-1))                        G   18
          TERMB=(U(N9)-U(N9-1))/DOM                                G   19
          R9=R(N9)-DOM9/DOM*(R(N9)-R(N9-1))                        G   20
          RHO9=RHO(N9)-DOM9/DOM*(RHO(N9)-RHO(N9-1))                G   21
          VIS9=VISCO(N9)-DOM9/DOM*(VISCO(N9)-VISCO(N9-1))          G   22
          CUUP=R(N9)*R(N9)*RHO(N9)*U(N9)*VISCO(N9)                 G   23
          CUUP=CUUP+R9*R9*RHO9*U9*VIS9                             G   24
          CUUP=CUUP/(2.D+0*PEI)                                    G   25
          CUUM=R(N9-1)*R(N9-1)*RHO(N9-1)*U(N9-1)*VISCO(N9-1)       G   26
          CUUM=CUUM+R9*R9*RHO9*U9*VIS9                             G   27
          CUUM=CUUM/(2.D+0*PEI)                                    G   28
          G5=2.D+0*CUUP/(DOM*DOM9)                                 G   29
          G6=2.D+0*CUUM/(DOM*(0.9D+0-OM(N9-1)))                    G   30
          TERMA=G5*(U(N9)-U9)-G6*(U9-U(N9-1))                      G   31
          TERMA=TERMA/TERMB                                        G   32
          U9WIG=USUP*DSQRT(2.D+0)*DSQRT(1.D+0-PPO**((GAM-1.D+0)/GAM))   G   33
    C     USUP IS READ-IN IN BEGIN     IT SUPPRESSES THE B.L.      G   34
          TERMC=(U9WIG-U9)/DX*DPDX/(RHO9*U9)                       G   35
          TERMC=TERMC*PEI/TERMB                                    G   36
          AME=TERMA-TERMC                                          G   37
          AME=AME-0.1D+0*R(1)*AMI                                  G   38
          AME=AME/(0.9D+0*R(NP3))                                  G   39
          RETURN                                                   G   40
    6     AME=0.D+0                                                G   41
          RETURN                                                   G   42
          END                                                      G   43=
```

81

MASS

```
      SUBROUTINE MASS (XU,XD,AM)                                          I    1
      IMPLICIT REAL*8(A-H,O-Z)
C     APPLICABLE TO AN IMPERMEABLE-WALL SITUATION                        I    2
      AM=0.D+0                                                            I    3
      RETURN                                                             I    4
      END                                                                I    5-
```

PRE

```
      SUBROUTINE PRE (X,DPDXX)                                          K    1
      IMPLICIT REAL*8(A-H,O-Z)
      COMMON /GEN/ PEI,AMI,AME,DPDX,PREF(2),PR(2),P(2),DEN,AMU,XU,XD,XP, K    2
     1XL,DX,XSTEP,CSALFA,ALPHA,XR,REORS,GAM,ZETA,PPO,TWTO,YSTART,USUP,ID  A    4
     2IMEN,IHEAT,Z,TO,INTG/V/U(200),F(2,200),R(200),RHO(200),OM(200),Y(2 K    4
     300)/I/N,NP1,NP2,NP3,NEQ,NPH,KEX,KIN,KASE,KRAD                      K    5
      DIMENSION XX(300), POP(300)                                        K    6
      IF (INTG.NE.0) GO TO 1                                             K    7
      READ (5,3) LMAX                                                    K    8
      READ (5,4) (XX(L),POP(L),L=1,LMAX)                                 K    9
      WRITE (6,5)                                                        K   10
      WRITE (6,6) (XX(L),POP(L),L,L=1,LMAX)                             K   11
1     CONTINUE                                                          K   12
      L=1                                                               K   13
2     CONTINUE                                                          K   14
      L=L+1                                                             K   15
      IF (XX(L).LT.X) GO TO 2                                           K   16
      DPDX=(POP(L)-POP(L-1))/(XX(L)-XX(L-1))                            K   17
      PPO=POP(L-1)+DPDX*(X-XX(L-1))                                     K   18
      DPDXX=DPDX                                                        K   19
      DPDXX=DPDX*(GAM-1.D+0)/GAM                                        K   20
      RETURN                                                            K   21
C                                                                       K   22
3     FORMAT(I3)                                                        K   23
4     FORMAT(2E12.0)                                                    K   24
5     FORMAT(1H1,/,8X,'X',12X,'P/PO',/)                                K   25
6     FORMAT(1P2E14.5,I6)                                              K   26
      END                                                               K   27-
```

RAD

```
      SUBROUTINE RAD (X,R1,CALPHA)                                  L   1
      IMPLICIT REAL*8(A-H,O-Z)
      COMMON /GEN/ PEI,AMI,AME,DPDX,PREF(2),PR(2),P(2),DEN,AMU,XU,XD,XP,   L   2
     1XL,DX,XSTEP,CSALFA,ALPHA,XR,REORS,GAM,ZETA,PPO,TWTO,YSTART,USUP,ID   A   4
     2IMEN,IHEAT,Z,TO,INTG/V/U(200),F(2,200),R(200),RHO(200),OM(200),Y(2   L   4
     300)/I/N,NP1,NP2,NP3,NEQ,NPH,KEX,KIN,KASE,KRAD                        L   5
C     APPLICABLE TO NOZZLES WITH CONSTANT LONGITUDINAL RADIUS OF           L   6
C     CURVATURE OF THE CONVERGING SECTION- CONSTANT WALL HALF ANGLE OF     L   7
C     DIVERGING SECTION-AND WALL SLOPES MATCHED DOWNSTREAM OF THE THROAT   L   8
      IF (INTG.NE.0) GO TO 1                                              L   9
      PI2=3.141592650+0/2.D+0                                            L  10
      ALPHA=ALPHA*PI2/90.D+0                                             L  11
      COSALF=DCOS(ALPHA)                                                 L  12
      SINALF=DSIN(ALPHA)                                                 L  13
      ZWIG=XR*(1.D+0+SINALF)                                             L  14
      XWIG=XR*(PI2+ALPHA)                                                L  15
      RWIG=1.D+0+XR*(1.D+0-COSALF)                                       L  16
1     CONTINUE                                                            L  17
      IF (X.GE.XWIG) GO TO 2                                             L  18
      R(1)=1.D+0+XR*(1.D+0-DSIN(X/XR))                                   L  19
      CSALFA=DSIN(X/XR)                                                  L  20
      CALPHA=CSALFA                                                       L  21
      R1=R(1)                                                             L  22
      ZZ=XR*(1.D+0-DCOS(X/XR))                                           L  23
      GO TO 3                                                             L  24
2     CONTINUE                                                            L  25
      R(1)=(X-XWIG)*SINALF+RWIG                                          L  26
      CSALFA=COSALF                                                       L  27
      CALPHA=CSALFA                                                       L  28
      R1=R(1)                                                             L  29
      ZZ=(X-XWIG)*CSALFA+ZWIG                                            L  30
3     CONTINUE                                                            L  31
      IF(IDIMEN.EQ.0)R1=1.D+0
      ZZ=ZZ-XR                                                            L  32
      Z=ZZ                                                                L  33
      RETURN                                                              L  34
      END                                                                 L  35-
```

83

SLIP

```
      SUBROUTINE SLIP                                              M    1
      IMPLICIT REAL*8(A-H,O-Z)                                     M    2
      COMMON /GEN/ PEI,AMI,AME,DPDX,PREF(2),PR(2),P(2),DEN,AMU,XU,XD,XP,  M    2
     1XL,DX,XSTEP,CSALFA,ALPHA,XR,REORS,GAM,ZETA,PPO,TWTO,YSTART,USUP,ID  A    4
     2IMEN,IHEAT,Z,TO,INTG/I/N,NP1,NP2,NP3,NEQ,NPH,KEX,KIN,KASE,KRAD/V/U  M    4
     3(200),F(2,200),R(200),RHO(200),OM(200),Y(200)/B/BETA,GAMA(2),TAUI,  M    5
     4TAUE,AJI(2),AJE(2),INDI(2),INDE(2)                           M    6
      COMMON /L/ AK,ALMG/C/SC(200),AU(200),BU(200),CU(200),A(2,200),B(2,  M    7
     1200),C(2,200)                                                M    8
C     SLIP COEFFICIENTS NEAR THE I BOUNDARY FOR VELOCITY EQUATION  M    9
      CU(2)=0.D+0                                                  M   10
      CU(NP2)=0.D+0                                                M   11
      GO TO (1,2,3), KIN                                           M   12
1     BU(2)=0.D+0                                                  M   13
      AU(2)=1.D+0/(1.D+0+2.D+0*BETA)                               M   14
      GO TO 5                                                      M   15
2     SQ=84.D+0*U(1)*U(1)-12.D+0*U(1)*U(3)+9.D+0*U(3)*U(3)         M   16
      BU(2)=8.D+0*(2.D+0*U(1)+U(3))/(2.D+0*U(1)+7.D+0*U(3)+DSQRT(SQ))  M   17
      AU(2)=1.D+0-BU(2)                                            M   18
      GO TO 5                                                      M   19
3     BU(2)=0.D+0                                                  M   20
      CALL VEFF (2,3,EMU)                                          M   21
      AK1=1.D+0/DX-DPDX/(RHO(1)*U(1)*U(1))                         M   22
      AK2=-U(1)*AK1+DPDX/(RHO(1)*U(1))                             M   23
      AJ=RHO(1)*U(1)*.25D+0*(Y(2)+Y(3))**2/EMU                     M   24
      IF (KRAD.EQ.0) GO TO 4                                       M   25
      AU(2)=2.D+0/(2.D+0+AJ*AK1)                                   M   26
      CU(2)=-.5D+0*AJ*AK2*AU(2)                                    M   27
      GO TO 5                                                      M   28
4     CU(2)=1.D+0/(2.D+0+3.D+0*AJ*AK1)                             M   29
      AU(2)=CU(2)*(2.D+0-AJ*AK1)                                   M   30
      CU(2)=-CU(2)*4.D+0*AJ*AK2                                    M   31
C     SLIP COEFFICIENTS NEAR THE E BOUNDARY FOR VELOCITY EQUATION  M   32
5     GO TO (6,7,8), KEX                                           M   33
6     AU(NP2)=0.D+0                                                M   34
      BU(NP2)=1.D+0/(1.D+0+2.D+0*BETA)                             M   35
      GO TO 9                                                      M   36
7     SQ=84.D+0*U(NP3)*U(NP3)-12.D+0*U(NP3)*U(NP1)+9.D+0*U(NP1)*U(NP1)  M   37
      AU(NP2)=8.D+0*(2.D+0*U(NP3)+U(NP1))/(2.D+0*U(NP3)+7.D+0*U(NP1)+DSQ  M   38
     *RT(SQ))                                                      M
      BU(NP2)=1.D+0-AU(NP2)                                        M   39
      GO TO 9                                                      M   40
8     AU(NP2)=0.D+0                                                M   41
      CALL VEFF (NP1,NP2,EMU)                                      M   42
      BK1=1.D+0/DX-DPDX/(RHO(NP3)*U(NP3)*U(NP3))                   M   43
      BK2=-U(NP3)*BK1+DPDX/(RHO(NP3)*U(NP3))                       M   44
      BJ=RHO(NP3)*U(NP3)*.25D+0*(2.D+0*Y(NP3)-Y(NP1)-Y(NP2))**2/EMU  M   45
      CU(NP2)=1.D+0/(2.D+0+3.D+0*BJ*BK1)                           M   46
      BU(NP2)=CU(NP2)*(2.D+0-BJ*BK1)                               M   47
      CU(NP2)=-CU(NP2)*4.D+0*BJ*BK2                                M   48
9     IF (NEQ.EQ.1) RETURN                                         M   49
C     SLIP COEFFICIENTS NEAR THE I BOUNDARY FOR OTHER EQUATIONS    M   50
      DO 20 J=1,NPH                                                M   51
      C(J,2)=0.D+0                                                 M   52
      C(J,NP2)=0.D+0                                               M   53
      GO TO (10,12,13), KIN                                        M   54
```

SLIP

```
   10      CALL FBC (XD,J,INDI(J),QI)                                   M   55
           IF (INDI(J).EQ.1) GO TO 11                                   M   56
           AJI(J)=QI                                                    M   57
           A(J,2)=1.D+0                                                 M   58
           B(J,2)=0.D+0                                                 M   59
           C(J,2)=8.D+0*(1.D+0+2.D+0*BETA)*PREF(J)*AJI(J)/(AK*AK*BETA*(1.D+0+  M   60
          1BETA)*(1.D+0+BETA)*(3.D+0*RHO(2)+RHO(3))*U(3))               M   61
           GO TO 15                                                     M   62
   11      F(J,1)=QI                                                    M   63
           A(J,2)=(1.D+0+BETA-GAMA(J))/(1.D+0+BETA+GAMA(J))             M   64
           B(J,2)=1.D+0-A(J,2)                                          M   65
           GO TO 15                                                     M   66
   12      A(J,2)=(U(2)+U(3)-8.D+0*U(1))/(5.D+0*(U(2)+U(3))+8.D+0*U(1))  M   67
           GF=(1.D+0-PREF(J))/(1.D+0+PREF(J))                           M   68
           A(J,2)=(A(J,2)+GF)/(1.D+0+A(J,2)*GF)                         M   69
           B(J,2)=1.D+0-A(J,2)                                          M   70
           GO TO 15                                                     M   71
   13      B(J,2)=0.D+0                                                 M   72
           CALL SOURCE (J,1,CS,DS)                                      M   73
           AK1=1.D+0/DX-DS                                              M   74
           AK2=-AK1*F(J,1)-CS                                           M   75
           AJF=AJ*PREF(J)                                               M   76
           IF (KRAD.EQ.0) GO TO 14                                      M   77
           A(J,2)=2.D+0/(2.D+0+AJF*AK1)                                 M   78
           C(J,2)=-.5D+0*AJF*AK2*A(J,2)                                 M   79
           GO TO 15                                                     M   80
   14      C(J,2)=1.D+0/(2.D+0+3.D+0*AJF*AK1)                           M   81
           A(J,2)=C(J,2)*(2.D+0-AJF*AK1)                                M   82
           C(J,2)=-C(J,2)*4.D+0*AJF*AK2                                 M   83
   C       SLIP COEFFICIENTS NEAR THE E BOUNDARY FOR OTHER EQUATIONS    M   84
   15      GO TO (16,18,19), KEX                                        M   85
   16      CALL FBC (XD,J,INDE(J),QE)                                   M   86
           IF (INDE(J).EQ.1) GO TO 17                                   M   87
           AJE(J)=QE                                                    M   88
           B(J,NP2)=1.D+0                                               M   89
           A(J,NP2)=0.D+0                                               M   90
           C(J,NP2)=-8.D+0*(1.D+0+2.D+0*BETA)*PREF(J)*AJE(J)/(AK*AK*BETA*(1.D  M   91
          1+0+BETA)*(1.D+0+BETA)*(RHO(NP1)+3.D+0*RHO(NP2))*U(NP1))      M   92
           GO TO 20                                                     M   93
   17      F(J,NP3)=QE                                                  M   94
           B(J,NP2)=(1.D+0+BETA-GAMA(J))/(1.D+0+BETA+GAMA(J))           M   95
           A(J,NP2)=1.D+0-B(J,NP2)                                      M   96
           GO TO 20                                                     M   97
   18      B(J,NP2)=(U(NP2)+U(NP1)-8.D+0*U(NP3))/(5.D+0*(U(NP2)+U(NP1))+8.D+0  M   98
          **U(NP3))                                                     M   98
           GF=(1.D+0-PREF(J))/(1.D+0+PREF(J))                           M   99
           B(J,NP2)=(B(J,NP2)+GF)/(1.D+0+B(J,NP2)*GF)                   M  100
           A(J,NP2)=1.D+0-B(J,NP2)                                      M  101
           GO TO 20                                                     M  102
   19      A(J,NP2)=0.D+0                                               M  103
           CALL SOURCE (J,NP3,CS,DS)                                    M  104
           BK1=1.D+0/DX-DS                                              M  105
           BK2=-BK1*F(J,NP3)-CS                                         M  106
           BJF=BJ*PREF(J)                                               M  107
           C(J,NP2)=1.D+0/(2.D+0+3.D+0*BJF*BK1)                         M  108
           B(J,NP2)=C(J,NP2)*(2.D+0-BJF*BK1)                            M  109
```

SLIP

```
         C(J,NP2)=-C(J,NP2)*4.D+0*BJF*BK2                                    M 110
   20    CONTINUE                                                            M 111
         RETURN                                                             M 112
         END                                                                M 113-
```

SOLVE

```
         SUBROUTINE SOLVE (A,B,C,F,NP3)                                      N  1
         IMPLICIT REAL*8(A-H,O-Z)                                           N  2
   C     THIS SOLVES EQUATIONS OF THE FORM                                   N  2
   C     F(I) = A(I)*F(I+1) + B(I)*F(I-1) + C(I)                             N  3
   C     FOR I=2,NP2                                                         N  4
         DIMENSION A(NP3), B(NP3), C(NP3), F(NP3)                            N  5
         NP2=NP3-1                                                           N  6
         B(2)=B(2)*F(1)+C(2)                                                 N  7
         DO 1 I=3,NP2                                                        N  8
         T=1.D+0/(1.D+0-B(I)*A(I-1))                                         N  9
         A(I)=A(I)*T                                                         N 10
   1     B(I)=(B(I)*B(I-1)+C(I))*T                                           N 11
         DO 2 I=2,NP2                                                        N 12
         J=NP2-I+2                                                           N 13
   2     F(J)=A(J)*F(J+1)+B(J)                                               N 14
         RETURN                                                             N 15
         END                                                                N 16-
```

WALL

```
         SUBROUTINE WALL                                                     R  1
         IMPLICIT REAL*8(A-H,O-Z)                                           R  1
         COMMON /GEN/ PEI,AMI,AME,DPDX,PREF(2),PR(2),P(2),DEN,AMU,XU,XD,XP,   R  2
        1XL,DX,XSTEP,CSALFA,ALPHA,XR,REORS,GAM,ZETA,PPO,TWTO,YSTART,USUP,ID    A  4
        2IMEN,IHEAT,Z,TO,INTG/V/U(200),F(2,200),R(200),RHO(200),OM(200),Y(2   R  4
        300)/I/N,NP1,NP2,NP3,NEQ,NPH,KEX,KIN,KASE,KRAD/B/BETA,GAMA(2),TAUI,   R  5
        4TAUE,AJI(2),AJE(2),INDI(2),INDE(2)                                   R  6
   C     CALCULATION OF BETA FOR THE I BOUNDARY                              R  7
   1     YI=.5D+0*(Y(2)+Y(3))                                                R  8
         UI=.5D+0*(U(2)+U(3))                                                R  9
         RH=.25D+0*(3.D+0*RHO(2)+RHO(3))                                     R 10
         RE=RH*UI*YI/VISCO(1)                                                R 11
         FP=DPDX*YI/(RH*UI*UI)                                               R 12
         AM=AMI/(RH*UI)                                                      R 13
   C     FOR LAMINAR FLOW AND AM=0 (NEED DIFFERENT EXPRESSION IF F=0)        R 14
         S=1.D+0/RE-FP/2.D+0                                                 R 15
         BETA=RE*(S+FP+AM)                                                   R 16
         TAUI=S*RH*UI*UI                                                     R 17
         IF (NEQ.EQ.1) RETURN                                                R 18
   C     CALCULATION OF GAMA 'S FOR THE I BOUNDARY                           R 19
         DO 2 J=1,NPH                                                        R 20
   C     FOR LAMINAR FLOW AND LIMITING ZERO AM                              R 21
         SF=1.D+0/(PR(J)*RE)                                                 R 22
         GAMA(J)=RE*PR(J)*(SF+AM)                                            R 23
         IF (INDI(J).EQ.1) AJI(J)=SF*RH*UI*(2.D+0*F(J,1)-F(J,2)-F(J,3))*.5D   R 24
        *+0
   2     CONTINUE                                                            R 25
         RETURN                                                             R 26
         END                                                                R 27-
```

The following is an example input to the boundary-layer computer code.
See subroutines BEGIN and PRE for input formats.

00321004150087							
2.880E 05	.667	.85	1.4	.0	.0	642.	.9999
.1	1.0	.1	.85	.01	.000001		
022							
0.0	.5283						
32.1	.4398						
64.2	.3609						
96.3	.3012						
128.4	.2533						
160.5	.2151						
192.6	.1850						
224.7	.1612						
256.8	.1470						
288.9	.1370						
321.	.1278						
353.1	.1220						
385.2	.1128						
417.3	.1077						
449.4	.1027						
481.5	.1003						
513.6	.0965						
545.7	.0950						
577.8	.0943						
609.9	.0935						
642.	.0935						
9000.	.0935						

APPENDIX B
DATA REDUCTION COMPUTER CODE

MAIN

```
C     THIS IS A DATA REDUCTION PROGRAM
C     INPUT IS PT1, TW/TO, XME, GAMMA, REYNOLDS NUMBER PER FOOT, AND
C        PT2 DISTRIBUTION
C     UNITS OF PT1 AND PT2 MUST BE CONSISTENT
C     THE INPUT XME IS FOR A FIRST GUESS ONLY
C     IF THE INPUT TW/TO IS ZERO THEN THE WALL IS TAKEN AS ADIABATIC
C     OUTPUT IS VELOCITY, TEMPERATURE, BOUNDARY-LAYER THICKNESS, BOUNDARY-
C        LAYER DISPLACEMENT THICKNESS, BOUNDARY-LAYER NOMEMTUM THICKNESS,
C        SHAPE FACTOR, MACH NUMBER, TBAR, AND SKIN FRICTION
C     HEAT FLUX CAN ALSO BE DETERMINED (SEE THE CORRESPONDING LAB REPORT)
      DIMENSION Y(100),PT2(100),PT2P1(100),XM(100),TOTOE(100)
      DIMENSION U(100),T(100),TBAR(100),RHO(100),RHOU(100)
      DIMENSION CF(100),CCC(100),CC(100)
      CF(1)=.001
      READ(5,2)NUM
      DO 10 LL=1,NUM
      READ(5,1) PT1,TWTO,XME,G,R
      READ(5,2)NE
      READ(5,3)(Y(N),PT2(N),N=1,NE)
C     READ(5,1) PT1,TWTO,XME,G,R
C     READ(5,2)NE
C     READ(5,3)(Y(N),PT2(N),N=1,NE)
1     FORMAT(8E10.0)
2     FORMAT(I3)
3     FORMAT(2E10.0)
      GP1=G+1.
      GM1=G-1.
      D=(GP1/2.)**(G/GM1)
      IF(XME.LE.1.)XME=SQRT(2./GM1*((PT1/PT2(1))**(GM1/G)-1.))
      XE=XME*XME
      IF(XME.GT.1.) CALL XEDGE(PT2(NE),PT1,G,XME,XE)
      P1=PT1/(1.+GM1*XE/2.)**(G/GM1)
      PT2(1)=P1
      X=XE
      XM(NE)=SQRT(XE)
      DO 4 N=1,NE
4     PT2P1(N)=PT2(N)/P1
      J = NE-1
      DO 5 N=1,J
      I=NE-N
      IF(PT2P1(I).LE.D)X=2./GM1* (PT2P1(I)**(GM1/G)-1.)
      IF(PT2P1(I).GT.D) CALL XDIST(PT2P1(I),G,X)
      XM(I)=SQRT(X)
5     CONTINUE
      XME=XM(NE)
      A=GM1*XME*XME
      CALL PR(XME,G,A,P)
      HW=TWTO*(1.+A/2.)
      C1=1.+A/2.-HW
      IF(TWTO.EQ.0.)C1=0.
      D=SQRT(2.*A*HW+C1*C1)
      IF(TWTO.EQ.0.)D=SQRT(A*2.*(1.+A/2.))
      U(1)=0.
      DO 7 K=1,NE
      C=(XM(K)/XM(NE))**2
      CALL VT(A,HW,C1,D,P,C,T(K),U(K))
```

MAIN

```
        CALL TEMP(A,HW,C1,Q,P,U(K),DHDV,T(K))
        IF(K.EQ.1)T(K)=HW
        TBAR(K)=(T(K)+A*U(K)*U(K)/2.-HW)/(1.+A/2.-HW)
        RHO(K)=1./T(K)
        RHOU(K)=RHO(K)*U(K)
        CCC(K)=1.-RHOU(K)
        CC(K)=RHOU(K)*(1.-U(K))
        TOTOE(K)=(T(K)+A*U(K)*U(K)/2.)/(1.+A/2.)
        IF (K.NE.1) CF(K)=CF(K-1)
        IF(K.NE.1)CALL SKIN(R,CF(K),G,XME,Y(K),U(K))
        T(K+1)=T(K)
7       CONTINUE
        PT2PT1=PT2(NE)/PT1
        CALL SUM(Y,CCC,NE,VINT1)
        CALL SUM(Y,CC,NE,VINT2)
        CALL CFI(XME,R,VINT2,SQCF)
        CALL PLUS      (SQCF, Y,RHO,R,NE,CCC,CC,VINT1,VINT2,A,HW,C1,Q,P)
        CFF=SQCF*SQCF
        SHAPE=VINT1/VINT2
        DO 15 M=1,NE
        IF(U(M).GT.0.99)GO TO 16
15      CONTINUE
16      DELTA=Y(M-1)+(0.99-U(M-1))*(Y(M)-Y(M-1))/(U(M)-U(M-1))
        IF(TWTO.EQ.0.)WRITE(6,11)P,G,PT2PT1,R,DELTA,VINT1,VINT2,SHAPE,CFF
11      FORMAT(1H1,39X,'THIS DATA REDUCTION SHOT IS FOR AN ADIABATIC WALL'
       1 ,//  ,40X,'RECOVERY FACTOR = 0.8800',//,40X,'PRANDTL NUMBER = ',
       2  F6.4,//,40X,'GAMMA = ',F6.4,//,40X,'PT2E/PT1 = ',1PE10.4,//,
       3 40X,'FREE-STREAM UNIT REYNOLDS NO. PER FOOT = ',1PE10.4,//,
       4 40X,'DELTA(IN) =', 1PE11.4,//,40X,'DELTA STAR(IN) =', 1PE11.4,//,
       5 40X,'THETA(IN) =', 1PE11.4,//,40X,'SHAPE FACTOR =', 1PE11.4,//,
       6 40X,'CF (BASED ON RE-THETA EQ OF R. & M. REP. NO. 3712) =',
       7 1PE11.4,///)
        IF(TWTO.NE.0.)WRITE(6,12)P,G,PT2PT1,R,DELTA,VINT1,VINT2,SHAPE,CFF
12      FORMAT(1H1,39X,'THIS DATA REDUCTION SHOT IS FOR A NON-ADIABATIC WA
       1LL',//,40X,'RECOVERY FACTOR = 0.8800',//,40X,'PRANDTL NUMBER = ',
       2  F6.4,//,40X,'GAMMA = ',F6.4,//,40X,'PT2E/PT1 = ',1PE10.4,//,
       3 40X,'FREE-STREAM UNIT REYNOLDS NO. PER FOOT = ',1PE10.4,//,
       4 40X,'DELTA(IN) =', 1PE11.4,//,40X,'DELTA STAR(IN) =', 1PE11.4,//,
       5 40X,'THETA(IN) =', 1PE11.4,//,40X,'SHAPE FACTOR =', 1PE11.4,//,
       6 40X,'CF (BASED ON RE-THETA EQ OF R. & M. REP. NO. 3712) =',
       7 1PE11.4,///)
        WRITE(6,8)
8       FORMAT(    /,7X,'Y',11X,'PT2',8X,'TO/TOE',10X,'M',10X,'U/UE', 9X,
       1 'T/TE', 9X,'TBAR',7X,'RHO/RHOE',2X,'RHO*U/(RHOE*UE)',4X,'CF',/)
        WRITE(6,6)(Y(N),PT2(N),TOTOE(N),XM(N),U(N),T(N),TBAR(N),RHO(N),
       1RHOU(N),CF(N),N=1,NE)
6       FORMAT (1P10E13.5)
        WRITE(6,18)
18      FORMAT(///)
10      CONTINUE
        STOP
        END
```

XEDGE

```
      SUBROUTINE XEDGE(W,Z,G,Y,X)
      X=Y*Y
      GP1=G+1.
      GM1=G-1.
      C=W/Z
1     F=(GP1*X/(GM1*X+2.))**(G/GM1)*(GP1/(2.*G*X-GM1))**(1./GM1)-C
      DFDX=(F+C)*G/GM1*(          2./(X*(GM1*X+2.))-2./(2.*G*X-GM1))
      XNEW=X-F/DFDX
      IF(ABS((X-XNEW)/XNEW).LT.0.0001)GO TO 2
      X=XNEW
      GO TO 1
2     X=XNEW
      RETURN
      END
```

XDIST

```
      SUBROUTINE XDIST(B,G,X)
      GP1=G+1.
      GM1=G-1.
1     F=(GP1*X/2.)**(G/GM1)*(GP1/(2.*G*X-GM1))**(1./GM1)-B
      DFDX=(F+B)*G/X*(2.*X-1.)/(2.*G*X-GM1)
      XNEW=X-F/DFDX
      IF(ABS((X-XNEW)/XNEW).LT.0.0001)GO TO 2
      X=XNEW
      GO TO 1
2     X=XNEW
      RETURN
      END
```

PR

```
      SUBROUTINE PR(XM,G,A,P)
C     CALCULATES PRANDTL NUMBER FOR A RECOVERY FACTOR OF 0.88
      R=.88
      AL=5.*7./2.
      AL1=AL+1.
      AL2=AL+2.
      BE=4.*AL
      A=(G-1.)*XM*XM
      D=SQRT(2.*A*(1.+A/2.))
      CALL TINYF(A,HW,0.,D,0.,F0)
      CALL TINYF(A,HW,0.,D,1.,F1)
      HONE=A*BE/(AL1*AL2)+A/2.+F1-F0
      P=1.-A*(R-1.)/(2.*HONE)
      RETURN
      END
```

SKIN

```
SUBROUTINE SKIN (R,CF,GAM,XM,Y,U)
C1=5.75
C2=5.10
OMEGA=.768
RE=R*Y/12.
X=SQRT(CF/2.)
Z=1.+.88*((GAM-1.)/2.)*XM**2
Z=SQRT(Z)
SIGMA=(((GAM-1.)/2.)*XM**2)/(1.+(((GAM-1.)/2.)*XM**2))
SQSIG=SQRT(SIGMA)
1 GA=C1*ALOG10(RE*X*Z**(-2.*(.5+OMEGA)))+C2
G=GA-(1./(SQSIG*X*Z))*ARSIN(SQSIG*U)
DGDX=(C1/(2.3*X))+(1./(SQSIG*(X**2)*Z))*ARSIN(SQSIG*U)
XNEW=X-G/DGDX
IF (ABS((XNEW-X)/XNEW).LT.0.0001)  GO TO 2
X=XNEW
GO TO 1
2 X=XNEW
CF=2.*X**2
RETURN
END
```

SUM

```
SUBROUTINE SUM(X,Y,NE,VINT)
C   X IS THE INDEPENDENT VARIABLE
C   Y IS THE DEPENDENT VARIABLE
DIMENSION X(100),Y(100)
VINT=0.
NN=NE-1'
DO 1 I=1,NN
1    VINT=VINT+(X(I+1)-X(I))*(Y(I+1)+Y(I))/2.
RETURN
END
```

PLUS

```
      SUBROUTINE PLUS(SQCF, Y,RHO,R,NE,CCC,CC,VINT1,VINT2,A,HW,C1,D,P)
      DIMENSION Y(100),RHO(100),CCC(100),CC(100),YP(100),UP(100)
      DIMENSION CCCP(100),CCP(100),TP(100)
C     THIS SUBROUTINE USES THE WOLL MODEL TO DETERMINE Y AND U NEAR THE
C     WALL TO IMPROVE THE CALCULATIONS OF THETA AND DELTA STAR
      YE=138./RHO(1)*SQRT(2.)/SQCF*12./R
      DO 1 I=2,NE
      IF(Y(I).GT.YE)GO TO 2
    1 CONTINUE
    2 N=I
      DY=Y(N)-YE
      CALL SUM(Y,CCC,N,VINT1W)
      CALL SUM (Y,CC,N,VINT2W)
      VINT1=VINT1-VINT1W
      VINT2=VINT2-VINT2W
      YPLUS=0.
      YP(1)=0.
      UP(1)=0.
      CCP(1)=0.
      CCCP(1)=1.
      DO 3 J=2,70
      YPLUS=YPLUS+2.
      UPLUS=ATAN(8.*TAN(0.09*YPLUS/8.))/0.09
      YP(J)=YPLUS/RHO(1)**1.268*SQRT(2.)/SQCF*12./R
      UP(J)=UPLUS*SQCF/SQRT(2.*RHO(1))
      CALL TEMP(A,HW,C1,D,P,UP(J),DHDV,TP(J))
      CCCP(J)=1.-UP(J)/TP(J)
    3 CCP(J)=UP(J)/TP(J)*(1.-UP(J))
      JJ=70
      CALL SUM(YP,CCCP,JJ,VINT1P)
      CALL SUM(YP,CCP,JJ,VINT2P)
      VINT1=VINT1+VINT1P+(CCCP(JJ)+CCC(N))/2.*DY
      VINT2=VINT2+VINT2P+(CCP(JJ)+CC(N))/2.*DY
      RETURN
      END
```

```
                         CFI
      SUBROUTINE CFI(XME,R,VINT2,SQCF)
C     THIS SUBROUTINE SOLVES FOR CF USING EQUATION (22) OF THE WINTER
C     AND GAUDET REPORT R.& M. NO. 3712 DECEMBER 1970
      FD=1.+.056*XME*XME
      FC=SQRT(1.+.2*XME*XME)
      C=FD*R/12.*VINT2
      G=0.3894
      H=4.632
      XNEW=0.002**0.5
 55   X=XNEW
      F=1.0-H*X
      TEXP=EXP(0.537/X)
      XNEW=X-((G*F*TEXP-C)/(G*F*TEXP*(-0.537/X**2)-H*TEXP))
      S=ABS((XNEW-X)/XNEW)
      IF(S.LT.0.0001)GO TO 100
      GO TO 55
 100  CONTINUE
      SQCF=XNEW
      RETURN
      END
```

The following is an example input to the data reduction computer code. See MAIN for input formats.

```
001
17.68        0.          .8          1.4          3819000.
021
 .0          13.53
 .0056       14.71
 .034        14.94
 .077        15.18
 .11         15.28
 .177        15.75
 .206        15.9
 .2492       16.
 .2778       16.11
 .3208       16.16
 .3495       16.37
 .3924       16.41
 .421        16.54
 .4641       16.62
 .507        16.67
 .5357       16.69
 .5786       16.77
 .6216       16.92
 .65         17.07
 .6932       17.16
1.4          17.68
```

NOMENCLATURE

A $(\gamma - 1)M_\infty^2$

a Constant in Eq. (6)

C Defined by Eq. (13)

c Constant in Eq. (48), equal to 4

c_f Local skin-friction coefficient, $\dot{\tau}_w / (1/2 \rho_\infty U_\infty^2)$

c_h Stanton number, $- \dot{q}_w / \rho_\infty U_\infty (h_{aw} - h_w)$

c_p Specific heat at constant pressure

c_v Specific heat at constant volume

E e/U_τ^2

e Turbulent kinetic energy per unit mass, $(<u^2> + <v^2> + <w^2>)/2$

$\bar{e}$ $e/H_{o,\infty}$

F_c $(1 + 0.2 M_\infty^2)^{1/2}$

F_δ $1 + 0.056 M_\infty^2$

f Function defined by Eqs. (60) and (67)

H Specific total enthalpy, also used for shape factor, δ^*/θ

$\bar{H}$ H/h_∞

$\hat{H}$ $H/H_{o,\infty}$

h Specific enthalpy

h' Fluctuating local static enthalpy

$\bar{h}$ h/h_∞

$\bar{h}_o$ Zeroth-order $\bar{h}$

$\bar{h}_1$ First-order $\bar{h}$

k	Molecular thermal conductivity
k_t	Eddy thermal conductivity
L	Dissipation length, $\bar{L} = L/s$
ℓ	Prandtl mixing length
ℓ'	Integral scale length of turbulence
M	Mach number
m	$\bar{u} = \eta^{1/m}$, used herein as m = 7
$\dot{m}$	Mass flux
Pr	Prandtl number, $\mu\, c_p/k$
Pr_m	Mixed Prandtl number, $c_p\, (\mu + \mu_t)/(k + k_t)$
Pr_t	Turbulent Prandtl number, $c_p\, \mu_t/k_t$
p	Mean pressure
$\bar{p}$	$(\gamma - 1)p/(\gamma p_o)$
p'_o	Impact pressure
$\dot{q}$	Heat-transfer rate
$Re_{d,c}$	Reynolds number based on pipe diameter and velocity at pipe center
$Re_{d,m}$	Reynolds number based on pipe diameter and mean velocity
Re_δ	Reynolds number based on boundary-layer thickness and free-stream velocity
$Re_{o,s}$	Reynolds number, $\rho_o\, (2H_{o,\infty})^{1/2}\, s/\mu_o$
$Re_{\infty,x}$	Reynolds number, $\rho_\infty\, U_\infty x/\mu_\infty$
r	Recovery factor, $r = (T_{aw} - T_\infty)/(T_{o,\infty} - T_\infty)$
$\bar{r}$	Defined by Eq. (5)

s	Reynolds-analog factor, $s = c_f/2c_h$ (also used for characteristic length)
T	Mean static temperature
$\overline{T}$	$(T_o - T_w)/(T_{o,\infty} - T_w)$
t	Time
U	Mean velocity in x-direction
$\overline{U}$	$U/(H_{o,\infty})^{1/2}$
U_τ	Friction velocity $(\tau_w/\rho_w)^{1/2}$
u	Fluctuating velocity in x-direction
$\overline{u}$	U/U_∞
u^+	$U/(\tau_w/\rho_w)^{1/2}$
$-\langle uv \rangle$	Reynolds stress, a bar over this quantity indicates normalization with respect to $H_{o,\infty}$
V	Mean velocity in y-direction
$\overline{V}$	$V/(H_{o,\infty})^{1/2}$
v	Fluctuating velocity in y-direction
w	Fluctuating velocity in z-direction
x	Coordinate along body surface
$\overline{x}$	x/s
y	Coordinate normal to body surface
$\overline{y}$	y/s
y^+	$\rho_w U_\tau y/\mu_w$
z	Coordinate completing right-hand system with x and y
α	A constant equal to 0.18 in Section 3.0 and equal to $(5/2)m$ in Section 4.0
β	$c(5/2)m$

γ c_p/c_v

Δ Defined by Eq. (62) for constant temperature wall and by Eq. (69) for an adiabatic wall

δ Boundary-layer thickness defined as the value of y where $U/U_\infty = 0.99$

$\delta*$ Boundary-layer displacement thickness

ϵ A constant equal to zero or 1/8 in Section 3.0 and equal to $(1 - Pr_m)$ in Section 4.0

ζ Defined by Eq. (61) for constant temperature wall and by Eq. (68) for an adiabatic wall; also exponent of T in power law relation for viscosity

η y/δ

$\bar{\theta}$ Local wall angle

θ Boundary-layer momentum thickness

μ Molecular viscosity

$\bar{\mu}$ μ/μ_0

μ_t Eddy viscosity

ρ Density

$\bar{\rho}$ ρ/ρ_0

σ $\dfrac{\gamma-1}{2} M_\infty^2 \Big/ \left(1 + \dfrac{\gamma-1}{2} M_\infty^2\right)$

σ_e Schmidt number for turbulent kinetic energy

τ Total shear stress

τ_t Turbulent shear stress

ϕ Stream function

ω Transformed stream function

ν μ/ρ

SUBSCRIPTS

aw   Adiabatic wall

E   Outer edge of boundary layer

I   Inner edge of boundary layer

o   Local total conditions, except $\bar{h}_o$

w   Wall conditions

∞ Free-stream conditions

SPECIAL NOTATION AND CLARIFICATION

$< >$ Indicates time average, e.g. $<uv> = \displaystyle\lim_{t \to \infty} \frac{1}{2t} \int_{-t}^{t} (uv) \, dt'$

The variables denoted in the nomenclature as mean quantities are understood to be time averaged.